ISSN 2667-4211

ESKİŞEHİR TECHNICAL UNIVERSITY JOURNAL OF SCIENCE AND TECHNOLOGY

A – Applied Sciences and Engineering

Volume 23 Number 4 - December - 2022

ESKİŞEHİR TECHNICAL UNIVERSITY JOURNAL OF SCIENCE AND TECHNOLOGY
A- Applied Sciences and Engineering
Eskişehir Teknik Üniversitesi Bilim ve Teknoloji Dergisi A – Uygulamalı Bilimler ve Mühendislik

Volume: 23 / Number: 4 / December - 2022

Eskişehir Technical University Journal of Science and Technology A - Applied Sciences and Engineering (ESTUJST-A) is a peer-reviewed and refereed international journal published by Eskişehir Technical University. Since 2000, it has been regularly published and distributed biannually and it has been published quarterly and only electronically since 2016.
The journal accepts only manuscripts written in English.

The journal issues are published electronically in **March, June**, **September**, and **December**.

Eskişehir Technical University Journal of Science and Technology A - Applied Sciences and Engineering is an international peer-reviewed and refereed journal published by Eskişehir Technical University.

The journal is dedicated to the dissemination of knowledge in applied sciences and engineering disciplines.

The journal aims to publish high quality, original international scientific research articles with specific contributions to the literature in the field of engineering and applied sciences. The journal publishes research papers in the fields of applied science and technology such as Physics, Biology, Mathematics, Statistics, Chemistry and Chemical Engineering, Environmental Sciences and Engineering, Civil Engineering, Earth and Atmospheric Sciences, Electrical and Electronical Engineering, Computer Science and Informatics, Materials Sciences and Engineering, Mechanical Engineering, Mining Engineering, Industrial Engineering, Aeronautics and Astronautics, Pharmaceutical Sciences.

The journal publishes original research articles and special issue articles. All articles are peer-reviewed and the articles that have been evaluated are ensured to meet with researchers as soon as possible.

"Anadolu Üniversitesi Bilim ve Teknoloji Dergisi A - Uygulamalı Bilimler ve Mühendislik (Anadolu University Journal of Science and Technology A - Applied Sciences and Engineering)" published within Anadolu University started to be published within Eskişehir Technical University which was established due to statute law 7141, in 2018. Hence, the name of the journal is changed to " Eskişehir Technical University Journal of Science and Technology A - Applied Sciences and Engineering (Eskişehir Teknik Üniversitesi Bilim ve Teknoloji Dergisi A - Uygulamalı Bilimler ve Mühendislik)".

Indexed by **DOAJ** - Directory of Open Access Journals, **EBSCO** and **ULAKBIM**

ESKİŞEHİR TECHNICAL UNIVERSITY JOURNAL OF SCIENCE AND TECHNOLOGY
A- Applied Sciences and Engineering
Eskişehir Teknik Üniversitesi Bilim ve Teknoloji Dergisi A – Uygulamalı Bilimler ve Mühendislik

Volume: 23 / Number: 4 / December – 2022

Owner / Publisher: Prof. Dr. Adnan ÖZCAN for Eskişehir Technical University

CONTACT INFORMATION
Eskişehir Technical Unıversity Journal of Science and Technology
Eskişehir Technical University, Institute of Graduate Programs, 26470 Eskişehir, TURKEY
Phone: +90 222 213 7485
e-mail : btda@eskisehir.edu.tr

ESKİŞEHİR TECHNICAL UNIVERSITY JOURNAL OF SCIENCE AND TECHNOLOGY
A- Applied Sciences and Engineering

Eskişehir Teknik Üniversitesi Bilim ve Teknoloji Dergisi A – Uygulamalı Bilimler ve Mühendislik

Volume: 23 / Number: 4 / December - 2022

ESKİŞEHİR TECHNICAL UNIVERSITY JOURNAL OF SCIENCE AND TECHNOLOGY
A- Applied Sciences and Engineering
Eskişehir Teknik Üniversitesi Bilim ve Teknoloji Dergisi A – Uygulamalı Bilimler ve Mühendislik

ABOUT

Eskişehir Technical University Journal of Science and Technology A - Applied Sciences and Engineering (ESTUJST-A) is a peer-reviewed and refereed international journal published by Eskişehir Technical University. Since 2000, it has been regularly published and distributed biannually and it has been published quarterly and only electronically since 2016.

The journal accepts only manuscripts written in English.

The journal issues are published electronically in **MARCH, JUNE, SEPTEMBER**, and **DECEMBER.**

AIM AND SCOPE

Eskişehir Technical University Journal of Science and Technology A - Applied Sciences and Engineering is an international peer-reviewed and refereed journal published by Eskişehir Technical University.

The journal is dedicated to the dissemination of knowledge in applied sciences and engineering disciplines.

The journal aims to publish high quality, original international scientific research articles with specific contributions to the literature in the field of engineering and applied sciences. The journal publishes research papers in the fields of applied science and technology such as Physics, Biology, Mathematics, Statistics, Chemistry and Chemical Engineering, Environmental Sciences and Engineering, Civil Engineering, Earth and Atmospheric Sciences, Electrical and Electronical Engineering, Computer Science and Informatics, Materials Sciences and Engineering, Mechanical Engineering, Mining Engineering, Industrial Engineering, Aeronautics and Astronautics, Pharmaceutical Sciences.

The journal publishes original research articles and special issue articles. All articles are peer-reviewed and the articles that have been evaluated are ensured to meet with researchers as soon as possible.

PEER REVIEW PROCESS

Manuscripts are first reviewed by the editorial board in terms of its its journal's style rules scientific content, ethics and methodological approach. If found appropriate, the manuscript is then send to at least two renown referees by editor. The decision in line with the referees may be an acceptance, a rejection or an invitation to revise and resubmit. Confidential review reports from the referees will be kept in archive. All submission process manage through the online submission systems.

OPEN ACCESS POLICY

This journal provides immediate open access to its content on the principle that making research freely available to the public supports a greater global exchange of knowledge.

PRICE POLICY

Eskişehir Technical University Journal of Science and Technology A - Journal of Applied Sciences and Engineering is an English, peer-reviewed, scientific, free of charge open-access-based journal. The author is not required to pay any publication fees or article processing charges (APCs) for peer-review administration and management, typesetting, and open-access. Articles also receive Digital Object Identifiers (DOIs) from the CrossRef organization to ensure they are always available.

ETHICAL RULES

You can reach the Ethical Rules in our journal in full detail from the link below:

https://dergipark.org.tr/en/pub/estubtda/policy

Ethical Principles and Publication Policy

Policy & Ethics

Assessment and Publication

As a peer-reviewed journal, it is our goal to advance scientific knowledge and understanding. We adhere to the guideline and ethical standards from the Committee on Publication Ethics (COPE) and the recommendations of ICMJE (International Committee of Medical Journal Editors) regarding all aspects of publication ethics and cases of research and publication misconduct to ensure that all publications represent accurate and original work and that our peer review process is structured without bias. We have outlined a set of ethical principles that must be followed by all authors, reviewers, and editors.

All manuscripts submitted to our journals are pre-evaluated in terms of their relevance to the scope of the journal, language, compliance with writing instructions, suitability for science, and originality, by taking into account the current legal requirements regarding copyright infringement and plagiarism. Manuscripts that are evaluated as insufficient or non-compliant with the instructions for authors may be rejected without peer review.

Editors and referees who are expert researchers in their fields assess scientific manuscripts submitted to our journals. A blind peer review policy is applied to the evaluation process. The Editor-in-Chief, if he/she sees necessary, may assign an Editor for the manuscript or may conduct the scientific assessment of the manuscript himself/herself. Editors may also assign referees for the scientific assessment of the manuscript and make their decisions based on reports by the referees. The Editor-in-Chief makes the final decision regarding the publishing of the manuscript.

Articles are accepted for publication by the Editor-in-Chief in accordance with the COPE (Committee on Publication Ethics). Authors can access this information online via the journals' websites (https://publicationethics.org/). Articles are accepted for publication on the understanding that they have not been published and are not going to be considered for publication elsewhere. Authors should certify that neither the manuscript nor its main contents have already been published or submitted for publication in another journal.

The journal adapts the COPE guidelines to satisfy the high-quality standards of ethics for authors, editors, and reviewers:

Duties of Editors-in-Chief and co-Editors

The crucial role of the journal Editor-in-Chief and co-Editors is to monitor and ensure the fairness, timeliness, thoroughness, and civility of the peer-review editorial process. The main responsibilities of Editors-in-Chief are as follows:

• Selecting manuscripts suitable for publication while rejecting unsuitable manuscripts,
• Ensuring a supply of high-quality manuscripts to the journal by identifying important,
• Increasing the journal's impact factor and maintaining the publishing schedule,
• Providing strategic input for the journal's development,

Duties of Editors

The main responsibilities of editors are as follows:

• An editor must evaluate the manuscript objectively for publication, judging each on its quality without considering the nationality, ethnicity, political beliefs, race, religion, gender, seniority, or institutional affiliation of the author(s). Editors should decline any assignment when there is a potential for conflict of interest.
• Editors must ensure the document(s) sent to the reviewers does not contain information of the author(s) and vice versa.
• Editors' decisions should be provided to the author(s) accompanied by the reviewers' comments and recommendations unless they contain offensive or libelous remarks.
• Editors should respect requests (if well reasoned and practicable) from author(s) that an individual should not review the submission.
• Editors and all staff members should guarantee the confidentiality of the submitted manuscript.
• Editors should have no conflict of interest with respect to articles they reject/accept. They must not have a conflict of interest with the author(s), funder(s), or reviewer(s) of the manuscript.
• Editors should strive to meet the needs of readers and authors and to constantly improve the journal.

Duties of Reviewers/Referees

The main responsibilities of reviewers/referees are as follows:

• Reviewers should keep all information regarding papers confidential and treat them as privileged information.
• Reviews should be conducted objectively, with no personal criticism of the author.
• Reviewers assist in the editorial decision process and as such should express their views clearly with supporting arguments.
• Reviewers should complete their reviews within a specified timeframe (maximum thirty-five (35) days). In the event that a reviewer feels it is not possible for him/her to complete the review of the manuscript within a stipulated time, then this information must be communicated to the editor so that the manuscript could be sent to another reviewer.
• Unpublished materials disclosed in a submitted manuscript must not be used in a reviewer's personal research without the written permission of the author. Information contained in an unpublished manuscript will remain confidential and must not be used by the reviewer for personal gain.
• Reviewers should not review manuscripts in which they have conflicts of interest resulting from competitive, collaborative, or other relationships or connections with any of the authors, companies, or institutions connected to the papers.

• Reviewers should identify similar work in published manuscripts that has not been cited by the author. Reviewers should also notify the Editors of significant similarities and/or overlaps between the manuscript and any other published or unpublished material.

Duties of Authors

The main responsibilities of authors are as follows:

• The author(s) should affirm that the material has not been previously published and that they have not transferred elsewhere any rights to the article.
• The author(s) should ensure the originality of the work and that they have properly cited others' work in accordance with the reference format.
• The author(s) should not engage in plagiarism or in self-plagiarism.
• On clinical and experimental humans and animals, which require an ethical committee decision for research in all branches of science;
All kinds of research carried out with qualitative or quantitative approaches that require data collection from the participants by using survey, interview, focus group work, observation, experiment, interview techniques,
Use of humans and animals (including material/data) for experimental or other scientific purposes,
• Clinical studies on humans,
• Studies on animals,
• Retrospective studies in accordance with the law on the protection of personal data, (Ethics committee approval should have been obtained for each individual application, and this approval should be stated and documented in the article.)
Information about the permission (board name, date, and number) should be included in the "Method" section of the article and also on the first/last page.
During manuscript upload, the "Ethics Committee Approval" file should be uploaded to the system in addition to the manuscript file.
In addition, in case reports, it is necessary to include information on the signing of the informed consent/ informed consent form in the manuscript.
• The author(s) should suggest no personal information that might make the identity of the patient recognizable in any form of description, photograph, or pedigree. When photographs of the patient were essential and indispensable as scientific information, the author(s) have received consent in written form and have clearly stated as much.
• The author(s) should provide the editor with the data and details of the work if there are suspicions of data falsification or fabrication. Fraudulent data shall not be tolerated. Any manuscript with suspected fabricated or falsified data will not be accepted. A retraction will be made for any publication which is found to have included fabricated or falsified data.
• The author(s) should clarify everything that may cause a conflict of interests such as work, research expenses, consultant expenses, and intellectual property.
• The author(s) must follow the submission guidelines of the journal.
• The author(s) discover(s) a significant error and/or inaccuracy in the submitted manuscript at any time, then the error and/or inaccuracy must be reported to the editor.
• The author(s) should disclose in their manuscript any financial or other substantive conflicts of interest that might be construed to influence the results or interpretation of their manuscript. All sources of financial support should be disclosed under the heading of "Acknowledgment" or "Contribution".
• The corresponding author should ensure that all appropriate co-authors and no inappropriate co-authors are included in the paper and that all co-authors have seen and approved the final version of the paper and have agreed to its submission for publication. All those who have made

significant contributions should be listed as co-authors. Others who have participated in certain substantive aspects of the research should be acknowledged or listed under the heading of "Author Contributions".

Cancellations/Returns

Articles/manuscripts may be returned to the authors in order to increase the authenticity and/or reliability and to prevent ethical breaches, and even if articles have been accepted and/or published, they can be withdrawn from publication if necessary. The Editor-in-Chief of the journal has the right to return or withdraw an article/manuscript in the following situations:

• When the manuscript is not within the scope of the journal,
• When the scientific quality and/or content of the manuscript do not meet the standards of the journal and a referee review is not necessary,
• When there is proof of ruling out the findings obtained by the research, (When the article/manuscript is undergoing an assessment or publication process by another journal, congress, conference, etc.,)
• When the article/manuscript was not prepared in compliance with scientific publication ethics,
• When any other plagiarism is detected in the article/manuscript,
• When the authors do not perform the requested corrections within the requested time (maximum twenty-one (21) days),
• When the author does not submit the requested documents/materials/data etc. within the requested time,
• When the requested documents/materials/data etc. submitted by the author are missing for the second time,
• When the study includes outdated data,
• When the authors make changes that are not approved by the editor after the manuscript was submitted,
• When an author is added/removed, the order of the authors is changed, the corresponding author is changed, or the addresses of the authors are changed without the consent of the Editor-in-Chief,
• When a statement is not submitted indicating that approval of the ethics committee permission was obtained for the following (including retrospective studies):
• When human rights or animal rights are violated,

ETHICAL ISSUES

Plagiarism

The use of someone else's ideas or words without a proper citation is considered plagiarism and will not be tolerated. Even if a citation is given, if quotation marks are not placed around words taken directly from other authors' work, the author is still guilty of plagiarism. Reuse of the author's own previously published words, with or without a citation, is regarded as self-plagiarism.

All manuscripts received are submitted to iThenticate®, which compares the content of the manuscript with a database of web pages and academic publications. Manuscripts are judged to be plagiarized or self-plagiarized, based on the iThenticate® report or any other source of information, will be rejected. Corrective actions are proposed when plagiarism and/or self-plagiarism is detected after publication. Editors should analyze the article and decide whether a corrected article or retraction needs to be published.

Open-access theses are considered as published works and they are included in the similarity checks.

iThenticate® report should have a maximum of 11% from a single source, and a maximum of 25% in total.

Conflicts of Interest

Eskişehir Technical University Journal of Science and Technology A - Applied Sciences and Engineering should be informed of any significant conflict of interest of editors, authors, or reviewers to determine whether any action would be appropriate (e.g. an author's statement of conflict of interest for a published work, or disqualifying a referee).

Financial

The authors and reviewers of the article should inform the journal about the financial information that will bring financial gain or loss to any organization from the publication of the article.

*Research funds; funds, consulting fees for a staff member; If you have an interest, such as patent interests, you may have a conflict of interest that needs to be declared.

Other areas of interest

The editor or reviewer may disclose a conflict of interest that, if known, would be embarrassing (for example, an academic affiliation or rivalry,a close relationship or dislike, or a person who may be affected by the publication of the article).

Conflict of interest statement

Please note that a conflict of interest statement is required for all submitted manuscripts. If there is no conflict of interest, please state "There are no conflicts of interest to declare" in your manuscript under the heading "Conflicts of Interest" as the last section before your Acknowledgments.

AUTHOR GUIDELINES

All manuscripts must be submitted electronically.

You will be guided stepwise through the creation and uploading of the various files. There are no page charges. Papers are accepted for publication on the understanding that they have not been published and are not going to be considered for publication elsewhere. Authors should certify that neither the manuscript nor its main contents have already been published or submitted for publication in another journal. We ask a signed copyright to start the evaluation process. After a manuscript has been submitted, it is not possible for authors to be added or removed or for the order of authors to be changed. If authors do so, their submission will be cancelled.

Manuscripts may be rejected without peer review by the editor-in-chief if they do not comply with the instructions to authors or if they are beyond the scope of the journal. After a manuscript has been accepted for publication, i.e. after referee-recommended revisions are complete, the author will not be permitted to make any changes that constitute departures from the manuscript that was accepted by the editor. Before publication, the galley proofs are always sent to the authors for corrections. Mistakes or omissions that occur due to some negligence on our part during final printing will be rectified in an errata section in a later issue.

This does not include those errors left uncorrected by the author in the galley proof. The use of someone else's ideas or words in their original form or slightly changed without a proper citation is considered plagiarism and will not be tolerated. Even if a citation is given, if quotation marks are not placed around words taken directly from another author's work, the author is still guilty of plagiarism. All manuscripts received are submitted to iThenticateR, a plagiarism checking system, which compares the content of the manuscript with a vast database of web pages and academic publications. In the received iThenticateR report; The similarity rate is expected to be below 25%. Articles higher than this rate will be rejected.

Uploading Articles to the Journal
Authors should prepare and upload 2 separate files while uploading articles to the journal. First, the Author names and institution information should be uploaded so that they can be seen, and then (using the additional file options) a separate file should be uploaded with the Author names and institution information completely closed. When uploading their files with closed author names, they will select the "Show to Referee" option, so that the file whose names are closed can be opened to the referees.

Style and Format
Manuscripts should be **single column** by giving one-spaced with 2.5-cm margins on all sides of the page, in Times New Roman font (font size 11). Every page of the manuscript, including the title page, references, tables, etc., should be numbered. All copies of the manuscript should also have line numbers starting with 1 on each consecutive page.

Manuscripts must be upload as word document (*.doc, *.docx vb.). **Please avoid uploading *texts in *.pdf format.***

Symbols, Units and Abbreviations
Standard abbreviations and units should be used; SI units are recommended. Abbreviations should be defined at first appearance, and their use in the title and abstract should be avoided. Generic names of chemicals should be used. Genus and species names should be typed in italic or, if this is not available, underlined.

Manuscript Content
Articles should be divided into logically ordered and numbered sections. Principal sections should be numbered consecutively with Arabic numerals (1. Introduction, 2. Formulation of problem, etc.) and subsections should be numbered 1.1., 1.2., etc. Do not number the Acknowledgements or References sections. The text of articles should be, if possible, divided into the following sections: Introduction, Materials and Methods (or Experimental), Results, Discussion, and Conclusion.

Title and contact information
The first page should contain the full title in sentence case (e.g., Hybrid feature selection for text classification), the full names (last names fully capitalised) and affiliations (in English) of all authors (Department, Faculty, University, City, Country, E-mail), and the contact e-mail address for the clearly identified corresponding author. The first page should contain the full title, abstract and keywords (both English and Turkish).

Abstract
The abstract should provide clear information about the research and the results obtained, and should not exceed 300 words. The abstract should not contain citations and must be written in Times New Roman font with font size 9.

Keywords
Please provide 3 to 5 keywords which can be used for indexing purposes.

Introduction
The motivation or purpose of your research should appear in the “Introduction”, where you state the questions you sought to answer, and then provide some of the historical basis for those questions.

Methods
Provide sufficient information to allow someone to repeat your work. A clear description of your experimental design, sampling procedures, and statistical procedures is especially important in papers describing field studies, simulations, or experiments. If you list a product (e.g., animal food, analytical device), supply the name and location of the manufacturer. Give the model number for equipment used.

Results
Results should be stated concisely and without interpretation.

Discussion
Focus on the rigorously supported aspects of your study. Carefully differentiate the results of your study from data obtained from other sources. Interpret your results, relate them to the results of previous research, and discuss the implications of your results or interpretations.

Conclusion
This should state clearly the main conclusions of the research and give a clear explanation of their importance and relevance. Summary illustrations may be included.

Acknowledgments
Acknowledgments of people, grants, funds, etc. should be placed in a separate section before the reference list. The names of funding organizations should be written in full.

References
AMA Style should be used in the reference writing of our journal. If necessary, at this point, the reference writings of the articles published in our article can be examined.

Citations in the text should be identified by numbers in square brackets. The list of references at the end of the paper should be given in order of their first appearance in the text. All authors should be included in reference lists unless there are 10 or more, in which case only the first 10 should be given, followed by 'et al.'. Do not use individual sets of square brackets for citation numbers that appear together, e.g., [2,3,5–9], not [2], [3], [5]–[9]. Do not include personal communications, unpublished data, websites, or other unpublished materials as references, although such material may be inserted (in parentheses) in the text. In the case of publications in languages other than English, the published English title should be provided if one exists, with an annotation such as "(article in Turkish with an abstract in English)". If the publication was not published with an English title, cite the original title only; do not provide a self-translation. References should be formatted as follows (please note the punctuation and capitalisation):

Journal articles
Journal titles should be abbreviated according to ISI Web of Science abbreviations.
Guyon I, Elisseeff A. An introduction to variable and feature selection. J Mach Learn Res 2003; 3: 1157-1182.

Izadpanahi S, Ozcınar C, Anbarjafari G, Demirel H. Resolution enhancement of video sequences by using discrete wavelet transform and illumination compensation. Turk J Elec Eng & Comp Sci 2012; 20: 1268-1276.

Books
Haupt RL, Haupt SE. Practical Genetic Algorithms. 2nd ed. New York, NY, USA: Wiley, 2004.
Kennedy J, Eberhart R. Swarm Intelligence. San Diego, CA, USA: Academic Press, 2001.

Chapters in books
Poore JH, Lin L, Eschbach R, Bauer T. Automated statistical testing for embedded systems. In: Zander J, Schieferdecker I, Mosterman PJ, editors. Model-Based Testing for Embedded Systems. Boca Raton, FL, USA: CRC Press, 2012. pp. 111-146.

Conference proceedings
Li RTH, Chung SH. Digital boundary controller for single-phase grid-connected CSI. In: IEEE 2008 Power Electronics Specialists Conference; 15–19 June 2008; Rhodes, Greece. New York, NY, USA: IEEE. pp. 4562-4568.

Theses
Boynukalın Z. Emotion analysis of Turkish texts by using machine learning methods. MSc, Middle East Technical University, Ankara, Turkey, 2012.

Tables and Figures
All illustrations (photographs, drawings, graphs, etc.), not including tables, must be labelled "Figure." Figures must be submitted in the manuscript.

All tables and figures must have a caption and/or legend and be numbered (e.g., Table 1, Figure 2), unless there is only one table or figure, in which case it should be labelled "Table" or "Figure" with no numbering. Captions must be written in sentence case (e.g., Macroscopic appearance of the samples.). The font used in the figures should be Times New Roman. If symbols such as ×, μ, η, or ν are used, they should be added using the Symbols menu of Word.

All tables and figures must be numbered consecutively as they are referred to in the text. Please refer to tables and figures with capitalisation and unabbreviated (e.g., "As shown in Figure 2…", and not "Fig. 2" or "figure 2").

The resolution of images should not be less than 118 pixels/cm when width is set to 16 cm. Images must be scanned at 1200 dpi resolution and submitted in jpeg or tiff format. Graphs and diagrams must be drawn with a line weight between 0.5 and 1 point. Graphs and diagrams with a line weight of less than 0.5 point or more than 1 point are not accepted. Scanned or photocopied graphs and diagrams are not accepted.

Figures that are charts, diagrams, or drawings must be submitted in a modifiable format, i.e. our graphics personnel should be able to modify them. Therefore, if the program with which the figure is drawn has a "save as" option, it must be saved as *.ai or *.pdf. If the "save as" option does not include these extensions, the figure must be copied and pasted into a blank Microsoft Word document as an editable object. It must not be pasted as an image file (tiff, jpeg, or eps) unless it is a photograph.

Tables and figures, including caption, title, column heads, and footnotes, must not exceed 16 × 20 cm and should be no smaller than 8 cm in width. For all tables, please use Word's "Create Table" feature, with no tabbed text or tables created with spaces and drawn lines. Please do not duplicate information that is already presented in the figures.

Article Corrections and Uploading to the System

Authors should upload the desired edits for their articles without destroying or changing the Template file of the article, by selecting and specifying the relevant edits as Colored, and also submit the Clean version of the article in 2 separate files (using the Additional file option if necessary). * In case of submitting a corrected article, a separate File in Reply to the Referees must be prepared and the "Reply to the Referees" option in the Add additional file option should be checked and uploaded. If a separate file is not prepared in response to the referees, the Author will definitely be asked to upload the relevant file again and the evaluation will be in the pending phase.

CONFLICT OF INTEREST STATEMENT

The authors are obliged to present the conflict of interest statement at the end of the article.

ESKİŞEHİR TECHNICAL UNIVERSITY JOURNAL OF SCIENCE AND TECHNOLOGY
A – Applied Sciences and Engineering
Volume: 23 / Number: 4 / December - 2022

CONTENTS

RESEARCH ARTICLE

ESKİŞEHİR TECHNICAL UNIVERSITY JOURNAL OF SCIENCE AND TECHNOLOGY
A- APPLIED SCIENCES AND ENGINEERING

2022, 23(4), pp. 233-243, DOI: 10.18038/estubtda.899963

CONTRIBITION OF MICRO-SILICA AND NANO-MONTMORILLONITE REINFORCEMENTS ON THE MECHANICAL PROPERTIES OF UV-CURABLE THERMOSET RESIN

Ayşe Çağıl KANDEMİR [1,*], Arda BAYTAROĞLU [1]

[1] Mechanical Engineering, Faculty of Engineering, TED University, Ankara, Turkey

ABSTRACT

UV-curable thermoset resins had been utilized in organic coating industry because of their benefits over conventional adhesives like fast curing, less energy consumption and equipment. In this article, the effects of micro and nano-scaled reinforcements on the mechanical properties of a UV-curable thermoset resin were investigated. The reinforcements are chosen to be nano-scaled Montmorillonite (MMT) and micro-scaled Silica (SiO_2). The reason for this choice is that the aforementioned particles are non-toxic, low-cost and in the case of MMT; abundant in nature. According to our knowledge, there is no study on the synergistic effects of those two additives in thermoset resins.

The instrumented microindentation test results reveal that maximum improvement on hardness (288%) was achieved by single addition of MMT thanks to the well-distributed silicate layers. Conversely, SiO_2 addition diminished both strength (-51%) and modulus (-68%) drastically which is attributed to the possible poor dispersion and weak surface attraction. On the other hand, when those additives were utilized together, the property improvements namely; hardness and modulus are observed to be in between of single addition of either additive. It is suggested that SiO_2 contribution does not disturb intercalated/exfoliated-MMT structure and similarly by simultaneous MMT reinforcement, quality of SiO_2 dispersion is not affected. It is concluded that one benefit of these SiO_2-MMT combinations over single MMT reinforcement could be related to plasticity since they result in less plasticity reduction of -22%-27% compared to MMT (-43%) with the further benefit of higher hardness improvement (+66%) than bare SiO_2 addition (-51%).

Keywords: Clay, Silicas, Composites, Film, Thermoset

1. INTRODUCTION

UV-curable thermoset resins had been utilized in organic coating industry because of their advantages like fast curing, less energy consumption and equipment in comparison with conventional curing methods. Crosslinking density of the thermoset resins could be increased to improve strength, though it leads to brittleness. The alternative for this is utilizing reinforcements by composite approach. In this study, nano-scaled Montmorillonite (MMT) and micro-scaled silica (SiO_2) were focused as they are non-toxic, low-cost and in the case of MMT; abundant in nature.

Studies show that both nano and micro-scaled silica particles either improve or diminish strength of thermoset matrices depending on mainly their surface compatibility [1– 3]. For instance, in the study of Ahmad et al. [1] nano-silica addition to epoxy resin diminished both strength and elastic modulus while in the study of Li et al. [2] both properties were improved thanks to the surface compatibility of composite constituents. In the study of Meng et. al., micro and nano silica reinforcements were utilized to toughen epoxy [3]. The study yielded that nano-silica could much more efficiently toughen the ductile epoxy matrix such that 738% and 60% improvements were achieved for 4 wt% nano and micro-silicas, respectively. This behavior is attributed to the higher surface area and smaller particle-particle distance of nano-silica.

*Corresponding Author: cagil.kandemir@tedu.edu.tr
Received: 19.03.2021 Published: 29.12.2022

There are many studies focusing on Montmorillonite (MMT) based adhesive composites [4– 9]. Silicate layers have very high aspect ratio (could be as high as 500) enabling effective stress transfer from matrix to MMT. In order to achieve this, intercalation/exfoliation level of them play a significant role. For instance, in the study of Menezes et al. [9] highest improvement in both strength and modulus of a dental adhesive is achieved by just 0.2 wt% exfoliated MMT addition while those properties declined with further MMT addition. This shows that dispersion quality and the exfoliation level are key parameters as increase in MMT concentration causes agglomeration. In the study of Alsagayar et al. [5] when MMT loading in epoxy resin exceeds 1 wt% both strength and modulus diminish because of poor dispersion pointing out the necessity of exfoliation.

The main aim of this study to investigate influence of nano-scaled MMT and micro-scaled SiO_2 on the mechanical properties of UV-curable thermoset resin. The reason for the choice of these particles is that they are non-toxic, low-cost and in the case of MMT; abundant in nature. According to our knowledge, there is no study on the mutual effects of those two particles in thermoset resins. The films of the composites were produced either on glass slides or as free-standing films. Dispersion of the particles was observed by XRD and FTIR analyses while mechanical behavior was tested via instrumented microindentation. In this study, plasticity was utilized to comment on the underlying deformation mechanisms. The outcomes were interpreted in terms of the size, shape, surface compatibility and dispersion of the particles.

2. EXPERIMENTAL

2.1. Materials

UV-curable thermoset resin is chosen as the polymer matrix having the commercial name of NOA 61 (Norland Optics). NOA 61 is not composed of volatile components, which is beneficial for long-term stability. As for the reinforcements, unmodified amorphous silica particles (1 μm) and organically modified- nanoclay (35-45% dimethyl dialkyl (C14-C18) amine modified Montmorillonite) were chosen for micro-scaled/ spherical and nano-scaled/ layered reinforcements, respectively. Silica particles and nanoclay were purchased from Sigma Aldrich and Nanografi (Ankara, Turkey), respectively.

2.2. Production of Composites

Firstly, an appropriate solvent was sought since the solvent-mixing method was going to be applied for composite production. The solvents: deionized water, ethanol and tetrahydrofuran were tried. Inspection by naked eye revealed that tetrahydrofuran is the most appropriate solvent for the particular UV-curable resin. Ethanol and deionized water usage as solvent resulted in more agglomerated morphology which was visible to naked eye while via tetrahydrofuran solvent, agglomeration was not observed. Similar results were also found in the previous study of the author with a comparable UV-curable resin [10–11].

The composite production consists of three main parts. Firstly, NOA 61 was dissolved in the solvent which is chosen to be tetrahydrofuran in magnetic stirrer for two hours. Secondly, reinforcements were induced to the solution and mixed for four hours by magnetic stirrer. Lastly, the solution was poured in either of the followings: to a Teflon plate or on a glass slide for XRD/ FTIR analyses, or microindentation test, respectively. Subsequently, UV-curing (365 nm-wavelength) was applied. The composite coatings which were exposed to micro-indentation test are shown in Figure 1 while standalone films taken from Teflon molds are shown in Figure 4. Designation and the weight percentages of composite constituents are shown in Table 1.

Table 1. Designation of the composite films and the weight percentages of their constituents.

	Polymer	**Polymer_ MMT**	**Polymer_MMT_ 2**	**Polymer_ SiO**	**Polymer_SiO_ MMT**	**Polymer_SiO_ MMT_2**
MMT	-	1 wt%	5 wt%		1 wt%	0.5 wt%
SiO_2	-	-	-	1 wt%	1 wt%	0.5 wt%

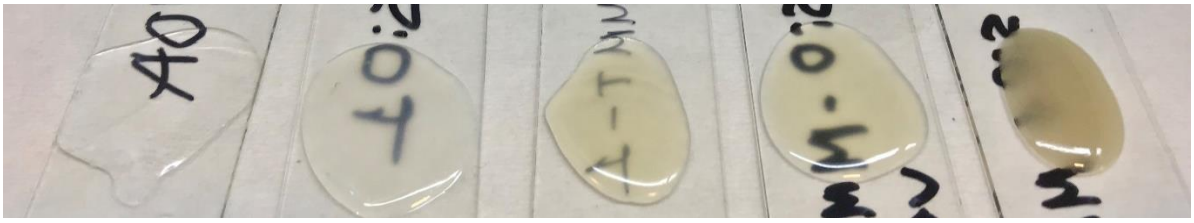

(a) **(b)** **(c)** **(d)** **(e)**

Figure 1. Polymer and composite coatings on glass slides which subsequently exposed to Micro-indentation test are shown: a)Polymer b) Polymer_SiO c) Polymer_MMT d) Polymer_SiO_MMT_2 e) Polymer_SiO_MMT.

2.3. X- ray Diffraction Analysis

To evaluate dispersity and the intercalation/exfoliation of Montmorrilonite silicate layers in thermoset resin, wide angle X- ray diffraction analysis (XRD) (Rigaku Ultima-IV, CuKa 40 kV, 40 mA) was conducted under a continuous scanning range of 2–10º in Middle East Technical University Central Laboratory.

2.4. FTIR Spectroscopy

Fourier Transformed Infrared Spectroscopy (FTIR) was accomplished in Middle East Technical University Central Laboratory (Bruker IFS 66/S) in order to confirm the surface compatibility of matrix with the reinforcements.

2.4. Mechanical Characterization

Instrumented micro-indentation test with Vickers indenter was conducted in Middle East Technical University Central Laboratory (CSM Instruments). The tests were accomplished by a maximum force of 5 mN. Hardness and Elastic Modulus values were calculated by using Oliver-Pharr method [25-26]. The equations used for the calculation of elastic modulus are revealed in (1) and (2). S is the slope of unloading curve, A is the contact area, β is the dimensionless parameter close to unity, E_{eff} is the effective modulus combining moduli of the indenter and the sample. υ, υ_i, E and Ei are Possion's ratio of sample, Possion's ratio of indenter, elastic modulus of sample and elastic modulus of indenter, respectively. The plasticity was measured by the ratio of the plastic work to the total work of force-indentation depth curves.

$$S = \beta \frac{2}{\sqrt{\pi}} Eeff\sqrt{A} \tag{1}$$

$$\frac{1}{Eeff} = \frac{1-v^2}{E} + \frac{1-vi^2}{Ei} \tag{2}$$

3. RESULTS

The results of XRD are represented in Figure 2. Sharp peaks does not exist in the patterns of Polymer, Polymer_MMT, Polymer_MMT_SiO and Polymer_MMT_SiO_2. In contrary, two distinctive peaks were found in Polymer_MMT which correspond to 2θ degress of 2.510º and 4.935º. FTIR Spectroscopy was accomplished for three samples; Polymer, Polymer_MMT and Polymer_SiO (Figure 3-4). There are no major peak differences in all of the FTIR patterns. However, in the case of Polymer_SiO; at the wave numbers of 522 cm^{-1} and 462 cm^{-1}there are two distinctive peaks differs from Polymer.

Micro-indentation test was applied in order to measure mechanical properties of the samples (Table 2, Figure 5). Hardness and Elastic Modulus values were calculated by using Oliver Pharr method [25-26]. Hardness of the samples were found to be 169.608±2.190, 657.394±116.394, 84.618±11.015, 282.166±15.00 and 126.906±23.705 for Polymer, Polymer_MMT, Polymer_SiO, Polymer_SiO_MMT and Polymer_SiO_MMT_2, respectively. While for the same samples elastic moduli were revealed to be 6.834±1.314, 7.613±0.337, 2.225±0.213, 5.022±0.567 and 3.288±0.432, respectively.

4. DISCUSSION

4.1. Interaction Between Matrix and the Reinforcements

The exact formula of the polymer (commercial name: NOA 61) is unknown. However, previous studies revealed that the main constituents of which are; mercapto-ester and tetrahydrofurfuryl metachrylate. The study of Castiriota et al. showed that main curing reaction occurs by the interaction of thiol group (R-SH) and C=C [12]. Consequently, the fully cured polymer should not have C=C and S-H bond. FTIR spectra of the polymer in Figure 3 does not show the specific peak of aliphatic C=C (1638 cm^{-1}) pointing out the efficient crosslinking while there exists a weak peak of S-H at 2570 cm^{-1}.

Insertion of 1 wt% of either SiO_2 or MMT neither increased the intensity of S-H peak nor led to formation of C=C peak (Figure 3). This could be interpreted as crosslinking density was not affected by the reinforcements. The peaks of Polymer_SiO are identical with the pristine polymer while two additional peaks (462 and 522 cm^{-1}) were observed for Polymer_MMT (Figure 3, Figure 4). This reveals that there is no considerable chemical interaction of polymer chains with unmodified-SiO_2 surface. On the contrary, interaction exists between MMT and the matrix indicating that organically-modified MMT surface is compatible with the polymer chains. This is also further confirmed by the XRD Analysis.

Figure 2 reveals XRD outcomes showing that addition of 5 wt% MMT in the polymer matrix (Polymer_MMT_2) resulted in two peaks. Since there were no visible peaks in the XRD pattern of the polymer (because of its amorphous structure), it can be said that these two peaks are directly due to MMT addition. The first sharp peak at $2\theta = 2.510°$ coincides to the interlayer spacing (d-spacing) of 3.517 nm. The calculated value of initial interlayer spacing of MMT is 2.658 nm. Looking at this result, increase of inter-gallery distance to 3.517 nm from 2.658 nm reveals that silicate layers are firmly intercalated by the molecular chains of the polymer. The second peak that occurred at $2\theta = 4.935°$ can be due to the second-order reflection since the calculations with the Bragg's Law indicates an interlayer spacing of 3.577 nm. Moreover, decreasing MMT loading to 1 wt% (Polymer_MMT) diminished all visible XRD Peaks which could be either interpreted as exfoliated microstructure was achieved with this particular composition or this could be resulted from decreased intensity. Nevertheless, this particular composition should have at least intercalated morphology with possible exfoliation as the FTIR (Figure 4) characterization reveals chemical interaction between nanocomposite constituents. It is also well-known from the literature that as the nanoclay concentration decreases, intercalation/exfoliation level increases. Because of these revelations, only Polymer_MMT was exposed to further mechanical test owing to its suggested better dispersion than Polymer_MMT_2.

Additionally, when equal amounts of MMT and SiO_2 (either 1 wt% or 0.5 wt%) were added together, similar to Polymer_MMT, sharp XRD peaks were not observed in their corresponding curves (Figure 2) suggesting that high dispersion quality was preserved.

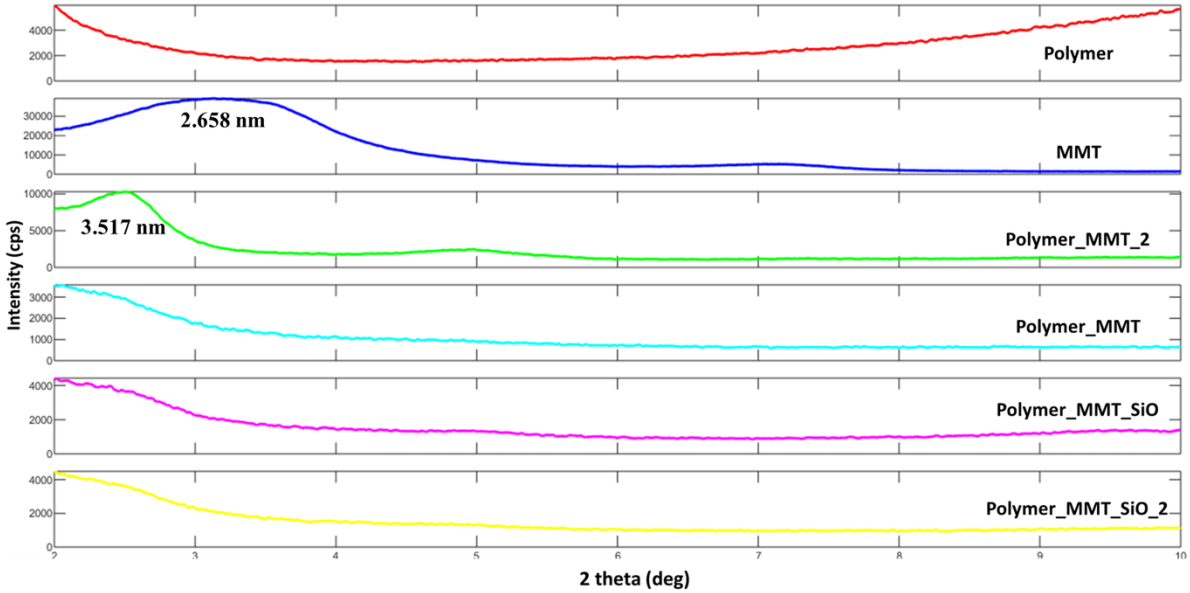

Figure 2. XRD outcomes of the polymer and composites are shown.

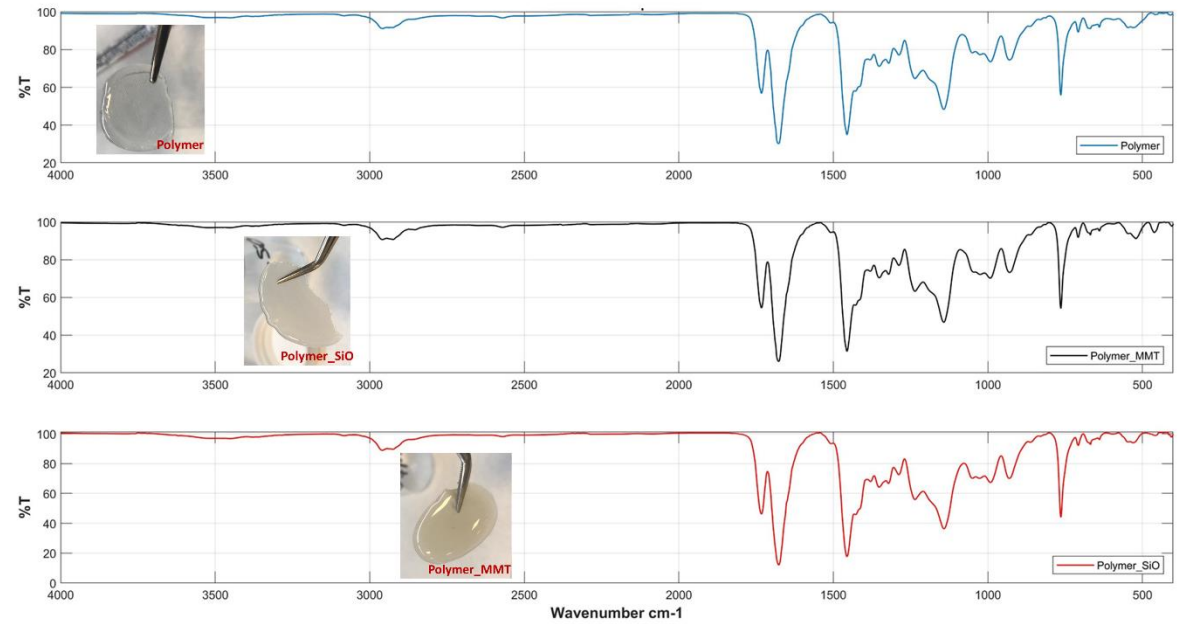

Figure 3. FTIR spectra of the polymer and composites.

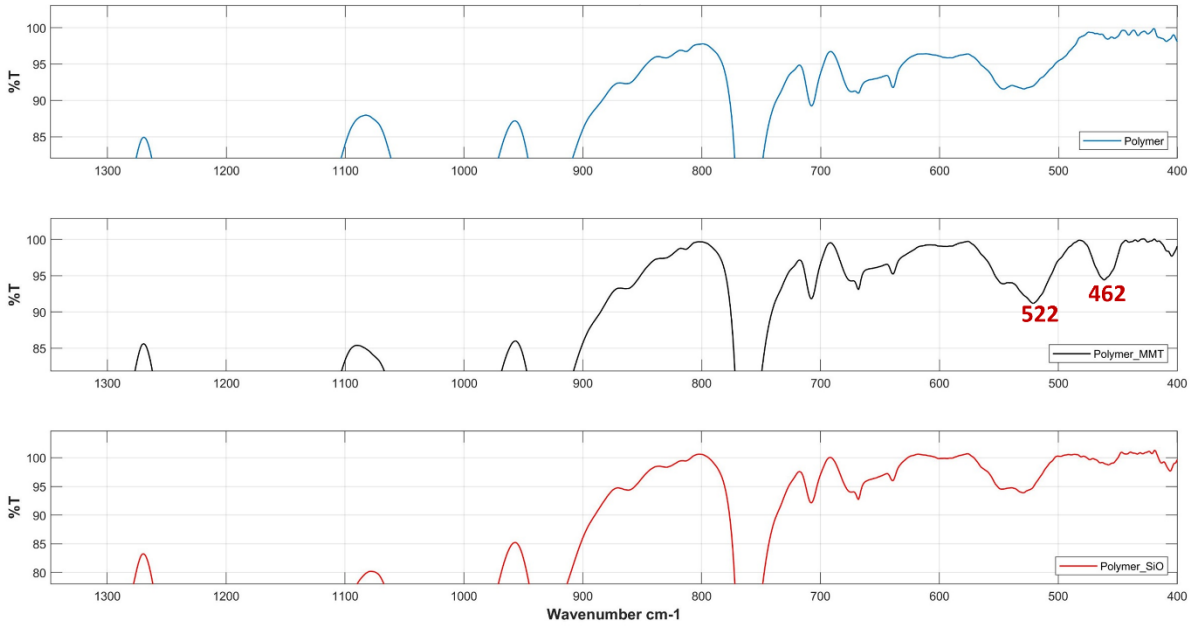

Figure 4. FTIR spectra concentrated on 400-1350 cm^{-1}.

4.2. Mechanical Properties

Micro-indentation test (Table 2, Figure 5) results reveal that the pristine polymer without any reinforcing agent has higher hardness (169.6 MPa) and elastic modulus (6.8 GPa) in comparison with its tensile test outcomes (tensile strength: 20 MPa, tensile modulus: 1 GPa; which are taken from the data sheet [13]). It should be noted that the results were obtained from a 'compressive test'. Generally, for most materials, hardness is 3-4 times higher than the tensile strength. Nevertheless, the results of this study indicate more than 8-fold overshoot of the strength. This could be attributed to the 'chain confinement effect' leading to chain entanglement in nm-scale.

It is seen that both polymer and composites are prone to creep throughout indentation because of their viscoelastic nature. Creep is basically increase in indentation depth right away after unloading, even though the applied force is diminishing, [14]. Creep might result in a 'nose effect' on unloading curve which disturbs elastic modulus measurement [14– 18]. It is suggested [17] to hold on at maximum load for a time period to reduce the creep effect, which was also conducted in this study, by holding all samples for 30 seconds to release viscoelasticity effect (Figure 5 a).

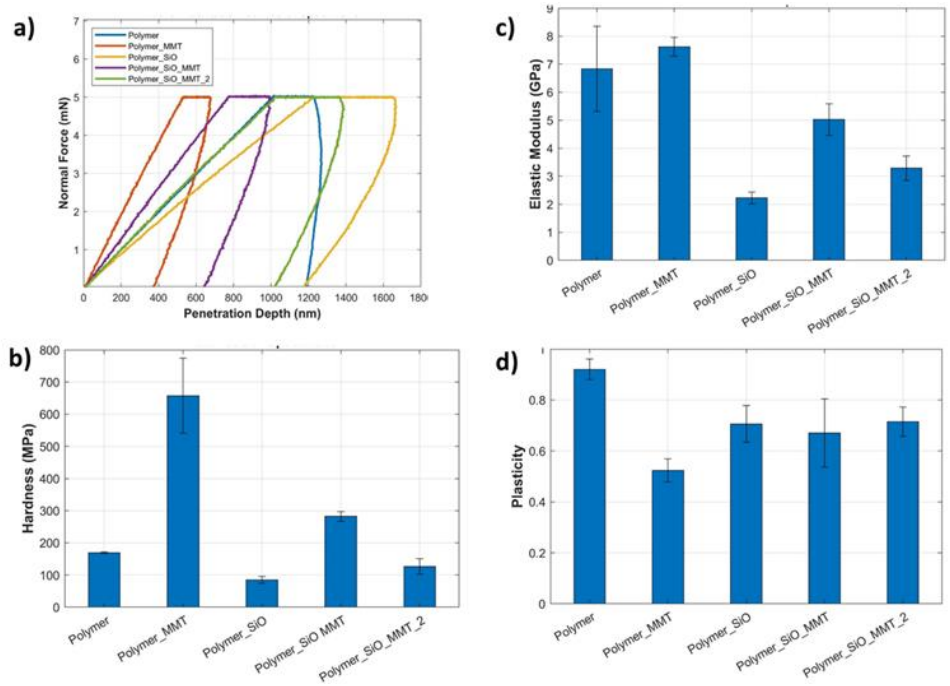

Figure 5. The results of micro-indentation test is shown; a) Representative Penetration Depth-Normal Force curves; b, c, and d represent Elastic Modulus, Hardness and Plasticity values of the specimens.

The plasticity was calculated by the ratio of the plastic work to the total work of force-indentation depth curves which is represented in Figure 6. The ratio of area under unloading curve to the area under loading curve indicates elastic part of work as it is suggested in the previous studies [19– 22] (Equation 3). The calculation was accomplished by numerical integration (multi-step trapezoidal method) and the creep segment of the curves were neglected.

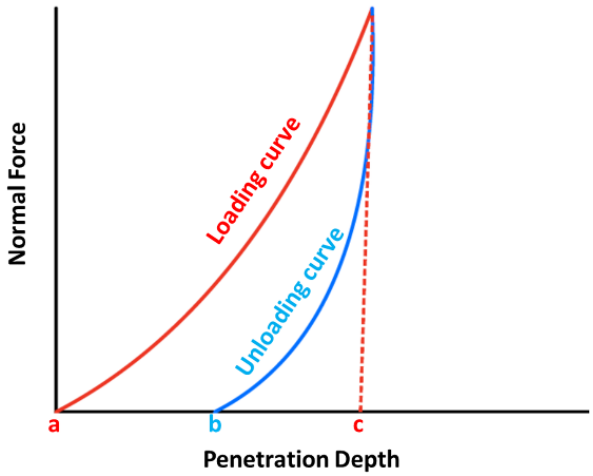

Figure 6. Plasticity was calculated by the ratio of area between the points of (a-b) to the area under loading curve (a-c).

$$Plasticity = \left[1 - \frac{Area\ under\ unloading\ curve}{Area\ under\ loading\ curve}\right] \quad (3)$$

It is seen that the polymer has rather high plasticity (90%) which means that the deformation is mostly unrecoverable when the polymer is unloaded which might be due to the highly cross-linked nature of the polymer. Being a glassy polymer the matrix of this study; NOA 61 is capable of plastic deformations explained by the recent studies. The broadly accepted mechanism consists of two steps [23]. Firstly, 'plasticity carrier polymer chains' are nucleated by the action of the applied load. Secondly, these nucleated plasticity carriers arrange themselves into local ordered-molecular structures which eventually form the macro scaled-plasticity carriers. This phenomenon is analogous to plastic deformation (such as by dislocations) in crystalline solids.

Insertion of 1 wt% MMT (Polymer_MMT) drastically improved the hardness by 288% (Table 2, Figure 5). In fact, the highest improvement in hardness was achieved by this particular nanocomposite. This points out efficient stress transfer from the matrix to reinforcement thanks to both high surface area of MMT and the compatibility between polymer matrix and organic modification of MMT. This is confirmed by both the intercalated/exfoliated silicate layers observed in XRD (Figure 2) and peaks of chemical attractions indicated by FTIR (Figure 4, 5). Elastic modulus of this particular nanocomposite is found to be similar to pristine polymer. Nevertheless, plasticity of the matrix was drastically reduced by 43%. This would occur because the movement of trapped polymer chains between silicate layers might be inhibited. Since this movement could be necessary to form 'local ordered-molecular structures' analogous to dislocations in metals, the blocked movement would reduce the percentage of plastic deformation.

Table 2. The results of the micro-indentation test

	Polymer	**Polymer_MMT**	**Polymer_SiO**	**Polymer_SiO_ MMT**	**Polymer_SiO_M MT_2**
Hardness (MPa)	169.608±2.190	657.394±116.394	84.618±11.015	282.166±15.00	126.906±23.705
Elastic Modulus (GPa)	6.834±1.314	7.613±0.337	2.225±0.213	5.022±0.567	3.288±0.432
Plasticity	0.918±0.035	0.524±0.072	0.706±0.045	0.671±0.134	0.715±0.057

Addition of 1 wt% SiO_2 led to decrease of both hardness and elastic modulus by 51% and 61%, respectively. There should be two reasons for that; firstly, the surface of unmodified-SiO_2 may not be compatible with the polymer matrix as there is no indicative peaks on FTIR curves (Figure 3, 4). Secondly, being a micro-scaled reinforcement, the total surface area of this particular reinforcement is not enough for efficient load transfer. It is well known that concentration of the micro-scaled particles should be optimum for efficient load transfer without leading to agglomeration. It is seen that SiO_2 particles rather act as stress concentration cites diminishing both strength and modulus. However, the plasticity reduction by SiO_2 additive is 21% lower than the reduction observed in Polymer_MMT. It is revealed that in polymer matrix, the surface compatibility of MMT is higher than SiO_2 which is confirmed by both FTIR and XRD (Figure 2, 4). Therefore, due to the loose bond between SiO_2 and the matrix, arrangement of polymer chains into plasticity carriers could become easier.

There seems to be no synergism for hardness and modulus when equal amounts of MMT and SiO_2 added together. The properties falls between the values obtained by the single addition of either MMT or SiO_2 such that simultaneous addition of SiO_2 and MMT changed hardness by -25% and +66% for the composites of Polymer_SiO_MMT_2 and Polymer_SiO_MMT, respectively. This might point out that neither SiO_2 contribution disturb intercalated/exfoliated-MMT structure, nor by simultaneous MMT reinforcement, quality of SiO_2 dispersion is affected. This suggestion is also supported by the preserved exfoliated nature of XRD curves for the SiO_2/MMT mixtures (Figure 2).

It should be noted that one benefit of these SiO_2/MMT combinations over single MMT reinforcement could be related to plasticity since they result in less plasticity reduction (-22% and -27% for Polymer_SiO_MMT_2 and Polymer_SiO_MMT, respectively). In addition to it, their contribution to hardness is higher than bare SiO_2 addition (Table 1). In the study of Fox-Rabinovich et al. [24], plasticity is proved to be contributed to wear resistance of inorganic coatings. This could also be applied to our study as the abrasive wear resistance of organic coatings could be calculated from hardness to elastic modulus ratio. This ratio, according to Fox-Rabinovich et al [24], is analogous to inverse of ratio of elastic work to total work of deformation which is proportional to the plasticity (Equation 4). Therefore, for the applications necessitating wear resistance, Polymer_SiO_MMT could be considered since this particular composite increases hardness of polymer by 66% with relatively small plasticity reduction (-27%).

$$Wear\ Resistance \approx \left[\frac{Area\ under\ unloading\ curve}{Area\ under\ loading\ curve}\right]^{-1} \tag{4}$$

5. CONCLUSION

The outcomes of this study reveal that, on the one hand, 1 wt% addition of MMT resulted in the highest hardness improvement (288%). This behavior is attributed to the intercalated/ exfoliated silicate layers which is confirmed by XRD. The particular peaks in FTIR spectrum also showed the compatibility of surface modification of MMT with the polymer. On the other hand, 1 wt% addition of SiO_2 diminished both the hardness and elastic modulus of the matrix, pointing out the inefficient load transfer from the matrix to the additive. The diminished mechanical properties stem from incompatibility between the surface of the composite constituents and the relatively lower surface area of micro-scaled SiO_2.

In the case of crosslinking density, FTIR spectra show that the addition of either additive leads to the same characteristic peaks of the polymer matrix, which could be interpreted as crosslinking density and adhesion quality were not affected.

Reinforcement by 1 wt% MMT and 1 wt% SiO_2 leads to lower hardness improvement (66%) than bare 1 wt% MMT addition (288%). Nevertheless, this combination resulted in 18% more plasticity than 1 wt% MMT, which could benefit wear resistance.

ACKNOWLEDGEMENTS

This study is funded by TED University Institutional Research Fund under grant number T-18-B2010-33018.

CONFLICT OF INTEREST

The authors stated that there are no conflicts of interest regarding the publication of this article.

REFERENCES

[1] Ahmad KZK, Ahmad SH, Tarawneh MA & Apte PR. Evaluation of Mechanical Properties of Epoxy / Nanoclay / Multi-Walled Carbon Nanotube Nanocomposites using Taguchi Method, 2012; 4: 80–86.

[2] Ahmad T & Mamat O. Studying the Effects of Adding Silica Sand Nanoparticles on Epoxy Based Composites. J Nanoparticle 2013.

[3] Alsagayar ZS, Rahmat AR, Arsad A & Mus SNHB. Tensile and Flexural Properties of Montmorillonite Nanoclay Reinforced Tensile and Flexural Properties of Montmorillonite Nanoclay Reinforced Epoxy Resin Composites. Adv Mat Res 2015; 1112: 373–376.

[4] Briscoe, BJ., Fiori, L, & Pelillo. Nano-indentation of polymeric surfaces. J Phys D Appl Phys, 1998; 31(19): 2395–2405.

[5] Donmez F, Kandemir AC & Kaplan CH. Biocompatible nanocomposite production via nanoclays with diverse morphology. Int J Polym Anal Charact 2022; 27 (13): 158-179.

[6] Bufford D, Liu Y, Wang J, Wang H & Zhang X. In situ nanoindentation study on plasticity and work hardening in aluminium with incoherent twin boundaries. Nat Commun 2014; 5.

[7] Castriota M, Fasanella A, Cazzanelli E, De Sio L, Caputo R & Umeton C. In situ polarized micro-Raman investigation of periodic structures realized in liquid-crystalline composite materials. Optics Express 2011; 19(11):10494.

[8] De Menezes LR & Da Silva EO. The use of montmorillonite clays as reinforcing fillers for dental adhesives. Mater Res 2016; 19(1): 236–242.

[9] Díez-Pascual AM, Gómez-Fatou, MA, Ania F & Flores A. Nanoindentation in polymer nanocomposites. Prog Mater Sci 2015; 67:1-95.

[10] Encalada-Alayola JJ, Veranes-Pantoja Y, Uribe-Calderón JA, Cauich-Rodríguez JV & Cervantes-Uc JM. Effect of type and concentration of nanoclay on the mechanical and physicochemical properties of bis-GMA/TTEGDMA dental resins. Polym 2020; 12(3)

[11] Fox-Rabinovich GS, Veldhuis SC, Scvortsov VN, Shuster LS, Dosbaeva GK & Migranov MS. Elastic and plastic work of indentation as a characteristic of wear behavior for cutting tools with nitride PVD coatings. Thin Solid Films 2004; 469(2): 505–512.

[12] Gerberich WW, Stauffer DD, Beaber AR & Mook WM. Connectivity between plasticity and brittle fracture: An overview from nanoindentation studies. Proceedings of the Institution of Mechanical Engineers, Part N: Journal of Nanoengineering and Nanosystems, 2007; 221(4): 139–156.

[13] Kandemir, AC, Erdem D, Ma H, Reiser A & Spolenak R. Polymer nanocomposite patterning by dip-pen nanolithography. Nanotechnology 2016; 27 (13):135303

[14] Kandemir AC, Ramakrishna SN, Erdem D, Courty D, & Spolenak R. Gradient nanocomposite printing by dip pen nanolithography. Comp Sci Tech 2017; 138: 186–200.

[15] Lam CK, Lau KT & Zhou LM. Nano-mechanical Creep Properties of Nanoclay / Epoxy Composite by Nanoindentation. Adv Comp Mater Struct 2007; 335: 669–672.

[16] Li Y, Li C, He J, Gao Y, & Hu Z. Effect of functionalized nano-SiO2 addition on bond behavior of adhesively bonded CFRP-steel double-lap joint. Constr Build Mater 2020; 244:118400

[17] Ma Z, Jiang D, Cui Y & Liu Y. The Development of Nanoclay-Epoxy Composite for Application in Ballistic Protection , SAE Technical Papers, 2018

[18] Meng Q, Wang CH, Saber N, Kuan H, Dai J, Friedrich K & Ma J. Nanosilica-toughened polymer adhesives. Mater Des, 2014; 61: 75–86.

[19] Milman YV, Chugunova SI & Goncharova IV. Plasticity determined by indentation and theoretical plasticity of materials. Bulletin of the Russian Academy of Sciences: Physics, 2009; 73(9):1215–1221.

[20] Milman YV, Chugunova SI, Goncharov IV & Golubenko AA. Plasticity of materials determined by the indentation method. Prog Phys Metals 2008; 19(3): 271-308

[21] Nai MH, Lim CT, Zeng KY & Tan VBC. Nanoindentation study of polymer based nanocomposites. J Metastable Nanocryst Mater 2005; 23: 363–366

[22] Norland Products Incorporated. (1966). Norland Optical Adhesives 61 Datasheet.

[23] Oleinik EF, Mazo MA, Strel'nikov IA, Rudnev SN & Salamatina OB. Plasticity Mechanism for Glassy Polymers: Computer Simulation Picture. Polym Sci - Series A. 2018; 60(1): 1-49

[24] Yasin S, Shakeel A, Iqbal T, Ahmad F, Mehmood H, Luckham PF & Ullah N. Effect of experimental conditions on nano-indentation response of low density polyethylene (LDPE). J Macromol Sci 2019; 56(7), 640–647.

[25] Oliver WC & Pharr GM. An Improved Technique for Determining Hardness and Elastic Modulus Using Load and Displacement Sensing Indentation Experiments. J Mater Res 1992; 7(6): 1564–1583.

[26] Oliver WC and Pharr GM. Measurement of Hardness and Elastic Modulus by Instrumented Indentation: Advances in Understanding and Refinements to Methodology. J Mater Res 2004; 19(01): 3–20.

ESKİŞEHİR TECHNICAL UNIVERSITY JOURNAL OF SCIENCE AND TECHNOLOGY
A- APPLIED SCIENCES AND ENGINEERING

2022, 23(4), pp. 244-255, DOI:10.18038/estubtda.1054195

APPLICATION OF HOOKE'S LAW TO ANGLE PLY LAMINA

Cagatay YILMAZ[1,*], Hafiz Qasim ALI [2], Mehmet YILDIZ [3]

[1*] Mechanical Engineering, Faculty of Engineering, Abdullah Gul University, Kayseri, Turkey
[2] Material Science and Nanoengineering, Faculty of Engineering and Natural Sciences, Sabancı University, Istanbul, Turkey
[3] Material Science and Nanoengineering, Faculty of Engineering and Natural Sciences, Sabancı University, Istanbul, Turkey

ABSTRACT

Aerospace-grade carbon fiber reinforced polymer composite plates with four different fiber orientations 0º, 30º, 45ºand 60º is produced with the autoclave curing method and subjected to tensile testing. The stress-strain curves of the composite specimens are compared with Hooke's law. It is observed that Hooke's law coincides precisely with the experimental results for samples containing fibers parallel to the loading direction. However, it does not coincide with samples where the fibers make a certain angle with the applied load direction. Moreover, it is reported that Hooke's law converges the experimental results for small strain values but diverges significantly from the experimental results at higher strain values.

Keywords: Hooke's law, Composite lamina, Tensile test, Angle ply lamina

1. INTRODUCTION

Laminated composites gained attention in major industries such as aerospace, defense, and automotive due to their versatile design, flexible manufacturing methods, and high strength-to-weight ratio. The usage of laminated composite makes the structure of the vehicle lighter and provides a longer range with the same amount of fuel. In order to use the laminated composite structure reliably within these industries, their modeling should be well understood and analyzed. If their modeling is well understood and precisely fits with the experimental finding, the need for mechanical characterization in the component development stage can be eliminated. The elimination of the mechanical characterization for laminated composite helps engineers to shorten component development time, thus reducing the costs.

Several experimental studies have been conducted to understand the experimental behavior of laminated composites [1–10], and finite element analyses are performed to simulate the behavior of laminated composites under certain loading conditions [11–13]. In addition to pure experimental or numerical studies, several studies present the correlation and validation to understand better the mechanical performance and failure behavior of the laminated composites[14–18].

A laminated composite can be modeled from two perspectives: micromechanics and macro mechanics. As per the micromechanics of a composite, a laminate consists of fiber and matrix. If the mechanical properties of fiber and matrix are known, then the whole laminate can be modeled by using these properties. In macro mechanics, a laminate is constructed from different laminae where each lamina can have a different fiber orientation. This difference in the orientation of fibers affects the mechanical properties of the laminate. The mechanical properties of laminate can be predicted by applying Hook's law to Classical Lamination Theory (CLT). CLT assumes that a laminate consists of different laminae and considers the angle of each lamina. It can be seen in the open literature that there are several studies that both use Hooke's law and CLT [19–22]. Since a laminate consists of several laminae, the application of Hooke's law should be well analyzed, validated, and understood in the lamina order.

*Corresponding Author: yilmaz.cagatay@agu.edu.tr
Received: 06.01.2022 Published: 29.12.2022

Hooke's law can be applied to lamina from a macro-mechanic perspective to explain the effect of varying fiber angles on stiffness in many textbooks [23–25]. These textbooks explain the application of Hooke's law for unidirectional and angle ply lamina and relate stress with strain. However, when the literature is investigated, it is seen that there is a lack of validation of Hooke's law with experimental data for angle ply composite lamina.

This research is an effort to fill the gap for a better understanding of whether Hook's law is confidently applicable for angle ply lamina or not. For that purpose, four different directions of carbon fiber reinforced polymeric lamina are produced through the autoclave curing method and then tested under tensile loading up to the failure point to acquire stress-strain data, which is then compared with Hooke's law.

2. MATERIALS AND METHODS

2.1. Materials and Sample Preparation

Carbon fiber prepreg, with a trading name of AX-6201XL-C, is obtained from Kordsa. The prepreg consists of unidirectional fibers with an aerial fiber weight of 300 gsm. Before laying up, the carbon fiber prepreg is cut with a dimension of 300x300 mm by using ZÜND G3-L3200 Digital Ply Cutter with desired fiber orientations. Four different composite plates are manufactured by an autoclave curing method. First, prepreg stacks are placed on a pre-treated steel plate with Axel Xtend 838 mold release agent. Two thermocouples (TC1 and TC 2) are attached to two different prepreg stacks with a heat-resistant tape called Flash Breaker. These thermocouples are used to monitor the temperature of prepreg stacks during autoclave curing. Prepreg stacks are covered with Airtech WL5200 release film, Airtech N10 breather fabric, and Airtech WL 7400 vacuum bag. The vacuum bag is sealed with Airtech AT 200Y sticky tape. Here, breather fabric is used for air evacuation inside the bagging, and release film prevents the sticking of breather fabric to prepreg stacks. Once the prepreg stacks are bagged, the vacuum leak test is performed for two minutes. At the end of the vacuum leak test, no vacuum leak is observed. Once every necessary step is completed for a secure autoclave run, a recipe is created in the autoclave software based on the prepreg manufacturer's recommendations. The autoclave is pressured with Nitrogen gas. The curing process parameters of four different prepreg stacks are depicted in Figure 1. Autoclave gage pressure (Pressure), autoclave temperature (AirTC), and part temperatures (TC1 and TC2) can be seen in Figure 1 (a), and the vacuum gage pressure inside the bag can be seen in Figure 1 (b).

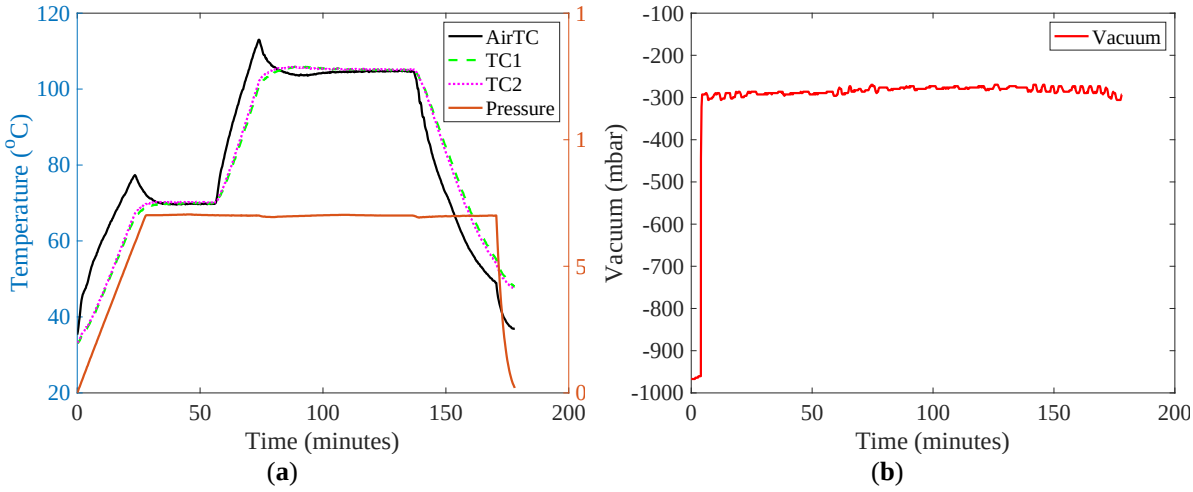

Figure 1. Curing condition for prepreg stack (a) Air temperature (AirTC), thermocouples attached to prepreg stacks (TC1 and TC2) and gauge pressure in the autoclave (Pressure), (b) gage vacuum inside the bagging

Once the autoclave cycle is completed, composite plates are carefully removed from the bagging materials. In order to prevent the composite plates from mixing with each other, the plates are immediately marked with their codes and fiber directions after they are cleared of the bag materials

A visual inspection is performed to check for any production imperfections. It is observed that composite plates are produced of good quality. The produced composite plates are then taken into dimensional quality inspection in order to check the homogeneity of thickness over the plates. It is seen that each composite plate has a homogeneous thickness of 1.2 mm. Once the quality of the composite plates is assured, they are sent to the tabbing station. The stacking sequence of composite plates and their codes along with their measured strength are given in Table 1.

Table 1. The configuration of plates and their code

Configuration	Code	Strength (MPa)
$[0]_4$	CY0	2112
$[30]_4$	CY30	70
$[45]_4$	CY45	58.6
$[60]_4$	CY60	41

The produced plates are tabbed with glass fiber reinforced polymer tabbing material for the tensile test. Glass fiber tabs are adhered to the produced test plate with 3M AF 163-2k adhesive film. The curing of the adhesive film is performed in a vacuum oven, and it is described in a previous publication [26]. First, the extraction of test coupons from the composite plates is attempted with the Poysan 3-axis router, and it is successful for the CY0, CY45, and CY60. However, it is seen that the CY30 test plate is so brittle that it is impossible to cut tensile test coupons with the router. Therefore, tensile test coupons from the CY30 plate are cut with a water jet (KUKA KR16 equipped with KMT Neoline 40i OEM water pressurizing system 3000 bar speed 250 mm/min). The tabbed tensile test coupons extracted from CY60 and CY0 test plates can be seen in Figure 2 (a &b), respectively. The dimensions of all test coupons are chosen per the ASTM D3039 standard and can be seen in Table 3.

2.2. Mechanical Testing

All mechanical tests are performed with a Universal Test Machine (UTM) (Instron 8803) equipped with a load cell of ±250 kN under the crosshead displacement of 2 mm/min. Axial strain data is recorded with a video extensometer (AVE 2.0), and transversal strain data is recorded with a mechanical extensometer (Epsilon 3542).

In order to analyze the reliability of Hooke's law for angle-ply lamina, material constants of the unidirectional lamina, namely, elastic modulus in the direction of fiber (E_{11}), elastic modulus in the perpendicular direction to fiber (E_{22}), the major Poisson's ratio, and in-plane shear modulus are needed. Among these material constants of the unidirectional lamina, E_{11}, E_{22}, and υ_{12}, are measured by applying the principles of ASTM D 3039 Standard Test Method for Tensile Properties of Polymer Matrix Composite Materials [27] and G_{12} is measured by following the ASTM D 3518 Standard Test Method for In-Plane Shear Response of Polymer Matrix Composite Materials by Tensile Test of a ±45° Laminate [28] standards. The material constant measured by following these standards is given in Table 2.

Table 2. Material constants of unidirectional lamina

Material constant	Value	Standard
E_{11}	128 GPa	ASTM D 3039
E_{22}	17.7 GPa	ASTM D 3039
υ_{12}	0.289	ASTM D 3039
G_{12}	14.4 GPa	ASTM D 3518

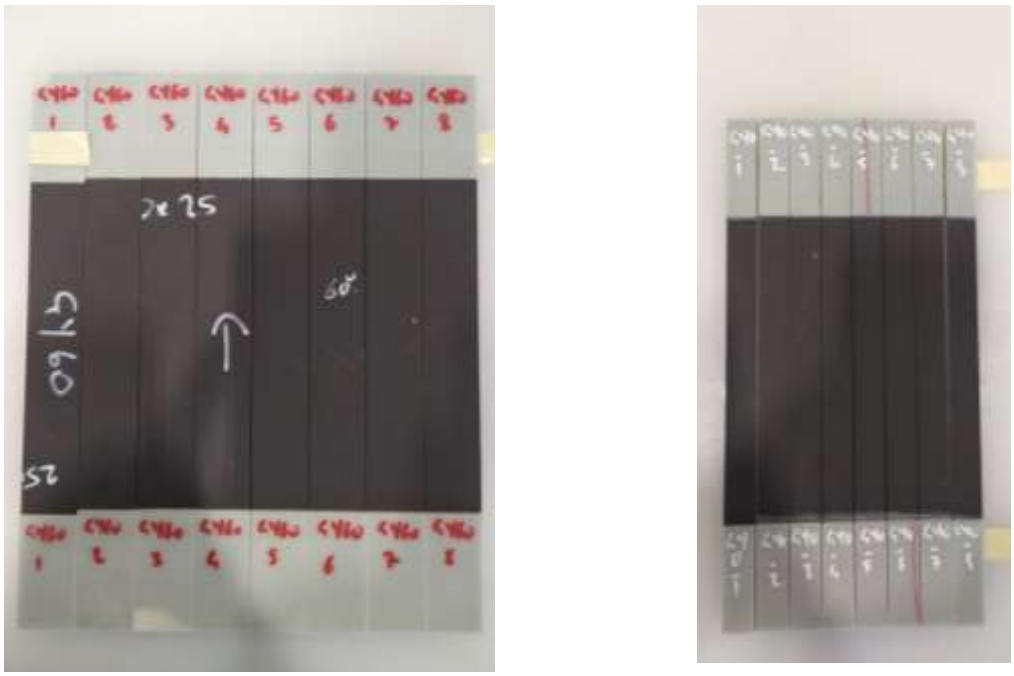

(a) (b)

Figure 2. Tensile test coupons ready to test, (a) CY60 coupons, (b) CY0 coupons

Table 3. Dimensions of coupons

Code	Gage length (mm)	Tab length (mm)	Width (mm)	Overall length (mm)
CY0	138	56	15	250
CY30	150	50	25	250
CY45	150	50	25	250
CY60	150	50	25	250

2.3. Hooke's Law

A plane stress assumption can be made if a thin plate experiences only in-plane loads. A thin plate has a relatively small thickness compared to its width and length. Therefore, a composite lamina can be treated as a thin plate. Under a plane stress assumption, three stress terms, σ_3, σ_{31}, σ_{23} are zero and the 3D stress-strain equation can be reduced to a 2D stress-strain equation. This two-dimensional stress-strain relation can be expressed with Equation (1)

$$\begin{bmatrix}\sigma_1\\ \sigma_2\\ \tau_{12}\end{bmatrix}=\begin{bmatrix}Q_{11} & Q_{12} & 0\\ Q_{12} & Q_{22} & 0\\ 0 & 0 & Q_{66}\end{bmatrix}\begin{bmatrix}\varepsilon_1\\ \varepsilon_2\\ \gamma_{12}\end{bmatrix} \quad (1)$$

In Equation (1), the direction of fibers is assumed as direction 1, while the direction perpendicular to fibers is referred to as direction 2.

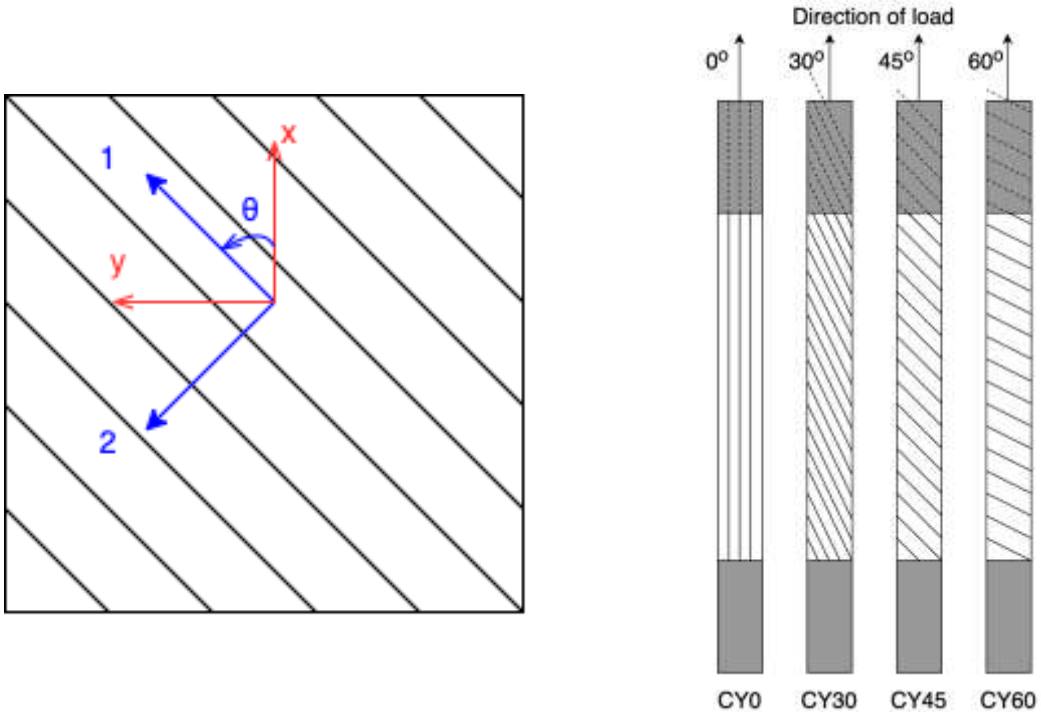

(a) (b)

Figure 3. (a) Global axes and material axes, (b) alignment of fiber for four different sets of the test sample

In an angled lamina, the stresses are applied at a certain angle with respect to the fiber direction. For angle ply lamina, stress is applied in accordance with the global coordinate system. The direction of load is referred to as the X-axis and the direction perpendicular to the load is referred to as the Y-axis.. (Figure 3 (a)). The angle between material and global axes is denoted by θ and is chosen as positive as the fiber turns out in a counterclockwise direction. The direction of fibers for four different sets of samples can be seen in Figure 3 (b). When stress is applied in global axes, the relation between stress and strain is given by Equation (2).

$$\begin{bmatrix}\sigma_x\\ \sigma_y\\ \tau_{xy}\end{bmatrix}=\begin{bmatrix}\bar{Q}_{11} & \bar{Q}_{12} & \bar{Q}_{16}\\ \bar{Q}_{12} & \bar{Q}_{22} & \bar{Q}_{26}\\ \bar{Q}_{16} & \bar{Q}_{26} & \bar{Q}_{66}\end{bmatrix}\begin{bmatrix}\varepsilon_x\\ \varepsilon_y\\ \gamma_x\end{bmatrix} \tag{2}$$

Here $[\bar{Q}\,]$are the transformed, reduced stiffness matrix and each element of $[\bar{Q}\,]$ can be calculated by Equation (3)

$$\begin{aligned}
\bar{Q}_{11} &= Q_{11}c^4 + Q_{22}s^4 + 2(Q_{12}+2Q_{66})s^2c^2,\\
\bar{Q}_{12} &= (Q_{11}+Q_{22}-4Q_{66})s^2c^2 + Q_{12}(s^4+c^4),\\
\bar{Q}_{22} &= Q_{11}s^4 + Q_{22}c^4 + 2(Q_{12}+2Q_{66})s^2c^2,\\
\bar{Q}_{16} &= (Q_{11}-Q_{12}-2Q_{66})c^3s - (Q_{22}-Q_{12}-2Q_{66})s^3c,\\
\bar{Q}_{26} &= (Q_{11}-Q_{12}-2Q_{66})cs^3 - (Q_{22}-Q_{12}-2Q_{66})s^3c,\\
\bar{Q}_{66} &= (Q_{11}+Q_{22}-2Q_{22})s^2c^2 + Q_{66}(s^4+c^4),
\end{aligned} \tag{3}$$

Here it can be seen that each element of the transformed, reduced stiffness matrix is related to four stiffness elements ($Q_{11}, Q_{12}, Q_{22}, Q_{66}$) and the constants $c = \cos\theta \ and \ s = \sin\theta$. The four stiffness elements are functions of four engineering constants ($E_1, E_2, \upsilon_{12}, \upsilon_{21}$) and can be seen in Equation (4).

$$Q_{11} = \frac{E_1}{1-\upsilon_{21}\upsilon_{12}},$$
$$Q_{12} = \frac{\upsilon_{12}E_2}{1-\upsilon_{21}\upsilon_{12}},$$
$$Q_{22} = \frac{E_2}{1-\upsilon_{21}\upsilon_{12}}, \quad (4)$$
$$Q_{66} = G_{12},$$

3. RESULTS

In order to see the response of Hooke's law on a lamina, first, CY0 samples are tested and analyzed with Hooke's law. Since CY0 samples are only composed of fibers parallel to the applied load, Hooke's law and experimental results are expected to converge to each other better when compared to angle ply lamina. Indeed, the results obtained to confirm this assumption. The experimental stress-strain curves and the response of Hooke's law for CY0 samples can be seen in Figure 4.

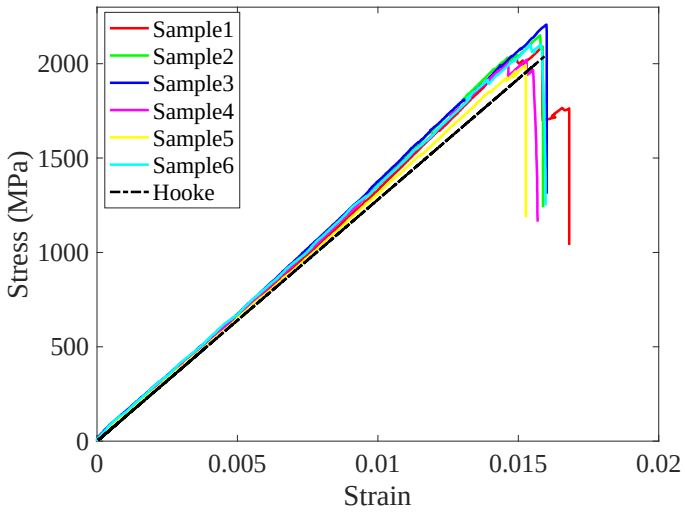

Figure 4. Experimental and Hooke's law stress-strain curve for CY0 samples.

Once it is confirmed that Hooke's law converges for the lamina with fibers aligned only in a direction parallel to load, Hooke's law is applied to the angle-ply laminate. The first angle ply lamina that the appropriate response of Hookes' law is examined to experimental results is the CY30. Although six different coupons are prepared for the test of CY30, only two of them are being tested successfully. The underlying reason behind this problem is the brittleness of CY30 samples. As mentioned in the "Materials and Sample Preparation section," the CY30 samples are so brittle that the extraction of samples is being done with a water jet. That brittleness also does not allow to conduct of tensile tests successfully. The stress-strain curves produced with Hooke's law and experiment can be seen in Figure 5 for CY30. Although Hooke's law produces results that agree with the experiment for CY0, the

situation is entirely different for CY30 samples. Hooke's law produces relatively close results with the experiment for small strain values while significantly deviating from experimental results for the high strain values. These relatively small strain values do not make sense in applying Hooke's law to the angle ply lamina. These small strain values are mostly not applicable, and an angle ply lamina can undergo higher strain values than Hooke's law.

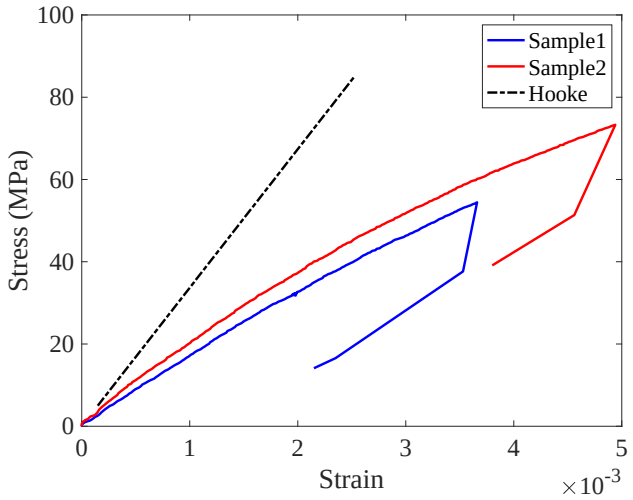

Figure 5. The comparison of stress-strain curves with Hooke's law for CY30 samples

Test coupons with 45 ° fibers, CY45, are tested to see that the error observed in CY30 specimens can be reduced. When the results obtained by Hooke's law and experiments are compared for CY45, it is clearly seen that in Figure 6, Hooke's law does not correlate with the experimental finding. Even though five different specimens are tested experimentally, and all indicate the same stress-strain curve, Hooke's law finding deviates from all the experimental stress-strain curves.

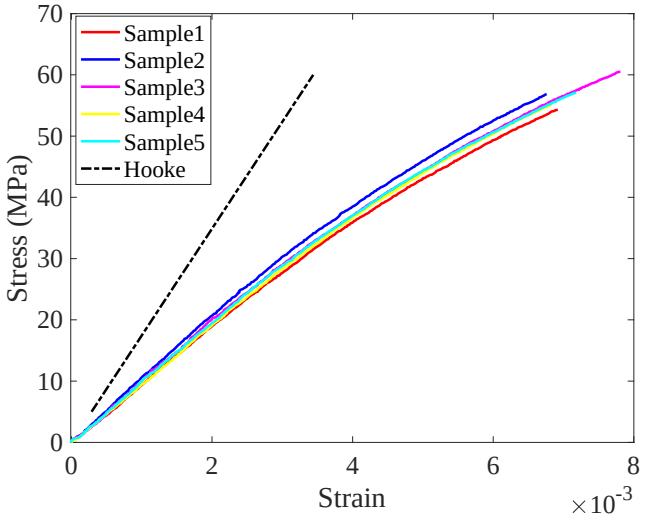

Figure 6. The comparison of stress-strain curves with Hooke's law for CY45

The last attempt is made with CY60 samples to see whether Hooke's law applies to the angle ply lamina. As shown in Figure 7, Hooke's law does not converge the experimental stress-strain curves for CY60

specimens. However, it can be seen from Figure 7 that Hooke's law produces better results for CY60 samples when compared to those of CY30 and CY45.

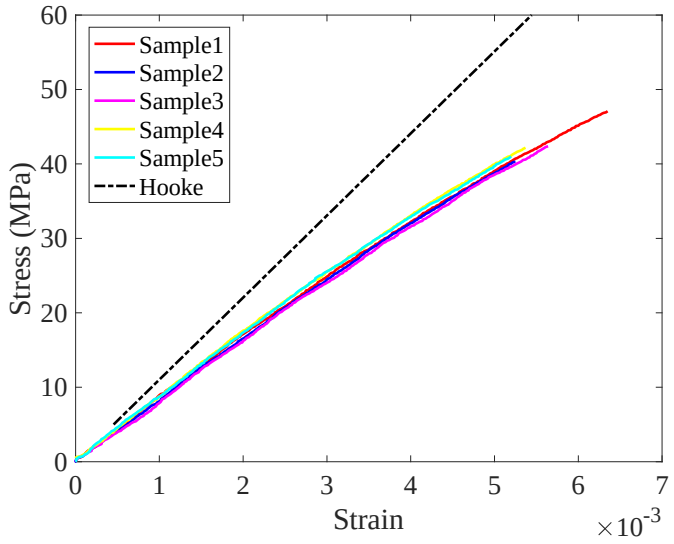

Figure 7. The comparison of stress-strain curves with Hooke's law for CY60

Four types of samples are being tested in this study, and their fracture images are taken and depicted in Figure 8. It can be seen from Figure 8 (a) that samples containing fibers parallel to load failed as if fibers exploded due to extensive splitting, and it is observed that the fibers are fringed. It is not possible to observe a clear fracture plane as can be observed from the other fractured samples. Figure 8 (b), (c), (d) represent the failed specimens from the CY30, CY45, and CY 60 batch, respectively. CY30, CY45, and CY 60 specimens indicate clear fracture planes and fracture angles based on the direction of fibers. It can be seen from Figure 8 (b-d) that as the angle of fibers with respect to load increases, the angle of the fracture plane also increases.

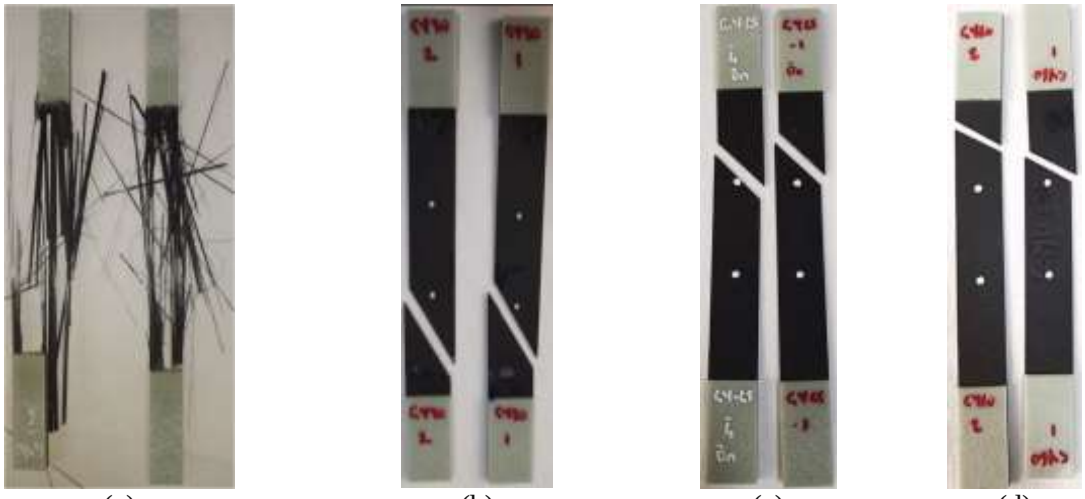

Figure 8. Fractured samples after tensile test; (a) CY0, (b) CY30, (c) CY45, (d) CY60

4. DISCUSSION

Herein, four different aerospace-grade angle ply laminates are produced with an autoclave manufacturing method, tested experimentally in ISO 17025 and AS 9100 certified laboratories, and the application of Hooke's law to the experimental results is analyzed. It is found that the correlation of Hooke's law with experimental results is very well for a laminate composed of only unidirectional fibers. When Hooke's law is applied for an angle ply lamina, there is a significant amount of deviation from the experimental stress-strain curves.

The autoclave used in test plate production is located at Advanced Composite Manufacturing (ACM) laboratory at Sabanci University Integrated Manufacturing Research and Application Center (SU IMC). The vacuum, pressure, and thermocouples found on the autoclave have all the annual calibrations and verifications, and the ACM is an AS 9100-certified laboratory. Technical personnel produces the test plates based on the written order, and all the technicians have the necessary training and at least two years of lamination experience to complete the given jobs accurately.

The Universal Testing Machine (UTM), mechanical and optical extensometers used in the mechanical testing of test coupons are also located Mechanical Testing laboratory at Sabanci University Integrated Manufacturing Research and Application Center (SU IMC). The UTM machine and extensometers also have annual calibration and verification after every six months. The mechanical testing laboratory is ISO 17025 and AS9100 certified. All the technical personnel who contribute to mechanical tests have the necessary training and experience.

Even though all the manufacturing and testing are done by qualified personnel and calibrated equipment in certified laboratories, the significant amount of divergence results produced by Hooke's law compared with the experimental results indicates the insufficiency of the theorem. According to obtained results for angle ply lamina, Hooke's law always overestimates the experimental results. This overestimation behavior of Hooke's law can be attributed to its linear elastic estimation of the relation between stress and strain. For the angle ply lamina, as the stress increases, the linear relationship between the stress and strain diminishes due to increased shear stress. The reason behind the deviation between Hooke's law predicted results and experimental results is the factor of an interface failure, which Hooke's law does not account for in the calculation.

5. CONCLUSION

Herein, the applicability of Hooke's law to the angle-ply laminate is analyzed. First, four different materials constants for unidirectional lamina, namely longitudinal elastic modulus (E_{11}), transverse elastic modulus (E_{22}), in-plane shear modulus (G_{12}), and major Poisson's ratio (υ_{12}) are measured. Then these measured material constants are fed into Hooke's law to investigate the appropriateness of Hooke's law for angle ply lamina. The following conclusions are drawn in this study:

1) The stress-strain curve produced by Hooke's law agrees well with the experimental stress-strain curve for unidirectional lamina.
2) However, the results generated by Hooke's law do not coincide well with the experimental results for angle ply lamina.
3) Hooke's law approaches the experimental stress-strain curve only for relatively small strains.
4) Therefore, the reliability of Hooke's law should be questioned for the angle-ply lamina, and this reliability problem should be considered when Hooke's law is taught in composite material courses at undergraduate and graduate levels.

ACKNOWLEDGMENTS

This work was partially supported by the Sabanci University Integrated Manufacturing Research (SU-IMC) and Application Center.

CONFLICT OF INTEREST

The authors stated that there are no conflicts of interest regarding the publication of this article.

REFERENCES

[1] Yilmaz C, Yildiz M. A study on correlating reduction in Poisson's ratio with transverse crack and delamination through acoustic emission signals. Polym Test 2017;63:47–53. https://doi.org/10.1016/j.polymertesting.2017.08.001.

[2] Yilmaz C, Akalin C, Gunal I, Celik H, Buyuk M, Suleman A, et al. A hybrid damage assessment for E-and S-glass reinforced laminated composite structures under in-plane shear loading. Compos Struct 2018;186:347–54. https://doi.org/10.1016/j.compstruct.2017.12.023.

[3] Yilmaz C, Akalin C, Kocaman ES, Suleman A, Yildiz M. Monitoring Poisson's ratio of glass fiber reinforced composites as damage index using biaxial Fiber Bragg Grating sensors. Polym Test 2016;53:98–107. https://doi.org/https://doi.org/10.1016/j.polymertesting.2016.05.009.

[4] Ali HQ, Emami Tabrizi I, Khan RMA, Tufani A, Yildiz M. Microscopic analysis of failure in woven carbon fabric laminates coupled with digital image correlation and acoustic emission. Compos Struct 2019;230:111515. https://doi.org/https://doi.org/10.1016/j.compstruct.2019.111515.

[5] Munoz V, Valès B, Perrin M, Pastor M-L, Welemane H, Cantarel A, et al. Damage detection in CFRP by coupling acoustic emission and infrared thermography. Compos Part B Eng 2016;85:68–75.

[6] Emami Tabrizi I, Alkhateab B, Seyyed Monfared Zanjani J, Yildiz M. Using digital image correlation for in situ strain and damage monitoring in hybrid fiber laminates under in-plane shear loading. Polym Compos 2021;n/a. https://doi.org/https://doi.org/10.1002/pc.26114.

[7] Saeedifar M, Saleh MN, El-Dessouky HM, Teixeira De Freitas S, Zarouchas D. Damage assessment of NCF, 2D and 3D woven composites under compression after multiple-impact using acoustic emission. Compos Part A Appl Sci Manuf 2020;132:105833. https://doi.org/https://doi.org/10.1016/j.compositesa.2020.105833.

[8] Strungar EM, Yankin AS, Zubova EM, Babushkin A V, Dushko AN. Experimental study of shear properties of 3D woven composite using digital image correlation and acoustic emission. Acta Mech Sin 2019:1–12.

[9] Khan RMA, Tabrizi IE, Ali HQ, Demir E, Yildiz M. Investigation on interlaminar delamination tendency of multidirectional carbon fiber composites. Polym Test 2020;90. https://doi.org/10.1016/j.polymertesting.2020.106653.

[10] Khan RMA, Saeidiharzand S, Emami Tabrizi I, Ali HQ, Yildiz M. A novel hybrid damage

monitoring approach to understand the correlation between size effect and failure behavior of twill CFRP laminates. Compos Struct 2021; 270: 114064. https://doi.org/https://doi.org/10.1016/j.compstruct.2021.114064.

[11] Evran S. Buckling temperature analysis of laminated composite plates with circular and semicircular holes. Eskişehir Tech Univ J Sci Technol A - Appl Sci Eng 2020;21:173–81.

[12] Ubaid J, Kashfuddoja M, Ramji M. Strength prediction and progressive failure analysis of carbon fiber reinforced polymer laminate with multiple interacting holes involving three dimensional finite element analysis and digital image correlation. Int J Damage Mech 2014;23:609–35.

[13] Hara E, Yokozeki T, Hatta H, Ishikawa T, Iwahori Y. Effects of geometry and specimen size on out-of-plane tensile strength of aligned CFRP determined by direct tensile method. Compos Part A Appl Sci Manuf 2010;41:1425–33. https://doi.org/https://doi.org/10.1016/j.compositesa.2010.06.003.

[14] Nicoletto G, Anzelotti G, Riva E. Mesoscopic strain fields in woven composites: experiments vs. finite element modeling. Opt Lasers Eng 2009;47:352–9.

[15] Tabrizi IE, Khan RMA, Massarwa E, Zanjani JSM, Ali HQ, Demir E, et al. Determining tab material for tensile test of CFRP laminates with combined usage of digital image correlation and acoustic emission techniques. Compos Part A Appl Sci Manuf 2019; 127. https://doi.org/10.1016/j.compositesa.2019.105623.

[16] Akın Ataş Oİ. Experımental characterisation and prediction of elastic properties of woven fabric reinforced textile composıte laminates. Eskişehir Tech Univ J Sci Technol A - Appl Sci Eng 2018;19:660–70.

[17] Merve Çobanoğlu Fahrettin Öztürk REE. Thermoforming process parameter optimization of thermoplastic pekk/cf and PPS. Eskişehir Tech Univ J Sci Technol A - Appl Sci Eng 2021;22:51–8.

[18] Massarwa E, Emami Tabrizi I, Yildiz M. Mechanical behavior and failure of glass/carbon fiber hybrid composites: Multiscale computational predictions validated by experiments. Compos Struct 2021;260:113499. https://doi.org/https://doi.org/10.1016/j.compstruct.2020.113499.

[19] Philippidis TP, Theocaris PS. The Transverse Poisson's Ratio in Fiber Reinforced Laminae by Means of a Hybrid Experimental Approach. J Compos Mater 1994;28:252–61. https://doi.org/10.1177/002199839402800304.

[20] Lim T-C. Coefficient of thermal expansion of stacked auxetic and negative thermal expansion laminates. Phys Status Solidi 2011;248:140–7. https://doi.org/https://doi.org/10.1002/pssb.200983970.

[21] Parnas L, Katırcı N. Design of fiber-reinforced composite pressure vessels under various loading conditions. Compos Struct 2002;58:83–95. https://doi.org/https://doi.org/10.1016/S0263-8223(02)00037-5.

[22] Vnučec Z. Analysis of the laminated composite plate under combined loads. 5th Int. Sci. Conf. Prod. Eng., 2005, p. 143–8.

[23] Migliaresi C. Chapter I.2.9 - Composites. In: Ratner BD, Hoffman AS, Schoen FJ, Lemons

JEBT-BS (Third E, editors., Academic Press; 2013, p. 223–41. https://doi.org/https://doi.org/10.1016/B978-0-08-087780-8.00024-3.

[24] Kaw AK. Mechanics of composite materials. CRC press; 2005.

[25] Öchsner A. Macromechanics of a Lamina BT - Foundations of Classical Laminate Theory. In: Öchsner A, editor., Cham: Springer International Publishing; 2021, p. 11–39. https://doi.org/10.1007/978-3-030-82631-4_2.

[26] Ali HQ, Yilmaz Ç, Yildiz M. The effect of different tabbing methods on the damage progression and failure of carbon fiber reinforced composite material under tensile loading. Polym Test 2022:107612. https://doi.org/https://doi.org/10.1016/j.polymertesting.2022.107612.

[27] Standard Test Method for Tensile Properties of Polymer Matrix Composite Materials n.d.

[28] Materials AS for T and. Standard Test Method for In-plane Shear Response of Polymer Matrix Composite Materials by Tensile Test of a ±45 ° Laminate. ASTM International; 2007.

ESKİŞEHİR TECHNICAL UNIVERSITY JOURNAL OF SCIENCE AND TECHNOLOGY
A- APPLIED SCIENCES AND ENGINEERING

2022, 23(4), pp. 256-275, DOI:10.18038/estubtda.1062978

IMPROVEMENT OF VOLTAGE STRESS ON MOTOR CONTROL HARDWARE VIA OPTIMAL LOCATION OF RC SNUBBER CIRCUIT

Mehmet Emin SARIAYDIN [1,*], Şener AĞALAR [2]

[*] Electrical & Electronics Engineering Department, Engineering Faculty, Eskişehir Technical University, Eskişehir, Turkey, eminsariaydin@gmail.com
[2] Electrical & Electronics Engineering Department, Engineering Faculty, Eskişehir Technical University, Eskişehir, Turkey, seneragalar@eskisehir.edu.tr

ABSTRACT

While the increase in the customer failure rate in the consumer electronics sector affects the manufacturers negatively in terms of cost. It has also become one of the issues that cause customer loss and customer satisfaction. In addition to the economic losses, during the production and distribution of the spare parts and products that are changed at the customer's home due to the reliability problems experienced in the field, extra carbon emissions are released to the nature for this operation. For these reasons, it has become important to reduce the rate of customer failure.

With the increase in electronic components, the quality and reliability precautions that may occur in the electronic circuits, have become the subject of study today. As in many white goods products, it is advantageous to have variable speed motors in refrigerators due to energy efficiency and energy regulation issues. For this reason, the compressor of refrigerator comes to the forefront as the component that dissipates the highest power proportionally. With the use of variable speed compressors, the need for an electronic board with including power conversion and motor driving capability has arisen.

In this paper, RC Snubber circuits have been studied in order to prevent quality problems that may occur due to high switching frequency in flyback converter topology, which is one of the DC-DC converters that provide isolation. The methods in the literature based on the location of the RC Snubber in the circuit and the determination of its related values were examined and experiments were made on the simulation program. At the same time, a test mechanism was set up on the variable speed compressor motor control card of the refrigerator and measurements were taken with the help of an oscilloscope. The measurements taken in the simulation program and the experimental environment were compared.

Keywords: Refrigerator, Compressor, FlybackConverter, Snubber, Powerquality

1. INTRODUCTION

In recent years, with the growing human need for energy and running out of the natural energy sources, human being should find alternative sources or use the existing ones efficiently. In this way, energy saving practices and precautions will reduce the effects of carbon dioxide emissions and global warming which are serious threat to the future of the world [1]. In case of considering the total energy demand, the energy demand in the residentials (28%) has an important place after transport consumption (32%) in EU. Figure 1 pie chart indicates the energy demand with percentages in EU [2].

*Corresponding Author: eminsariaydin@gmail.com.tr
Received: 25.01.2022 Published: 29.12.2022

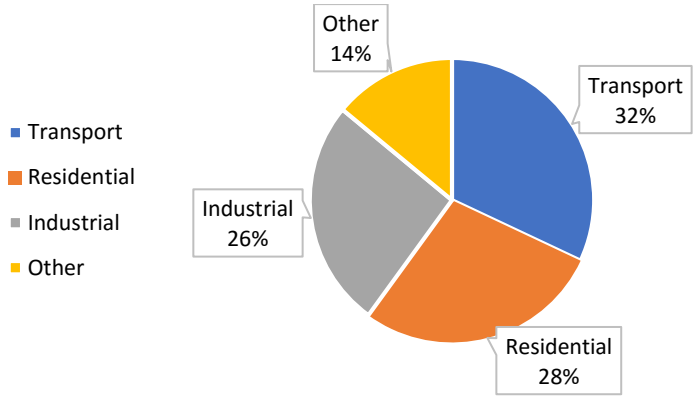

Figure 1. Energy demand percentages in EU

Accordingly, consumer electronics devices tend to consume less energy year by year. Figure 2 shows energy label usage on white goods product from 2015 to 2030 as classified business and low income household [3]. As a result of Figure 2, the number of high energy consumption products tends to decrease and the number of energy efficient product tend to increase by years. One of the providing method of producing energy efficient appliances is that use more electronic boards, components with including smart software.

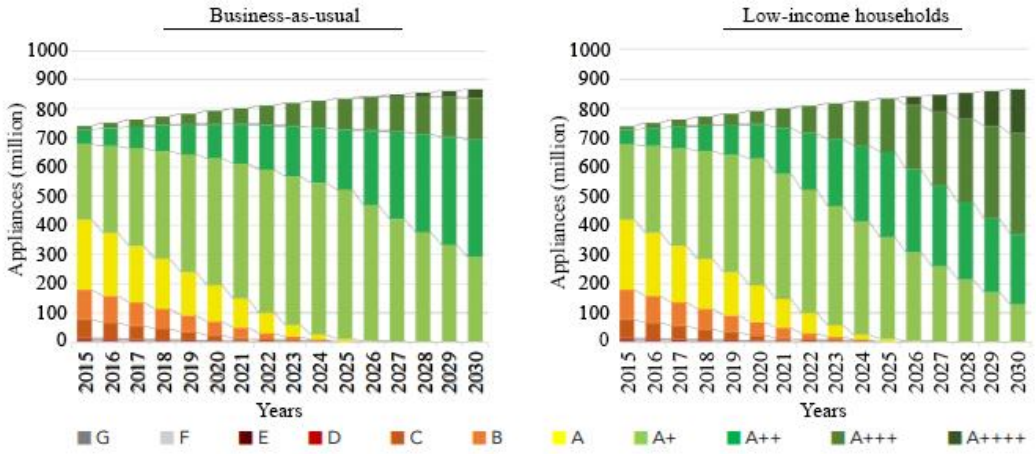

Figure 2. Household appliances energy label variation in case of number of appliances by years for 2015-2030[3]

While the number of electronic components and boards have been increasing day by day, their sustainability and repair costs are another rising issue for each consumer electronics manufacturer. A recent Eurobarometer survey indicated that the most common reason for purchasing a new digital device was the breakdown of the old product [4]. Also, according to conducted survey by Kantar TNS on behalf of Oslo Metropolitan University between 2018 and 2019, the electrical appliances that had broken down over the past two years are asked. Figure 3 indicates that respond of participants on survey. White goods appliances breaking down percentage takes a really important place like mobile phones. According to these results, while total white goods failures are 48%, mobile phone failures are 29%.

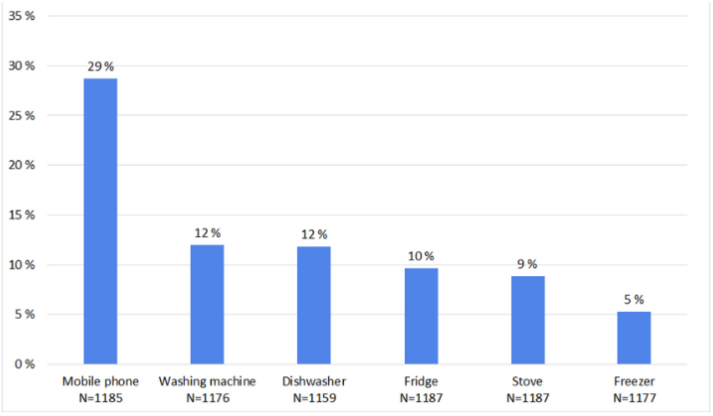

Figure 3. Proportional indication of the devices that have failed in the last two years of the survey participants (N: represents count of participant)[4]

In the view of such information, concentrate of decreasing repair quantities has been become as inevitable issue. In this study, one of the voltage stress decreasing circuit that is RC Snubber circuits on refrigerator compressor motor control board are examined. RC snubber location on circuit and RC value determination issue is examined with integrated of flyback converter circuit on refrigerator compressor motor control board.

Basically, the gas compression cycle refrigeration system is the heat transfer phenomena which provides to keep desired temperature in enclosed area, although outside of enclosed area temperature is varying. There are fundamentally four components of modern refrigeration systems which are compressor, condenser, expansion valve and evaporator. If it is wanted to be controlled more sensible in case of temperature and efficiency, more components could be added on refrigeration cycle such as sensors, actuators, electronic boards, smart cooling algorithms etc.

When it is considered about power or energy consumption perspective, the largest component of refrigerator is the compressor which is located back side of refrigerator. Also, refrigerator has auxiliary components which consume less power when it is compared to refrigerator compressor. These components could be defined as evaporator fans, condenser fan etc. Gas compression refrigeration cycle system flowchart is indicated in Figure 1.3 with the main lines [5].

In addition to four fundamental components of refrigerator, there is special refrigerant cooling liquid inside refrigerator system. This liquid swings round the refrigerator system cycle. The refrigerant cooling liquid may be fluid or gas form based on its characteristic inside refrigerator system. Also, it has a characteristic which transfers heat to the environment [6].

One of the extensive ways of DC-DC converter is flyback converter in terms of from high voltage to low voltage as providing isolation of SMPS topologies. Good measure of voltage and current stress are taken place on flyback circuit in case of relatively high frequencies. Due to natural characteristics of transformer, it stores related energy in case of switch on. Then, releases the energy to the output side of transformer during switch off time. Naturally, the windings of transformer are not distributed in case of coupling to the core. Because windings are isolated physically from each other. Therefore, there are energy stored between isolated windings which causes to occur leakage inductance [7].

Switching frequency increasing operation brings some drawbacks which could be defined as inefficiency, reliability problems and high EMI level. Also, voltage or current spikes, high dv/dt, di/dt or ringing signals could be occurred on implemented circuits. Particular snubber circuits are designed in order to take precautions to the unconformities which are mentioned above sentences. These unconformities create the aim of snubber circuits existence [8].

2. METHODS

It is really helpful to be able to observe the set up circuit on the simulation programs before putting it into practice. There is possible to manage recursive actions without using simulation programs in project. At the same time, simulation works could be used as pathfinder. Also, the results on simulation program gives clue about specific research issue.

On the other hand, there could be diversity between simulation program results and real experimental results. Rate of diversities depends on how real life parameters and dynamics are inserted on simulation programs. Sometimes, the ability of simulation programs can not enough to simulate real life variables with all parameters. One of the important things the difference between simulation and real life results is that interpret or estimate which parameters could cause the variation.

In this simulation work, behavior of flyback converter switching signal is examined. The mentioned circuit is used on refrigerator motor control board. The refrigerator motor control board input is chosen as 230Volt AC which is possible to represent house grid in European Region. Later on, AC house grid is rectified to DC supply signal. After rectification, this signal is forwarded to flyback converter as an input. Psim simulation circuit includes flyback converter which has a input of rectified house AC power supply and generates 15Volt output. Different types of RC circuits are applied to the flyback converter circuit on simulation program.

Before starting on experimental works on refrigerator compressor motor board, the simulation works are executed on Psim program. The signal between Drain and Source of flyback MOSFET are examined on simulation program. This signal characteristic is one of the important reasons of MOSFET failure issues in the long term at customers houses. The signal is aimed to examined about three criteria which is overshoot value, settling time and peak value. The fundamental definitions of these terms are explained in next paragraph.

Peak value could be defined as the maximum value of electrical signal or waveform in negative or positive side. Overshoot is the occurrence of a signal or function exceeding its target value. Undershoot is the same phenomenon in the opposite direction. Settling time is the time required for an output to reach and remain within a given error band following some input stimulus. Another useful definition is about ringing. Ringing is an unwanted oscillation on signal which could be voltage or current. If it is possible to obtain frequency of oscillation, it is called ringing frequency. Ringing frequency is assigned on oscillation part of signal. All related definitions are indicated on Figure 4 in order to visualize the used terms.

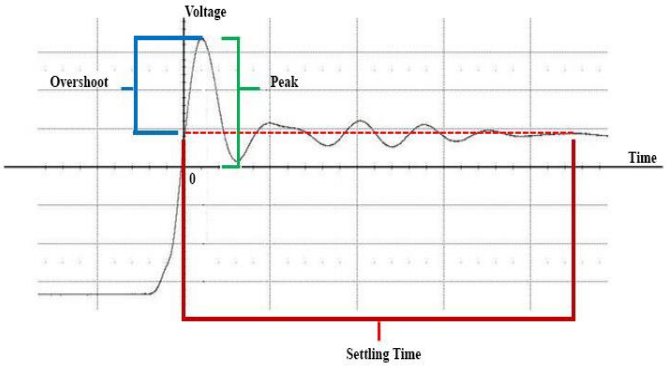

Figure 4. Explanation of Peak, Overshoot and Settling Time terms on sample signal

First of all, there is no snubber or additional circuit is used on flyback converter circuit in order to observe current status between drain and source pins of flyback converter MOSFET. Installed circuit on Psim simulation program is indicated with details in Figure 5.

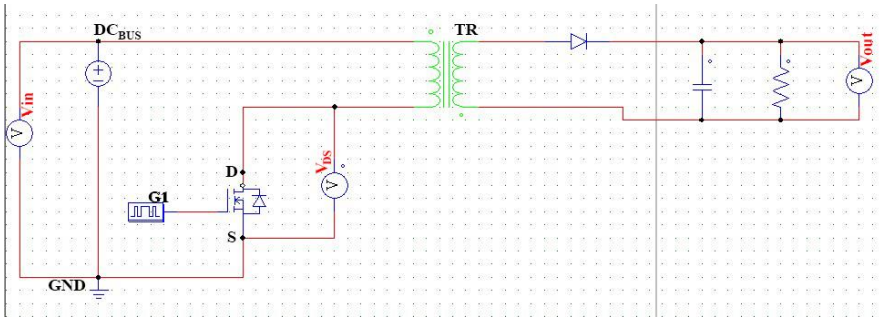

Figure 5: Flyback Converter circuit diagram without snubber on simulation program

The set up circuit includes DC voltage source(rectified from 230V AC power supply) as input, switching MOSFET, transformer and output passive components. The output of flyback converter is 15Volt which is necessary to supply other components of refrigerator motor control board.

As a first step, the signal between drain and source of MOSFET is observed on simulation circuit. In this circuit, existing component values of refrigerator compressor motor control board are used to simulate current situation. According to simulation program result, peak value, settling time and overshoot values are processed on Figure 6.

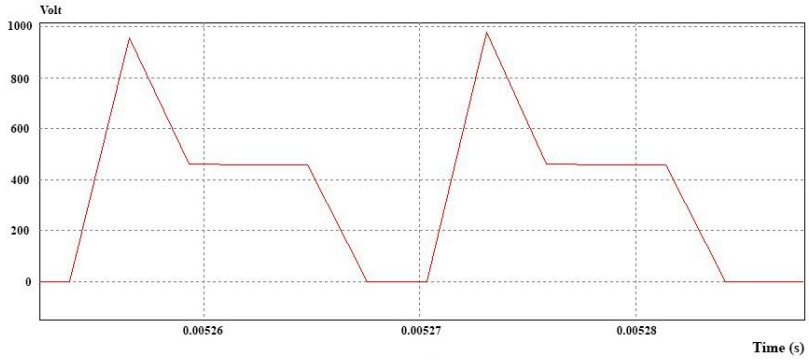

Peak (Voltage)	Settling Time (uS)	Overshoot (Voltage)
951	5	494

Figure 6. Obtained signal waveform which is measured between drain and source pins of MOSFET on simulation program in case of no snubber. Also, Peak, Overshoot and Settling time values are indicated

In this paperwork, two method of calculation RC values is examined about assigning appropriate RC values on refrigerator compressor motor control circuit flyback converter MOSFET. One of them is about assigning RC values on Buck converter [9]. Another one is related to obtain RC values on Flyback Converter [10]. The RC values are tried to assign on refrigerator compressor motor control board circuit. Below section includes about implementation of Ridley's method (2005) in case of RC values calculation.

The RC snubber circuit values should be designed based on used circuit type.

- As a first step, there are two measurements are needed to proceed next steps of calculations. One of them is total effective capacitance or the other one is leakage inductance. Capacitance is hard to define and measure when it compared to measure leakage inductance. It is a combination of nonlinear semiconductor junction capacitances, transformer winding capacitance, and any other stray capacitances such as heatsinks. In this case, measure leakage inductance is more useful with frequency response analyzer or LCR meter. LCR meter was used in order to measure leakage inductance on refrigerator compressor motor control hardware.

- A short circuit is implemented to secondary part of flyback transformer. Then, impedance of primary part of flyback transformer is measured. As expected, impedance value is varying depends on applied frequency. According to the method, ringing frequency of snubber signal was taken as reference. So, 6 micro Henry was measured, in case of refrigerator compressor motor control board ringing frequency(6.4Mhz) which is shown in Figure 7 as red dashed borders. Figure 9.4 indicates the signal between drain and source of MOSFET which is located on refrigerator compressor motor control board flyback converter as it could be seen zoomed format.

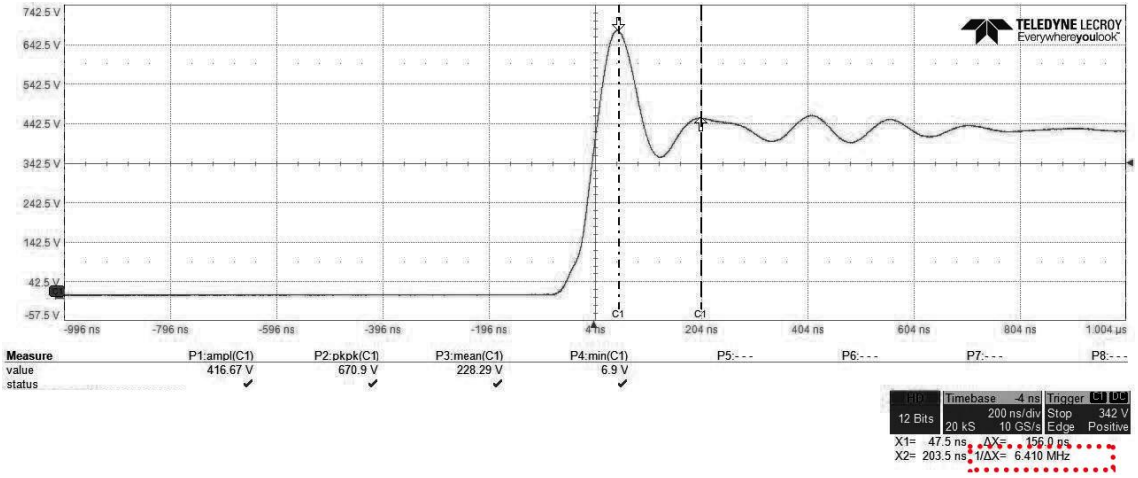

Figure 7. Obtained signal from oscilloscope which has ringing frequency 6.4 Mhz as it could be seen red dashed border

- Next step is that find characteristic impedance of flyback circuit. Below formula was used in order to calculate characteristic impedance. Z=R equalities is used when select resistor value. Also, characteristic impedance formula is indicated as below. According to below equation, appropriate resistor value is found as 200 Ohm.

$$Z = 2\ \pi\ L\ f_r$$

- After obtain resistor value, capacitor value should be calculated. According to method of Ridley (2005), below formula is used to find capacitance value of RC snubber circuit. In this case, 2nF capacitance value is founded.

$$C\ = \frac{1}{2\ \pi\ \ f_r\ \ R}$$

The resistor and capacitor values which are founded with Ridley's method (2005), are applied on simulation program based on refrigerator compressor motor control board flyback circuit. Also, the location of RC circuit is another critical working point. RC circuit could be connected to circuit as below combinations. Below combinations of RC circuit location on flyback converter is realized on simulation program with using RC values which is determined by the help of Ridley method (2005).

- Parallel connection of RC which is paralleled between drain and source pin of MOSFET
- Serial connection of RC which is paralleled between drain and source pin of MOSFET
- Parallel connection of RC which is paralleled between positive side of DC BUS signal and Drain pin of MOSFET
- Serial connection of RC which is paralleled between positive side of DC BUS signal and Drain pin of MOSFET

As a second step, a simulation circuit is set up as parallel connection of RC which is paralleled between drain and source pin of MOSFET. Figure 8 is indicated setting up circuit configuration on simulation program.

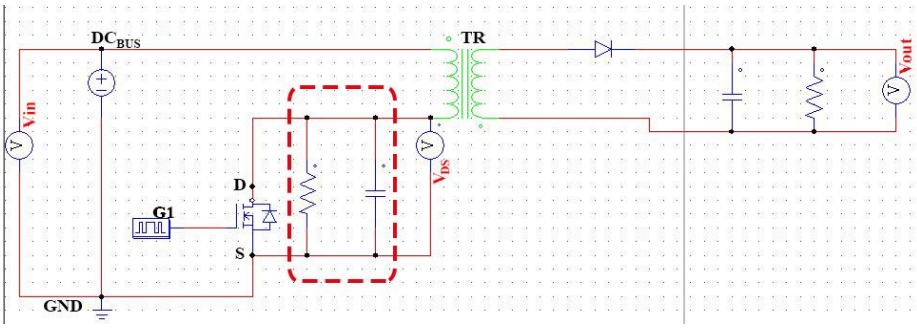

Figure 8. Flyback Converter circuit diagram, parallel connection of RC which is paralleled between drain and source pin of MOSFET on simulation program

When the circuit structure in Figure 8 is set up, the following signal is obtained which is shown on Figure 9. In this case, the signal between drain and source of MOSFET are acquired once again. The output of simulation program is shown on Figure 9.6. Also, peak value, settling time and overshoot values are processed on Figure 9. On the graph, the horizontal axis represents the time, the vertical axis the voltage.

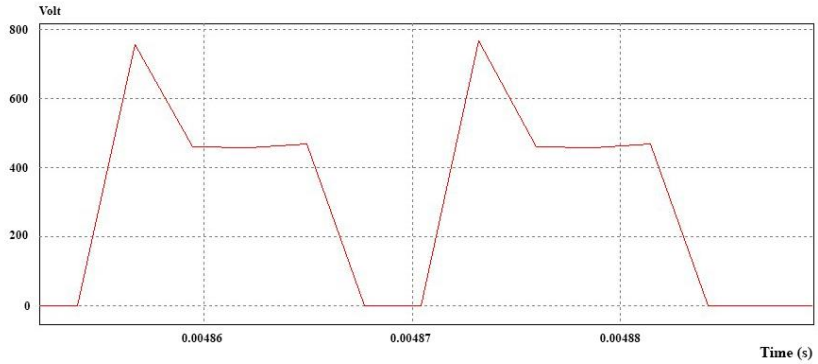

Peak (Voltage)	Settling Time (uS)	Overshoot (Voltage)
767	6	308

Figure 9. Measured signal between drain and source pins of mosfet on simulation program in case of parallel connection of RC which is paralleled between drain and source pin of mosfet. Also, Peak, Overshoot and Settling time values are indicated

In third phase of simulation work, serial connection of RC which is paralleled between drain and source pin of MOSFET. The setup circuit is close to conventional RC snubber circuits. Figure 10 shows the schematic of circuit that is realized on simulation program.

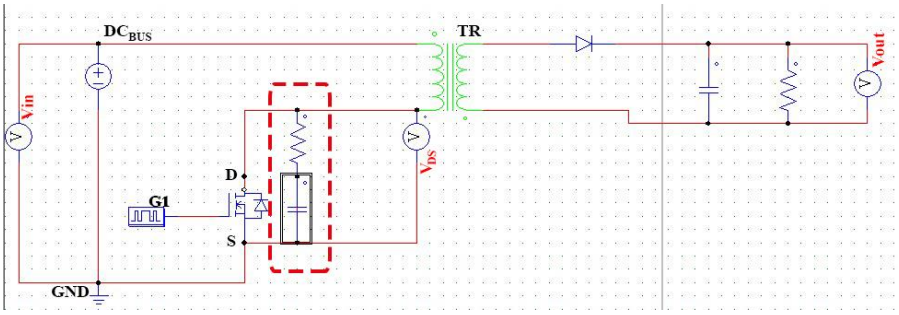

Figure 10. 4 Flyback Converter circuit diagram, serial connection of RC which is paralleled between drain and source pin of MOSFET on simulation program

When Figure 10 is applied on simulation program, the signal between drain and source of MOSFET are noted as below output signal. When this MOSFET signal is examined, peak value, settling time and overshoot values are added on Figure 11, numerically. On the graph, the horizontal axis represents the time, the vertical axis the voltage.

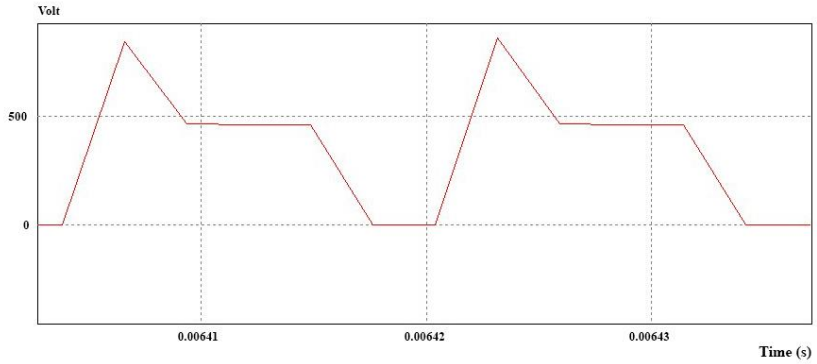

Peak (Voltage)	Settling Time (uS)	Overshoot (Voltage)
853	6	393

Figure 11. Measured signal between drain and source pins of MOSFET on simulation program in case of serial connection of RC which is paralleled between drain and source pin of MOSFET. Also, Peak, Overshoot and Settling time values are indicated

In the fourth step of simulation works, the circuit was set up which can be expressed as parallel connection of RC that is paralleled between positive side of DC BUS signal and Drain pin of MOSFET. Psim simulation program circuit representation is indicated in Figure 12.

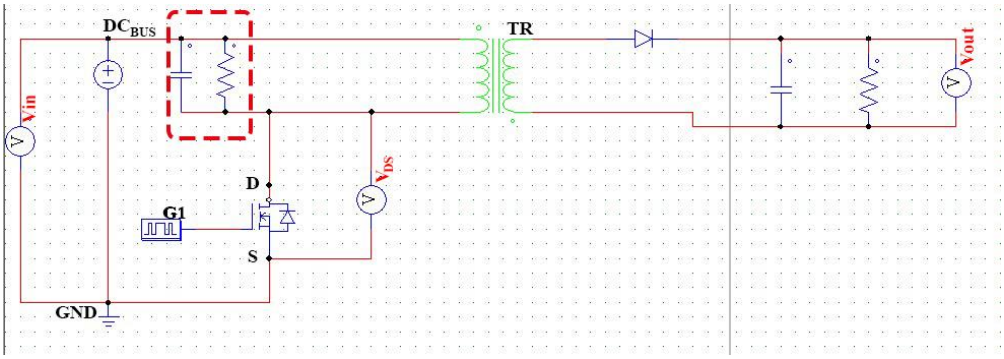

Figure 12. Flyback Converter circuit diagram, parallel connection of RC which is paralleled between positive side of DC BUS signal and Drain pin of MOSFET on simulation program

When the circuit in Figure 12 is implemented on simulation program, drain and source pins of the MOSFET is observed. Acquired waveform from simulation program could be seen in Figure 13. On the graph, the horizontal axis represents the time, the vertical axis the voltage. Similar to the previous situation, peak value, settling time and overshoot values are noted in Figure 13.

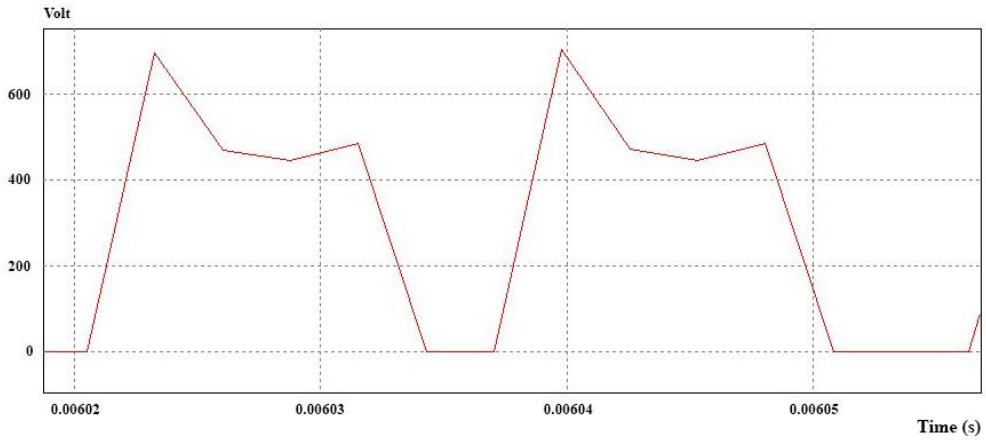

Peak (Voltage)	Settling Time (uS)	Overshoot (Voltage)
693	5	232

Figure 13. Measured signal between drain and source pins of MOSFET on simulation program in case of parallel connection of RC which is paralleled between positive side of DC BUS signal and Drain pin of MOSFET. Peak, Overshoot and Settling time values are indicated

In the last step of simulation work, another RC circuit location trial is examined. In this simulation work, serial connection of RC which is paralleled between positive side of DC BUS signal and Drain pin of MOSFET is set up on simulation program. The circuit representation is shown in the Figure 14 as below.

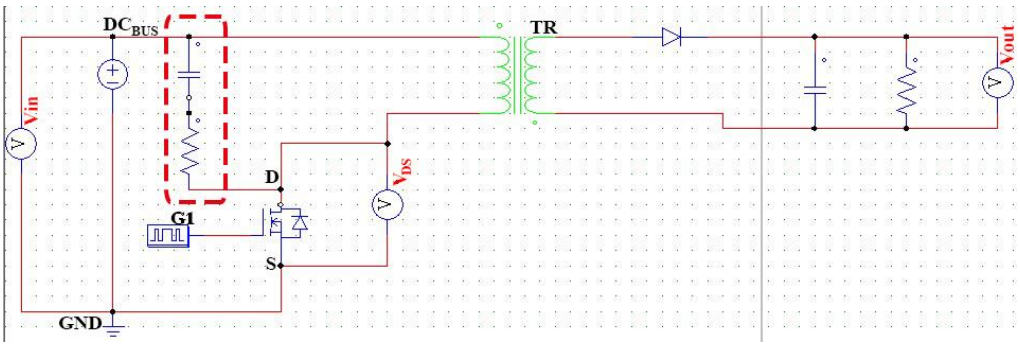

Figure 14. Flyback Converter circuit diagram, serial connection of RC which is paralleled between positive side of DC BUS signal and Drain pin of MOSFET on simulation program

The output between drain and source of MOSFET is obtained from simulation program. Obtained waveform is shown Figure 15. On the graph, the horizontal axis represents the time, the vertical axis the voltage. As in previous experiments, peak value, settling time and overshoot values are noted in Figure 15.

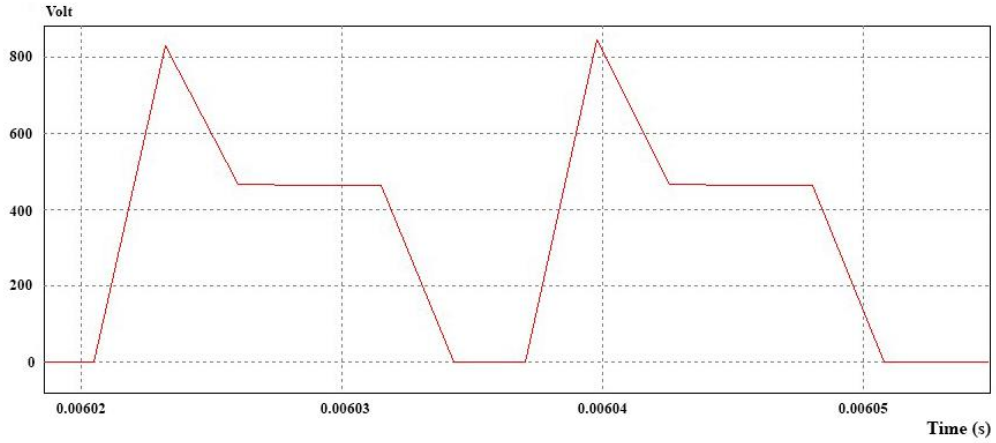

Peak (Voltage)	Settling Time (uS)	Overshoot (Voltage)
844	5	379

Figure 15. Measured signal between drain and source pins of MOSFET on simulation program in case of serial connection of RC which is paralleled between positive side of DC BUS signal and Drain pin ofMOSFET. Peak, Overshoot and Settling time values are indicated

The first method for assigning RC values and simulation works has been explained in previous paragraphs. In this section, about determination of RC values snubber circuit will be explained with details by using Rohm method (2016).

In Rohm method (2016), it obviously states that parasitic inductances and parasitic capacitances cause a resonance in input loop. In addition to this information, RC values calculation procedure is expressed in detail. The formulization of snubber resistor and snubber capacitor calculation is explained as below.

$$R_{SNUBBER} = 0.65 \times \sqrt{L_P} \Big/ \sqrt{C_{P2}}$$

$$C_{SNUBBER} = 8 \times C_{P2}$$

In this formula, C_{P2} can be calculated as divided by three of C_{P0}. C_{P0} is a capacitor that is connected between switch node and ground of circuit. C_{P0} is a capacitance value which the ringing frequency is decreased by a factor of 2. Therefore, in order to find snubber resistance and capacitance, there should be found C_{P2} and C_{P0} capacitance values according to formulization.

Before work on simulation program with RC values, there should be found $\mathrm{C_{P0}}$ capacitor value on real circuit that is specific on refrigerator compressor motor control board. The ringing frequency of obtained signals from simulation program does not readable. Because, in order to measure ringing frequency, at least 2 oscillation should be observed on signal.

According to Rohm method (2016), a target to find the capacitor value that halved the ringing frequency on refrigerator compressor motor control board. As it is seen on Figure 7, the ringing frequency of our circuit is 6.4 Mhz. Therefore, we expected to acquire approximately 3Mhz with addition of $\mathrm{C_{P0}}$ capacitor on refrigerator compressor motor control board flyback converter circuit. In this context, different capacitor values are connected on refrigerator compressor motor control flyback circuit. Firstly, 220 uF dc bus capacitor is selected as $\mathrm{C_{P0}}$ capacitor. The ringing frequency is obtained about 35Mhz as it could be seen in Table 1.

Table 1. Selected C_{P0} versus obtained ringing frequency on refrigerator compressor motor control board

Selected C_{P0} Capacitor	**Ringing frequency**
No RC component addition(current status)	6.4 Mhz
220 uf	35.3 Mhz
2 nf	5.7 Mhz
100 pf	5.3 Mhz

When the C_{P0} value is increased, ringing frequency is also increased. In line with this logic, the value of C_{P0} should be chosen smaller. Therefore, C_{P0} capacitor values are decreased until 100 pf which gives 5.3 Mhz ringing frequency. If this logic continues, about femto farad capacitor values could satisfy the demand which is half of ringing frequency. It does not reasonable to supply and obtain capacitor values in femtofarad value in our experimental environment. Due to this reason, it does not continue Rohm method(2016) recommended capacitor value on our refrigerator compressor motor control board.

Besides having an idea about the results by working with the simulation program, it is also important to prepare an experimental environment and observe what kind of results obtained in the real environment. In this paper, the refrigerator variable speed compressor motor control board is used to realize flyback converter snubber effects. Experimental studies were carried out on the flyback converter region on the refrigerator compressor motor control card. Flyback converter region is shown on refrigerator compressor motor control hardware in Figure 16.

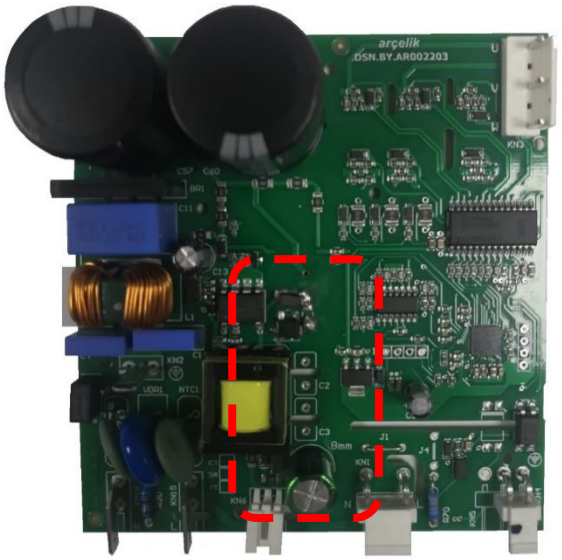

Figure 16. The indication of flyback converter region on refrigerator compressor motor control board

Variable speed compressor is placed at the back side of refrigerator. There is an evaporator tray on the variable speed compressor. Also, refrigerator compressor motor control board is combined with variable speed compressor on cooling product. AC power supply at home enters the refrigerator compressor motor control boards.

Electronic component modification on refrigerator compressor motor control board has been conducted with the help of auxiliary bread board. Because flyback converter structure has been already implemented on PCB of refrigerator compressor motor control board. Therefore, RC circuit modifications are executed on bread boards.

In order to measure between drain and source of MOSFET, Teledyne Lecroy (HDO4054) brand oscilloscope was used. Two wire are soldered on refrigerator motor control board for connection of

oscilloscope. Each measurement is executed with variable speed compressor connected to variable speed compressor motor control board. Also, experiments are executed at Arçelik Refrigerator - Compressor Plant R&D laboratory, Turkey. The experiment environment could be seen in Figure 17 with details.

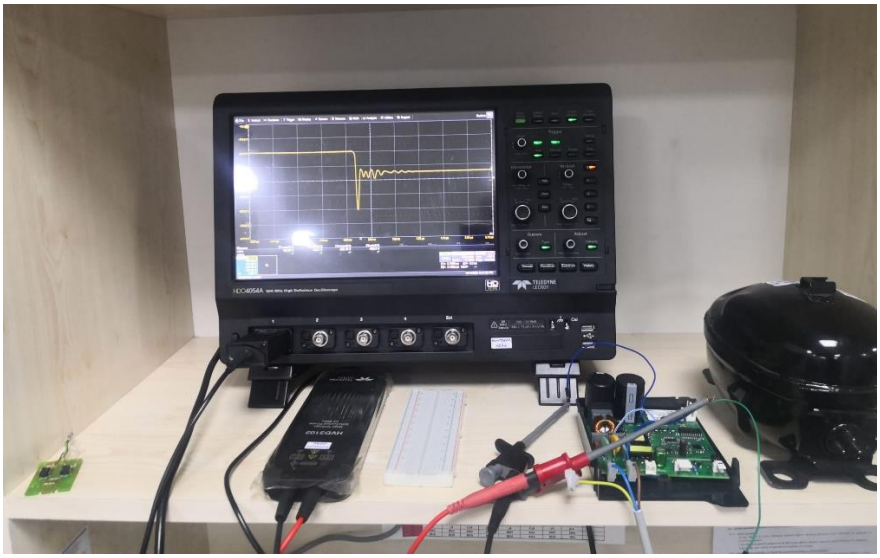

Figure 17. Indication of experimental environment which includes, ossiloscope, variable speed compressor, refrigerator compressor motor control board

Experimental works is another important point for many projects. The detailed information about experimental test environment was given in previous pharagraphs. After simulation works with different scenarios of RC circuit addition, combination of RC circuits is applied on experimental test environment.

In this section, experimental works are explained step by step. Two RC snubber values estimation methods was evaluated in simulation part which is Ridley & ROHM methods. However, second method RC values is not feasible for our refrigerator compressor motor control board circuit as explained in previous part. For this reason, first method RC values was implemented on refrigerator compressor motor control board and explained in detail. In addition, different combination of location of RC circuit is implemented on refrigerator compressor motor control board as simulation works are executed on previous section of paper.

The first experiment is about no snubber on flyback converter of refrigerator compressor motor control board as default. The purpose of this experiment is that see current state of refrigerator compressor motor control board in case of the signal between drain and source of flyback converter MOSFET. The simulation result was shown in previous section without snubber RC on flyback converter. In this case, the circuit representation for refrigerator compressor motor control board is indicated as Figure 18. The experimental result is shown in Figure 18. The signal which is captured by way of oscilloscope measurement, between drain and source of flyback converter MOSFET. The settling time, peak and overshoot value are indicated in table which is located in Figure 18.

Overshoot	340,5	**a.** Peak, Overshoot and Settling time values
Settling Time	50	
Peak	670,9	

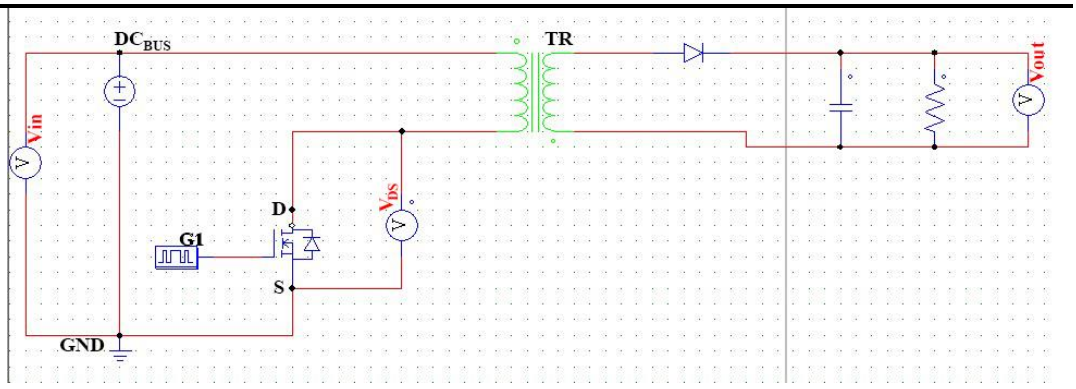

b. Flyback Converter circuit representation without snubber on simulation program

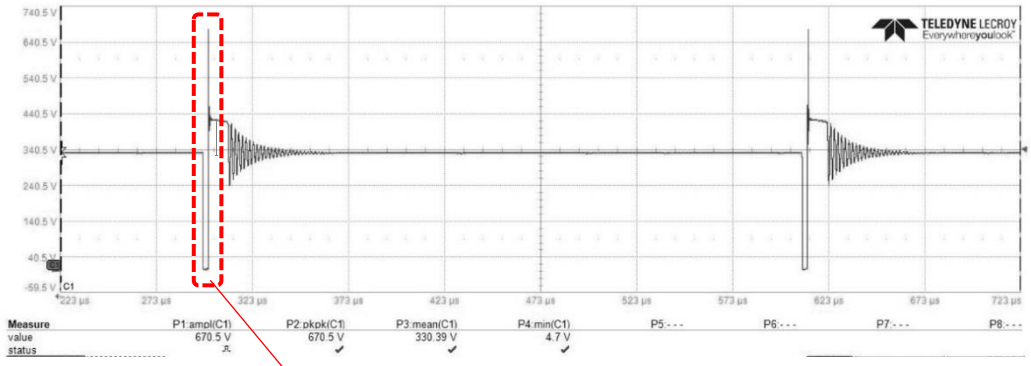

c. Obtained signal waveform which is measured between drain and source pins of MOSFET on simulation program in case of no snubber. Red dashed border indicates the zoomed format of signal.

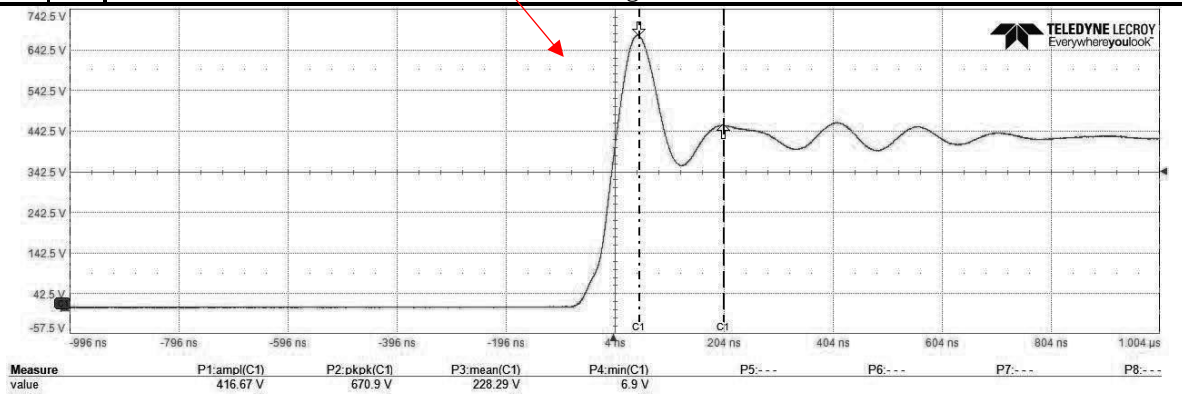

d. Zoomed signal in part C.

Figure 18. Obtained signal waveform which is measured between drain and source pins of MOSFET on simulation program in case of no snubber. Also, Peak, Overshoot and Settling time values are indicated

As the second step of experimental work, the RC circuit addition is implemented on refrigerator compressor motor control board. This modification could be expressed as parallel connection of RC which is paralleled between drain and source pin of MOSFET. In this circuit, all circuit component values are taken by refrigerator compressor motor control board except RC values. The circuit diagram of the set up circuit is shown as Figure 19. The output signal is gathered with using oscilloscope. The signal measurement is taken between drain and source pin of flyback converter MOSFET. In this measurement, the settling time, overshoot and peak values are examined and added on table.

Overshoot 325,2

Setting Time 50

Peak 656,5

. a. Peak, Overshoot and Settling time values

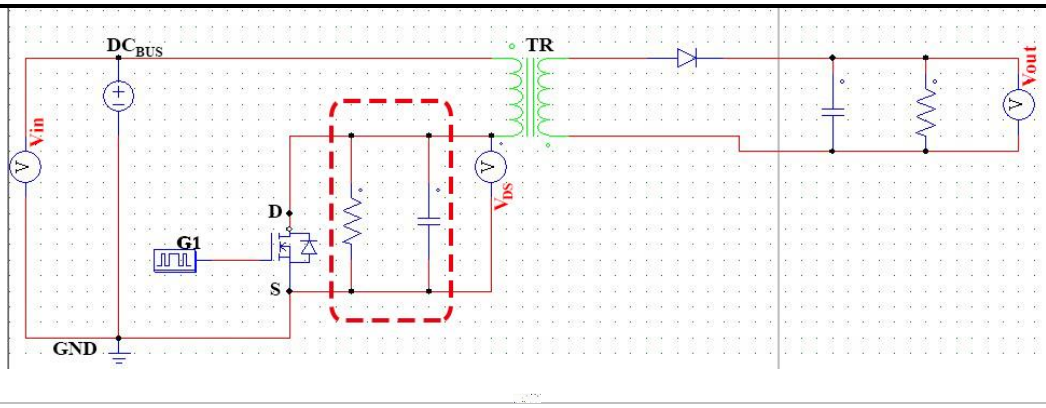

b. Flyback Converter circuit diagram, parallel connection of RC which is paralleled between drain and source pin of MOSFET on simulation program

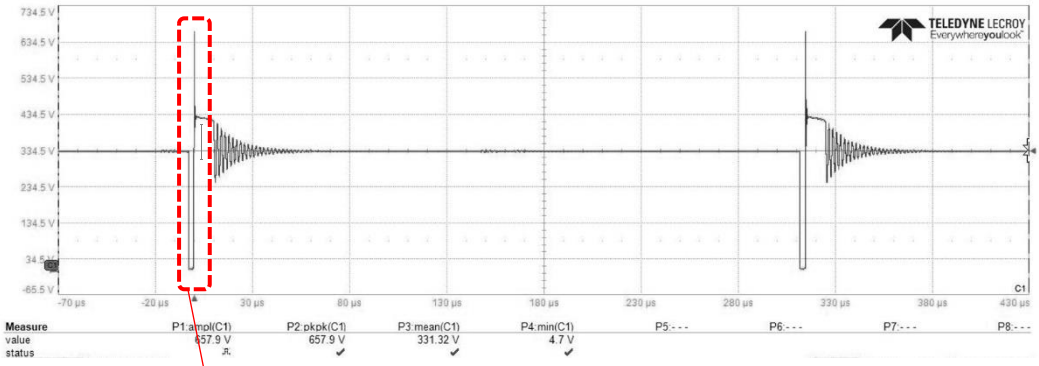

c. Obtained signal waveform which is measured between drain and source pins of mosfet on simulation program in case of parallel connection of RC which is paralleled between drain and source pin of MOSFET. Red dashed border indicates the zoomed format of signal.

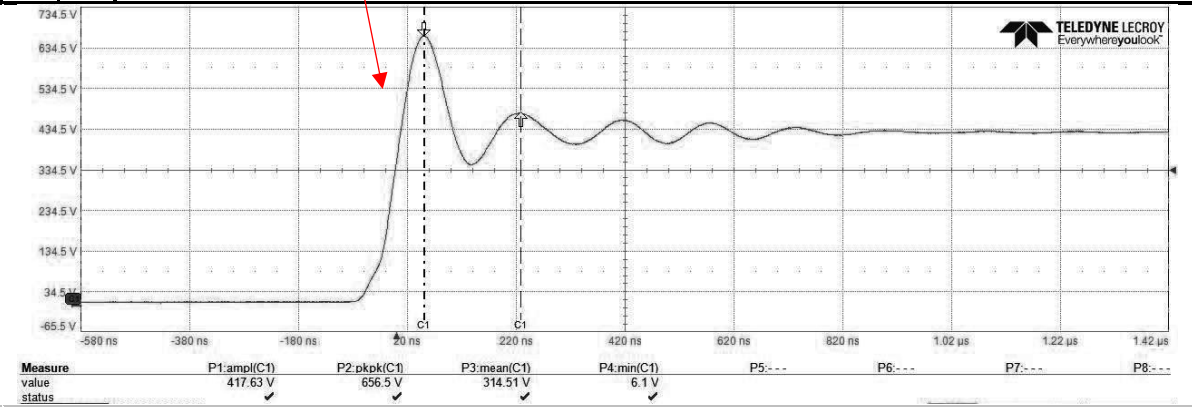

d. Zoomed signal in part C.

Figure 19. Measured signal between drain and source pins of MOSFET on simulation program in case of serial connection of RC which is paralleled between drain and source pin of MOSFET. Peak, Overshoot and Settling time values are indicated

In the third step, different combination of RC circuit location is implemented which is compatible with simulation section. In this part, set up circuit could be represented as serial connection of RC which is paralleled between drain and source pin of MOSFET. The combination of RC circuit is implemented on refrigerator compressor motor control board. The schematic representation of flyback converter circuit with addition of RC values is shown in Figure 20. The signal is measured that between drain and source pin of flyback converter MOSFET. The obtained signal is examined with criteria of settling time,

overshoot value and peak value. All mentioned and related values are processed on the Figure 10.3 with detail.

Overshoot	327,2	**a.** Peak, Overshoot and Settling time values
Settling Time	50	
Peak	658,3	

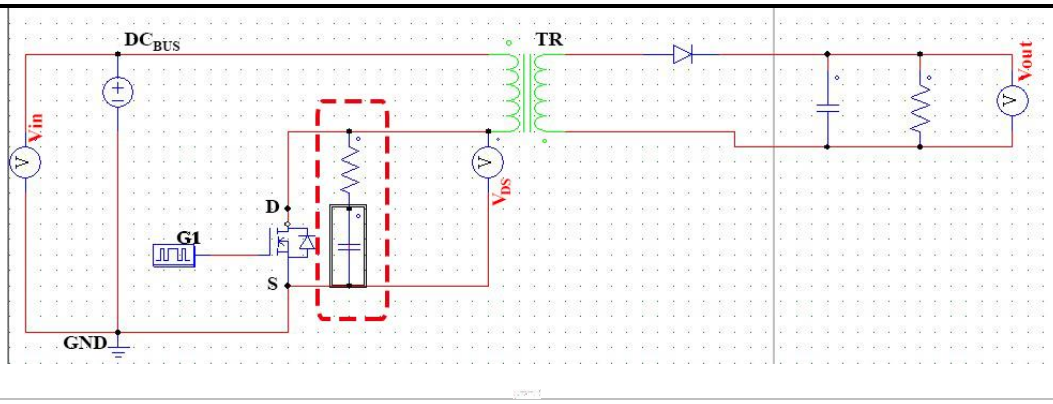

b. Flyback Converter circuit diagram, serial connection of RC which is paralleled between drain and source pin of MOSFET on simulation program

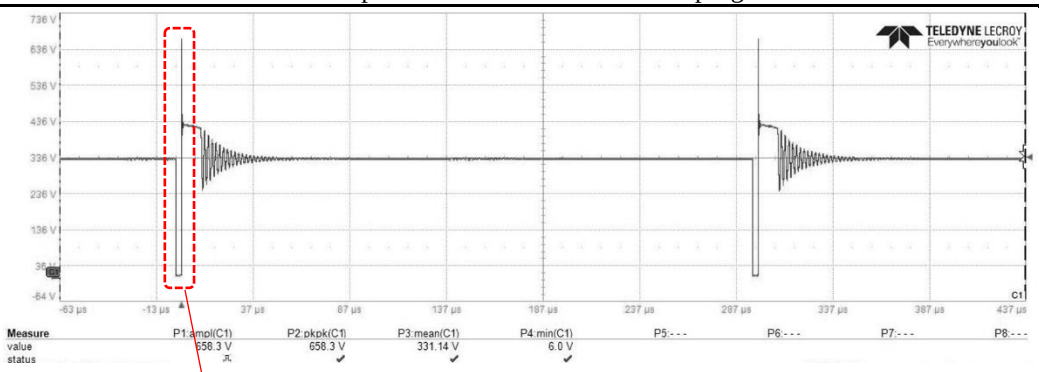

c. Obtained signal waveform which is measured between drain and source pins of MOSFET on simulation program in case of serial connection of RC which is paralleled between drain and source pin of MOSFET. Red dashed border indicates the zoomed format of signal

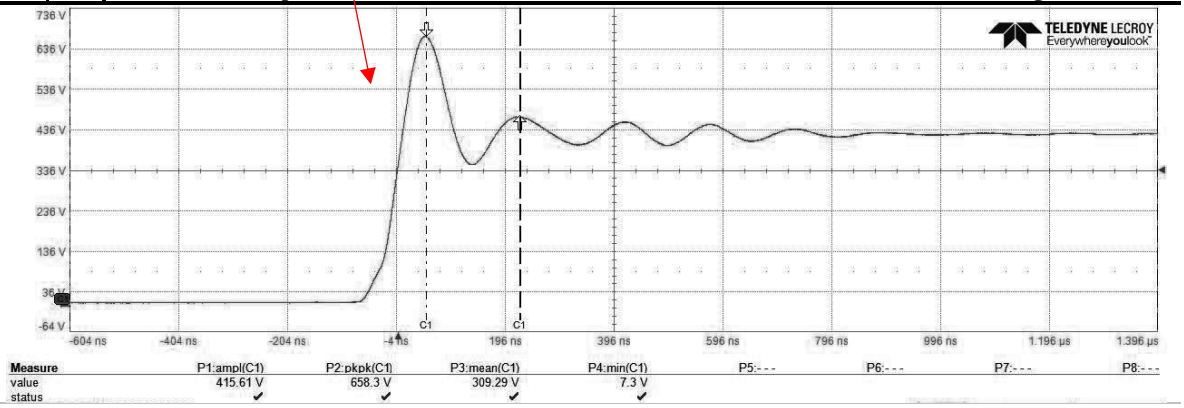

d. Zoomed signal in part C.

Figure 20. Measured signal between drain and source pins of MOSFET on simulation program in case of serial connection of RC which is paralleled between drain and source pin of MOSFET. Peak, Overshoot and Settling time values are indicated

In the fourth and fifth step, the location of RC circuit is shifted from between drain and source pins of mosfet to between dc bus signal and drain pin of mosfet. As a mention from fourth step, the circuit could be expressed as rarallel connection of RC which is paralleled between positive side of DC BUS signal and Drain pin of mosfet. The set up circuit is shown as schematic view on Figure 21. Also, settling time, peak value and overshoot values of oscilloscope measured signal are indicated on Figure 21.

Overshoot	215,1	**a.** Peak, Overshoot and Settling time values
Setting Time	50	
Peak	544,3	

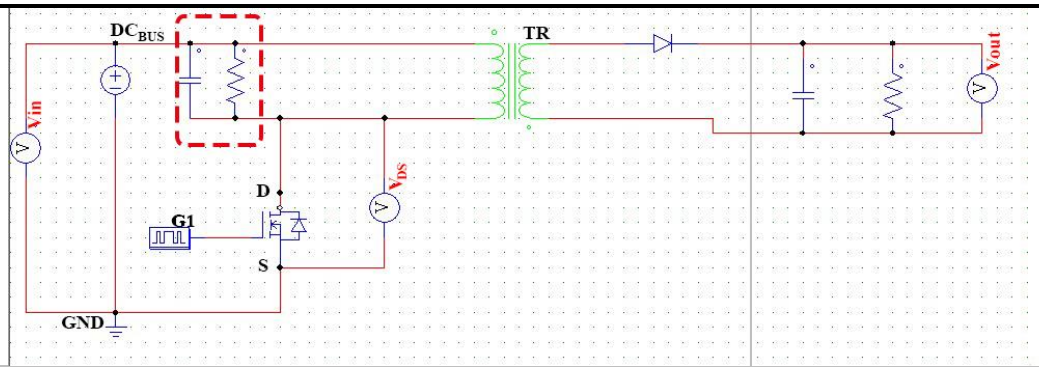

b. Flyback Converter circuit diagram, parallel connection of RC which is paralleled between positive side of DC BUS signal and Drain pin of MOSFET on simulation program

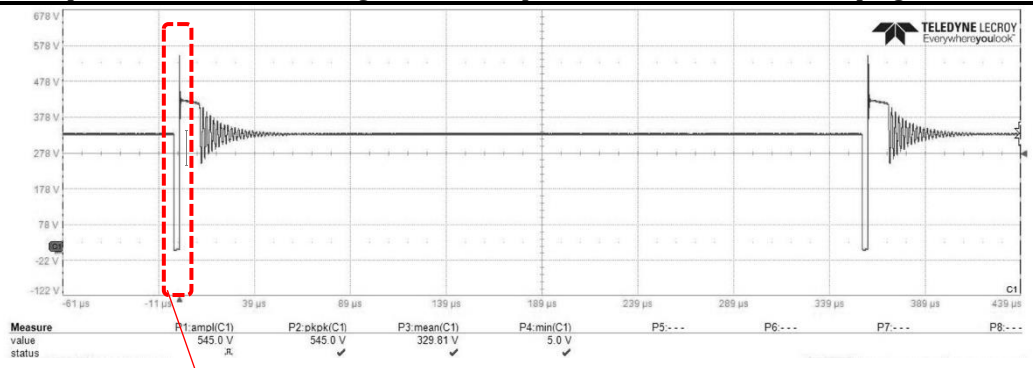

c. Obtained signal waveform which is measured between drain and source pins of MOSFET on simulation program in case of parallel connection of RC which is paralleled between positive side of DC BUS signal and Drain pin of MOSFET. Red dashed border indicates the zoomed format of signal

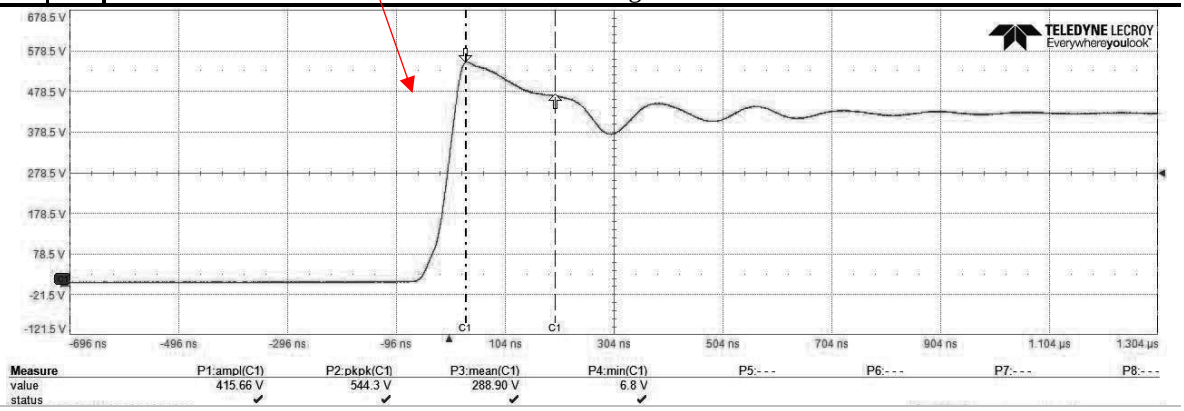

d. Zoomed signal in part C.

Figure 21. Measured signal between drain and source pins of MOSFET on simulation program in case of serial connection of RC which is paralleled between drain and source pin of MOSFET. Peak, Overshoot and Settling time values are indicated

In the last step of experimental test, RC circuit location is represented as serial connection of RC which is paralleled between positive side of DC BUS signal and Drain pin of MOSFET. The schematic circuit is indicated in Figure 22. The drain and source pins are measured with aid of oscilloscope on refrigerator compressor motor control board Also, captured signal settling time, overshoot value, peak value is added on Figure 22.

Overshoot	331,2	**a.** Peak, Overshoot and Settling time values
Settling Time	50	
Peak	661,7	

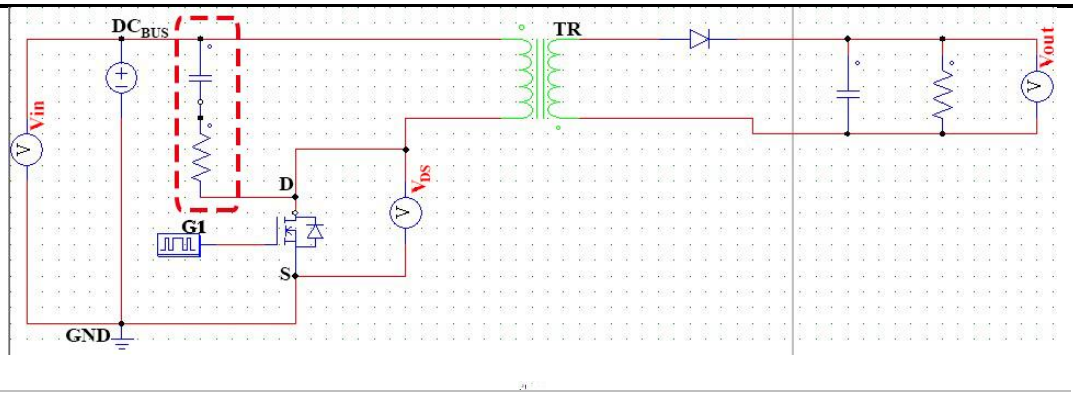

b. Flyback Converter circuit diagram, serial connection of RC which is paralleled between positive side of DC BUS signal and Drain pin of MOSFET on simulation program

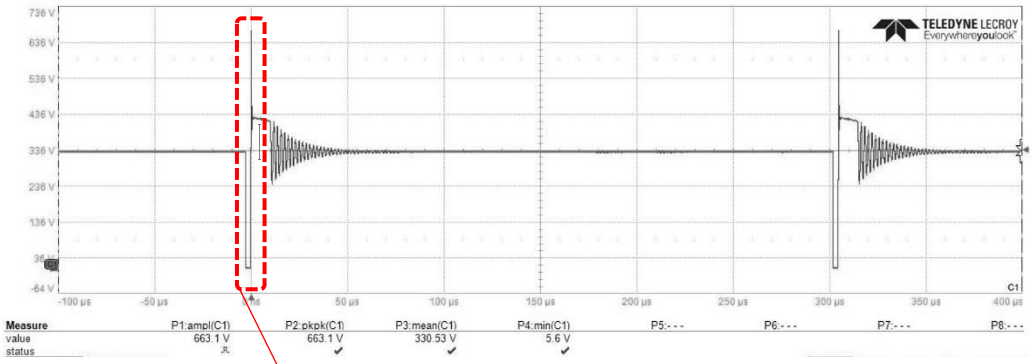

c. Obtained signal waveform which is measured between drain and source pins of MOSFET on simulation program in case of serial connection of RC which is paralleled between positive side of DC BUS signal and Drain pin of MOSFET. Red dashed border indicates the zoomed format of signal

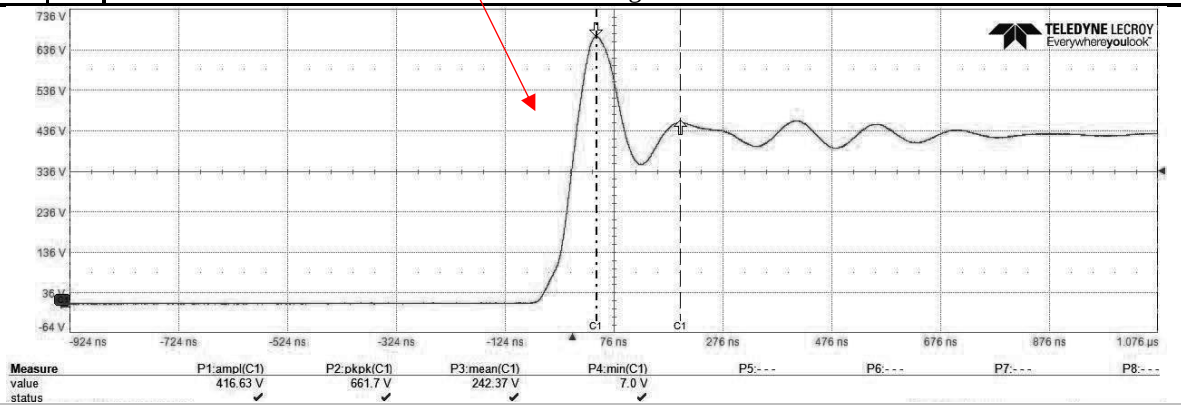

d. Zoomed signal in part C.

Figure 22. Measured signal between drain and source pins of MOSFET on simulation program in case of serial connection of RC which is paralleled between drain and source pin of MOSFET., Peak, Overshoot and Settling time values are indicated

3. RESULTS

Detailed table for three parameters could be seen in Table 2. When four location of RC circuit is examined, it could be said less peak and overshoot value are obtained with third location, according to simulation program Psim. The location of RC circuit is expressed as parallel connection of RC which is paralleled between positive side of DC BUS signal and Drain pin of MOSFET

Table 2. Peak, Settling time and overshoot values from no snubber situation to different location RC circuits in simulation program. RC location sequence is same as in simulation part

RC Location	Peak (Voltage)	Settling time (uS)	Overshoot (Voltage)
No RC	951	5	494
1	767	6	308
2	853	6	393
3	693	5	232
4	844	5	379

The circuits set up in the simulation study were also set up step by step during the experimental study. Table 3 indicates that no snubber circuit and four different location of RC circuit. Considering the peak value and overshoot value criteria, it is seen that third location of RC circuit is the most optimal method. Considering the settling time values, no significant difference was observed in all circuits.

Table 3. Peak, Settling time and overshoot values from no snubber situation to different location RC circuits on refrigerator compressor motor control board.. RC location sequence is same as in simulation part.

RC Location	Peak (Voltage)	Settling time (uS)	Overshoot (Voltage)
No RC	670	50	340
1	656	50	325
2	658	50	327
3	544	50	215
4	661	50	331

4. DISCUSSION

According to simulation program results, when evaluated in terms of settling time, it could not be said that there is a result that makes a significant or determinative difference. With the 3rd location, an improvement around 37% was observed compared to the circuit without any snubber circuit in case of peak value of signal during turn off instance. Also, at the same location of RC circuit, the improvement was achieved more than twice when the overshoot value was taken into account. Another consequence of this simulation work in case of RC snubber and snubberless case is that if RC circuit is used on four potential region of flyback converter, at least 25% improvement for overshoot value, %11 improvement for peak value will be obtained.

After evaluating the simulation results, experiments were carried out by making modifications on refrigerator compressor motor control board. With the 3rd location, an improvement around 23% was observed compared to the circuit without any snubber circuit in case of peak value of signal during turn off instance. Also, at the same location of RC circuit, the improvement was achieved around 58% when the overshoot value was taken into account.

5. CONCLUSION

Both simulation and experiments at laboratory were performed with 230 Volt AC and 50 Hertz frequency input voltage which simulates house grid. As in the simulation results, the 3rd circuit location of RC circuit gave the most optimum values in the experimental results in case of peak and overshoot value. At this point, it could be mentioned that the simulation and experimental results are compatible in terms of find optimum solution on flyback converter circuit of refrigerator compressor motor control board.

Although the experimental and simulation results are proportionally feasible with each other, they differ from each other in terms of numeric values which are peak value, settling time and overshoot value. On the other hand, minor differences could be seen in the waveform. There could be many reasons to not be able to transfer from real environment parameters to the simulation programs. Leakage inductance and leakage capacitance on real environment, refrigerator compressor motor control PCB path, traces and via effect, power sources losses, used component losses and their simulation models may have a couple of reasons for this deviation.

By using the RC values found by the method used, the electrical stress of the MOSFET in the flyback converter circuit is reduced. Also, one of the things that contributed to this situation is that using RC circuit in the most appropriate place on the refrigerator compressor motor control card. In this way, the longer-term working potential of the flyback converter MOSFET on the refrigerator compressor motor control card at customers home, has been occurred. In this way, there is chance to obtain an application with the potential to decrease the failure rate of the refrigerator compressor motor control board in case of MOSFET failures on flyback converter circuit.

In addition, due to voltage fluctuation in some regions, even higher peak and overshoot values may occur on the MOSFET of flyback converter. By applying this kind of methods, there was a potential to extend the life time of MOSFET by decreasing the peak and overshoot voltages. Looking at this situation from a broad perspective, besides reducing the service costs of the manufacturers, it also creates a beneficial situation for carbon emissions as less spare part boards will be produced and less fuel will be spent for spare part services. On the other hand, it has the potential to create a situation that will reflect positively on customer satisfaction.

CONFLICT OF INTEREST

The authors stated that there are no conflicts of interest regarding the publication of this article.

REFERENCES

[1] Yesilaydin I and Erbay LB. Numerical ınvestigation of flow losses through discharge line of household type refrigerator compressors. IOP Conf. Series: Materials Science and Engineering, 2015;90, pp. 1-10.

[2] Nepal R Musibau HO, Jamasb T. Energy consumption as an indicator of energy efficiency and emissions in the European Union: A GMM based quantile regression approach. Energy Policy, 2021;158, pp. 1-10.

[3] Mandel T, Brugger H, Guetlein MC, Schleich J. Integrating discrete choice experiments and bottom-up energy demand models to ınvestigate the long-term adoption of electrical appliances in response to energy efficiency policies. BEHAVE 2020-2021 the 6th European Conference on Behaviour Change for Energy Efficiency, 2021; Denmark, 209-212.

[4] Laitala K, Klepp IG, Haugrønning V, Throne-Holst H, Strandbakken P. Increasing repair of household appliances, mobile phones and clothing: Experiences from consumers and the repair industry. Journal of Cleaner Production, 2021; 282, 1-13.

[5] Kanargı ÖB. Evaluation of the performance of a household refrigerator using a variable speed compressor with 1d simulations. Unpublished Master's Thesis. İzmir: İzmir Institute of Technology, Mechanical Engineering, 2013.

[6] Yıldız L. Kompresör kabuğunun sayısal ve deneysel analizi. Unpublished Master's Thesis. İstanbul: İstanbul Technical University, Institute of Science, 2016.

[7] Patel HK. Voltage transient spikes suppression in flyback converter using dissipative voltage snubbers. 3rd IEEE Conference on Industrial Electronics and Applications, 2008; pp. 897-901.

[8] Mohammadi M and Ordonez M. Flyback lossless passive snubber. 2015 IEEE Energy Conversion Congress and Exposition (ECCE), 2015; pp. 5896-5901.

[9] ROHM Semiconductor (2016). Snubber Circuit for Buck Converter IC. Application Note.

[10] Ridley R. Flyback Converter Snubber Design. Switching Power Magazine, 2005.

ESKİŞEHİR TECHNICAL UNIVERSITY JOURNAL OF SCIENCE AND TECHNOLOGY
A- APPLIED SCIENCES AND ENGINEERING

2022, 23(4), pp. 276-290, DOI:10.18038/estubtda.1068351

OPTIMIZATION OF CHROMIUM AND LEAD BIOSORPTION IN WASTEWATER USING 3^3 FACTORIAL DESIGN

Berna YAZICI [1], Semra MALKOC [2], Ece OZGOREN [3,*], Nur DURSUN [4]

[1] Department of Statistics, Faculty of Science, Eskisehir Technical University, Eskisehir, Turkey
[2] Department of Environmental Engineering, Faculty of Engineering, Eskisehir Technical University, Eskisehir, Turkey
[3] Department of Statistics, Institute of Graduate Education, Eskisehir Technical University, Eskisehir, Turkey
[4] Department of Statistics, Faculty of Science, Eskisehir Technical University, Eskisehir, Turkey

ABSTRACT

In this study removing heavy metals, Cr (III), and Pb (II) from wastewater, Microorganism *Trichoderma* sp. biosorption was performed using Cr (III), and Pb (II) removal was taken into account. For this study, 3^3 Factorial Designs were used, and temperature (°C), biosorbent dosage (g/L), and pH were selected as the main factors for Cr (III), and Pb (II) metals and three levels of these factors were determined as low, medium, and high. In this study, which was carried out to increase the metal removal efficiency and biosorption capacity, the main factors and the significance of each interaction of these factors were examined with 3^3 Factorial Design. For this purpose, by conducting Analysis of Variance (ANOVA) via Response Surface Methodology and optimization, more detailed results were obtained regarding the factors affecting the efficiency of metal removal from wastewater.

Keywords: 3^3 Factorial Design, Optimization, Biosorption, Wastewater, Removal Efficiency

1. INTRODUCTION

Water pollution occurs in the form of a negative change in the physical, chemical, bacteriological, radioactive, and ecological properties of the water supply. Water pollution is a quality change that occurs as a result of anthropogenic effects, restricts or blocks used, and disrupts economic balances. Food and Agriculture Organization of the United Nations (FAO) defines water pollution as the disposal of substances into the water. This proves to be harmful to living resources and dangerous to human health. This pollution prevents activities such as fishing, and it may have detrimental effects on water quality [1].

There is no doubt that the accumulation of heavy metals constitutes the most dangerous dimension of chemical water pollution. The term heavy metal, used synonymously with trace metal, covers trace metals that are essential and those that are not. All of these are potential hazards for living organisms. The most important industrial activities that are effective in the spread of heavy metals to the environment are cement production, iron and steel industry, thermal power plants, glass production, garbage, and waste sludge incineration plants [2].

Heavy metals are toxic when they exceed the concentration limit both in the waters and in the living body where they are found. Especially in the living body, the effect varies depending on the type of creature and the structure of the metal ion, rather than depending on the concentration. For this reason, the maximum concentration restriction has been made, especially in the drinking water of regular consumption and in the food obtained from water sources, and it is necessary to keep it under constant control [3].

*Corresponding Author: eceozgoren@eskisehir.edu.trx
Received: 09.02.2022 Published: 29.12.2022

Physical and chemical methods used for heavy metal removal have a limited scope of use due to reasons such as high operating and maintenance costs and additional stress on the environment. Biosorption, in which biological methods are used to remove heavy metals and many other pollutants, is a process that means the removal of pollutants and harmful substances from the environment using microorganisms, such as bacteria, fungi, yeasts, and algae [4,5-6]

In this study, ANOVA via 3^3 Factorial Experiment Design was performed to examine the main and interaction effect of temperature, biosorbent dosage, and pH on the removal efficiency and biosorption capacity from wastewater by removing heavy metals. The main objective was to examine the optimum conditions for the Cr (III) and Pb (II) on two response variables from wastewater. After determining influential factors and their levels, the optimization analyses were applied to evaluate optimum combinations for removal efficiency and biosorption capacity from wastewater.

2. MATERIAL AND METHOD

2.1. Experimental Procedures

The fungal strain *Trichoderma* sp. was isolated from ceramic industrial sludge. One gram of the sludge was inoculated in the potato dextrose broth media amended with heavy metal ions solutions. The strain was isolated on potato dextrose agar media containing (gL^{-1}): agar 15.0, dextrose 20.0, potato extract 4, Streptomycin 0.03, at 25 °C and pH 5.6±0.2. The medium was sterilized by autoclaving at 1.5 atm pressure and 121°C temperature for 20 min. The pure colony was preserved on the slants at 4 °C and identified from morphological characterization with a microscope.

2.2. Experimental Design for Optimization

The aim of this study is to ensure that metal removal efficiency is as high as possible. Therefore, a Full Factorial Design with three levels of three factors was used. Factors affecting Cr (III) and Pb (II) in wastewater were selected as temperature (°C), biosorbent dosage (g/L), and pH, and three levels belonging to these three main factors were determined. These factors and levels are shown in Table 1 for Cr (III) and Pb (II) [7].

Temperature, biosorbent dosage, and pH were selected as the most important factors affecting metal removal efficiency and biosorption capacity as response variables, and a total of 108 experiments were carried out with 4 repetitions for low, medium, and high levels of these parameters.

The three main factors are determined, and three levels of these main factors will be examined with 3^3 Factorial Experiment Design. 27 experimental combinations including temperature (°C), biosorbent dosage (g/L), and pH factors and the interactions of these three factors, coded and quadratic coefficients are given in Table 2. The coded coefficients are 1, 0, and -1, respectively, while the quadratic coefficients are 1, -2, and 1. In addition, since the experiments were carried out in 4 repetitions, a total of 108 response results belonging with observation values were used in the statistical analysis.

Table 1. Factors and Levels for Cr (III) and Pb (II).

Factor	Level 1	Level 2	Level 3
A: Temperature (°C)	20	30	40
B: Biosorbent dosage (g/L)	1	3	5
C: pH	2	4	6

The mathematical model including main factors and their coded and quadratic combinations are given by Equation 1.

$$Y_{ijk} = \mu + A_i + B_j + C_k + AB_{ij} + AC_{ik} + BC_{jk} + ABC_{ijk} + \varepsilon_{ijk} \quad (1)$$

Where Y represents the response variable (e.g., the removal efficiency or the biosorption capacity), A, B and C are the independent variables (at low, medium and high levels), A_i, B_j, C_k ($i = j = k = 1,2,3$) represents the estimation of the main effect of the factor, whereas AB_{ij}, AC_{ik} and BC_{jk} represents the estimation of the second order interaction effect between factor i and j, i and k , j and k for the response variable. Moreover, the coefficient μ is constant term, ABC_{ijk} shows the third order interactions' estimation, and finally ε_{ijk} is a random error or residual component [8]. The main hypotheses regarding in this study are given in below.

H_0: A_i=B_j= C_k
H_1: At least one mean value is different from the others.

In the process of creating the experimental design and to obtain the ANOVA results, MINITAB 19 was used. The 3^3 Factorial Design Matrix is given in Table 2.

Table 2. 3^3 Factorial Design Matrix.

Experiment	Temperature (°C)		Biosorbent dosage (g/L)		pH		Coded Coefficient			Quadratic Coefficient		
	Cr (III)	Pb (II)	Cr (III)	Pb (II)	Cr (III)	Pb (II)	A	B	C	A	B	C
1	20	20	1	1	2	2	1	1	1	1	1	1
2	30	30	1	1	2	2	0	1	1	-2	1	1
3	40	40	1	1	2	2	-1	1	1	1	1	1
4	20	20	3	3	2	2	1	0	1	1	-2	1
5	30	30	3	3	2	2	0	0	1	-2	-2	1
6	40	40	3	3	2	2	-1	0	1	1	-2	1
7	20	20	5	5	2	2	1	-1	1	1	1	1
8	30	30	5	5	2	2	0	-1	1	-2	1	1
9	40	40	5	5	2	2	-1	-1	1	1	1	1
10	20	20	1	1	4	4	1	1	0	1	1	-2
11	30	30	1	1	4	4	0	1	0	-2	1	-2
12	40	40	1	1	4	4	-1	1	0	1	1	-2
13	20	20	3	3	4	4	1	0	0	1	-2	-2
14	30	30	3	3	4	4	0	0	0	-2	-2	-2
15	40	40	5	5	4	4	-1	0	0	1	-2	-2
16	20	20	5	5	4	4	1	-1	0	1	1	-2
17	30	30	5	5	4	4	0	-1	0	-2	1	-2
18	40	40	3	3	4	4	-1	-1	0	1	1	-2
19	20	20	1	1	6	6	1	1	-1	1	1	1
20	30	30	1	1	6	6	0	1	-1	-2	1	1
21	40	40	1	1	6	6	-1	1	-1	1	1	1
22	20	20	3	3	6	6	1	0	-1	1	-2	1
23	30	30	3	3	6	6	0	0	-1	-2	-2	1
24	40	40	5	5	6	6	-1	0	-1	1	-2	1
25	20	20	5	5	6	6	1	-1	-1	1	1	1
26	30	30	5	5	6	6	0	-1	-1	-2	1	1
27	40	40	3	3	6	6	-1	-1	-1	1	1	1

3. RESULTS AND DISCUSSION

3.1. Statistical Analyses

3.1.1. Analysis of Variance and Optimization for Removal Efficiency

In this study three main factors for each of the three levels are determined to apply Full Factorial Design on metal removal efficiency and biosorption capacity from wastewater. Analysis of Variance (ANOVA) was applied to statistically test the effect of these parameters on Cr (III) and Pb (II) biosorption. The full-factorial experimental design matrix in three factors and their levels of the response result were also represented in Appendix section. Moreover, the results of the analyses are shown in Table 3-6.

ANOVA is significant when the higher magnitude of the F-values, and the smaller value of p ($p < 0.0001$). The models F-values of 918.51 and 776.54 indicates that the models are significant Cr (III) and Pb (II) biosorption, showing that the models were perfectly fit with data. P values were obtained from ANOVA for all independent variables shown in Table 3 and 5, in that many variables measured low value ($p < 0.0001$), it revealed the model is significant. The competency of model was checked by analyzing Adj. R-squared (determination coefficient). The model was acceptable to predict the exact correlation between the response and significant variables, it shown the high Adj. R-squared values for two analyses (99.55% and 99.47%) value represented that the variation could be followed in the total response [9].

According to the ANOVA results in Table 3, for removal efficiency of the Cr (III) as a response variable, it was concluded that, main factors of A (temperature), B (biosorbent dosage), C (pH) and their second and third order interactions (A*B*C) have significance effect along with p-values less than 0.05 and High F-values.

Similarly, based to ANOVA results in Table 5 large F-values along with p-values less than 0.05 of main factors and interactions shows that the models are significant on removal efficiency of the Pb (II) from wastewater. In other words, main factors of A, B and C, their interactions (A*B, A*C and B*C) and third order interactions (A*B*C) have critical effect on response variable. Moreover, main effects and interactions in the model explain the removal efficiency of the Pb (II) at a rate of 99.47% as seen in Table 6.

Table 3. ANOVA Table for Removal Efficiency of the Cr (III)

Source	DF	Adj SS	Adj MS	F-value	P-value
Model	26	151169	5814.2	918.51	0.000
Linear	6	135766	22627.7	3574.67	0.000
A	2	86	43.1	6.80	0.002
B	2	7025	3512.7	554.93	0.000
C	2	128655	64327.4	10162.28	0.000
2^{nd}-Order Interactions	12	12653	1054.4	166.57	0.000
A*B	4	2442	610.4	96.43	0.000
A*C	4	2754	688.4	108.76	0.000
B*C	4	7458	1864.4	294.54	0.000
3^{rd}-Order Interactions	8	2750	343.7	54.30	0.000
A*B*C	8	2750	343.7	54.30	0.000
Error	81	513	6.3		
Total	107	151682			

Table 4. Model Summary for Cr (III) on the Removal Efficiency

S	R-sq	R-sq(adj)	R-sq(pred)
2.51595	99.66%	99.55%	99.40%

Table 5. ANOVA Table for Removal Efficiency of the Pb (II)

Source	DF	Adj SS	Adj MS	F-value	P-value
Model	26	152086	5849.4	776.54	0.000
Linear	6	127145	21190.8	2813.19	0.000
A	2	3725	1862.5	247.26	0.000
B	2	222	111.0	14.74	0.000
C	2	123198	61598.9	8177.57	0.000
2^{nd}-Order Interactions	12	17625	1468.7	194.98	0.000
A*B	4	2266	566.5	75.20	0.000
A*C	4	1960	490.1	65.06	0.000
B*C	4	13399	3349.7	444.68	0.000
3^{rd}-Order Interactions	8	7316	914.5	121.40	0.000
A*B*C	8	7316	914.5	121.40	0.000
Error	81	610	7.5		
Total	107	152696			

Table 6. Model Summary for Pb (II) on the Removal Efficiency

S	R-sq	R-sq(adj)	R-sq(pred)
2.74457	99.60%	99.47%	99.29%

In this part of the study, the main effects of low, medium and high levels of temperature (A), biosorbent dosage (B) and pH (C) for Cr (III) and Pb (II) on removal efficiency are shown in Figure 1(a) and Figure 1(b). In Figure 1(a), it was deduced that all the main factors A, B and C effective on removal efficiency. It can be deduced that the pH (C) has an important influence than biosorbent dosage (B) and temperature (A). Moreover, these results show that, biosorbent dosage (B) and pH (C) positively effects on the removal efficiency, while temperature (A) has negative effect. The results in Figure 1(b) shows the pH (C) has greatest and positively effect on the response variable and on the other hand temperature (A) and biosorbent dosage (B) have the weakest influence on the removal efficiency.

After examining the main effects, the interaction plots were obtained to evaluate every second order interaction effects on removal efficiency for Cr (III) and Pb (II) (Fig. 2(a) and Fig 2(b)) [10]. In these plots, non-parallel lines indicate that the effect of one factor on the response depends on the setting of the other factor. The greater lines depart from being parallel, the greater the strength of the interaction [8,11]. From Figure 2(a), it is seen that there is an interaction between A*B, A*C and B*C as the lines are non-parallel. This means that linear and quadratic combinations of A*B, A*C, and B*C are significant on removal efficiency for Cr (III). In addition to this, Figure 2(b) illustrates the interactions between A*B, A*C and B*C. As the lines non-parallel, it was concluded that there are all interactions are significant effect for Pb (II) on the removal efficiency.

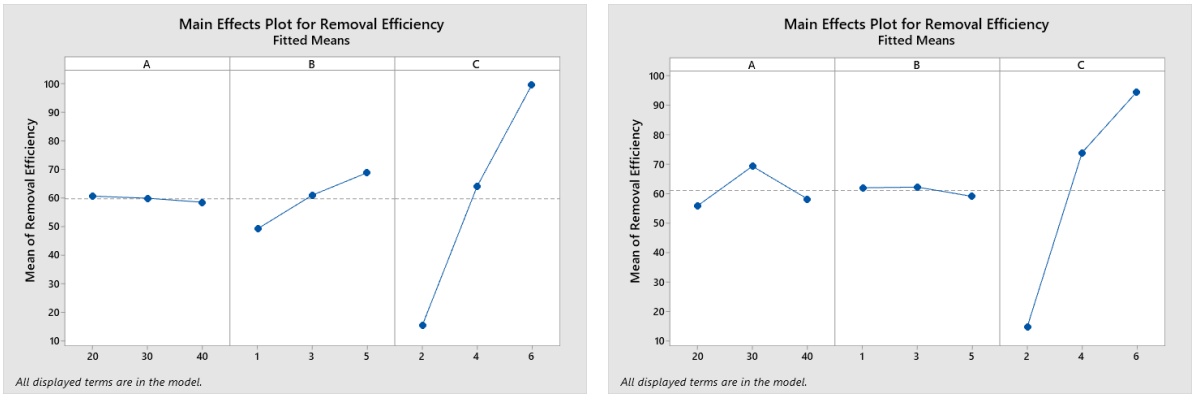

(a) **(b)**

Figure 1. (a): Main effects Plot for Cr (III) on the Removal Efficiency. (b): Main Effects Plot for Pb (II) on the Removal Efficiency.

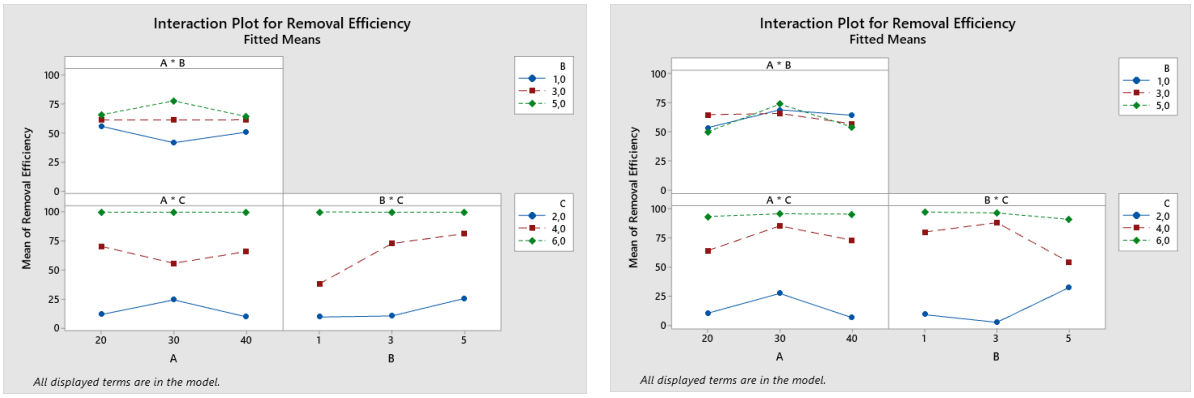

(a) **(b)**

Figure 2. (a): Interaction Plot for Cr (III) on the Removal Efficiency. (b): Interaction Plot for Pb (II) M on the Removal Efficiency.

According to all the results were obtained, it was concluded that, all the factors considered are important on the Cr (III) and Pb (II) on removal efficiency from wastewater. Accordingly, each main factors and their second and third order interactions should be included in the regression model for optimization. In the next step, the results of the regression and optimization model will be examined with three factors and their interactions for removal efficiency based on the first model.

The optimization analysis was implemented to determine convenient levels of all factors in ANOVA model and to obtain a regression equation for the removal efficiency. The regression equations were obtained in order to maximize Cr (III) (Eq. 2) and Pb (II) (Eq. 3) for removal efficiency response are given in below [12]. Besides, the optimization plots for Cr (III) and Pb (II) on removal efficiency are shown in Figure 3 and Figure 4.

$$y_{Removal\ Efficiency\ for\ Cr} = 59.70 + 1.191A - 9.16B - 39.931C - 3.788AB + 1.251AC - 9.23BC - 3.761ABC \quad (2)$$

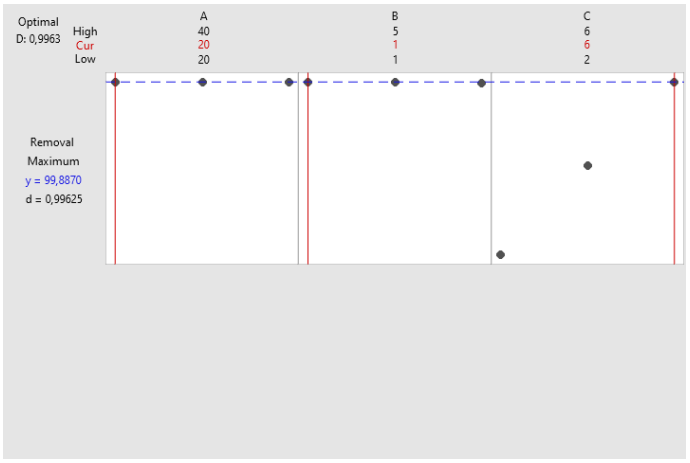

Figure 3. Optimization plot for Cr (III) on the removal efficiency.

According to Figure 3, for the optimization of the for Cr (III) on removal efficiency as a response variable, value of the objective function is calculated as 0.99625. This value changes from 0 to 1 and if closer to 1, this means that all factor levels supply optimum conditions [13]. This value (0.99625) also means that determined values belonging to all the factors provide best conditions for removal efficiency from wastewater. In case of A (temperature) 20 °C (low level), B (biosorbent dosage 1 g/L (low level) and C (pH) 6 pH (high level), the maximum value of removal efficiency could reach 99.8870%. As a result, the optimum conditions for Cr (III) on removal efficiency from wastewater are achieved keeping the temperature 20 °C, biosorbent dosage 1 g/L and pH 6 [10].

$$y_{Removal\ Efficiency\ for\ Pb} = 61.115 + 2.905A + 2.023B - 33.446C - 2.25AB + 3.501AC - 1.892BC - 5,.269ABC \quad (3)$$

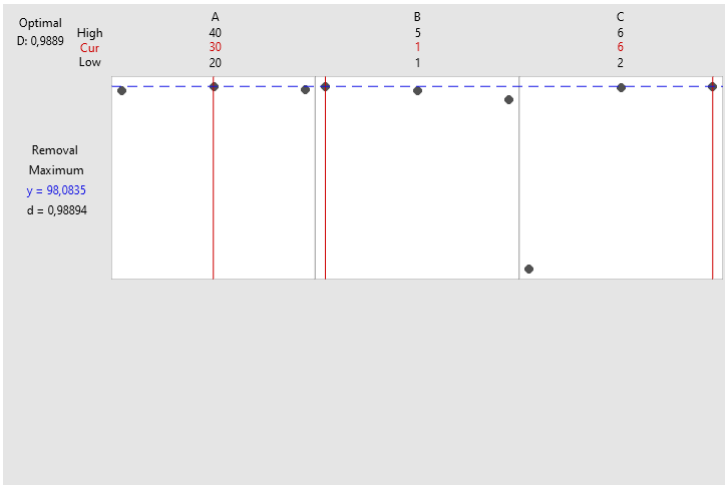

Figure 4. Optimization plot for Pb (II) on the removal efficiency.

The results of Figure 4 show that, for the optimization of the for Pb (II) on removal efficiency as a response variable, value of the objective function is calculated as 0.98894. This value means that determined values belonging to all the factors provide best conditions for removal efficiency from

wastewater. In case of A (temperature) 30 °C (medium level), B (biosorbent dosage) 1 g/L (low level) and C (pH) 6 (high level), the maximum value of removal efficiency could reach 98.0835%. As a result, the optimum conditions for Pb (II) on removal efficiency from wastewater are achieved keeping the temperature 30 °C, biosorbent dosage 1 g/L and pH 6 [10].

3.1.2. Analysis of Variance and Optimization for Biosorption Capacity

Analysis of Variance (ANOVA) was carried out to determine significant main factors and their interactions on biosorption capacity of Cr (III) and Pb (II) from wastewater. ANOVA was also used to identify the statistical significance of the experimental factors on biosorption capacity. The results of ANOVA for biosorption capacity on Cr (III) and Pb (II) are given in Table 7-Table 10.

According to the ANOVA results in Table 7, for biosorption capacity of the Cr (III) as a response variable, it was concluded that, main factors of A (temperature), B (biosorbent dosage) and C (pH) have significance effect ($p<0.05$). Since the F-values are also quite high, factors and interactions are considered statistically significant at %95 confidence level. Additionally, both A*B, A*C and B*C second order interactions, and A*B*C third order interactions have critical effect on biosorption capacity. Besides, when the Adj. R-squared and values were examined, it is seen that main factor and their interactions in the model explain the biosorption capacity of the Cr (III) at the rate of 98.99%.

Similarly, based to ANOVA results in Table 9 large F-values along with p-values less than 0.05 of main factors and interactions shows that the models are significant on biosorption capacity. In other words, based to the ANOVA results in Table 9 main factors of A, B and C, and their interactions (A*B, A*C and B*C) have critical effect on biosorption capacity of the Pb (II) from wastewater. Moreover, main effects and interactions in the model explain the biosorption capacity of the Pb (II) at a rate of 99.88% as seen in Table 10.

Table 7. ANOVA Table for Biosorption Capacity of the Cr (III)

Source	DF	Adj SS	Adj MS	F-value	P-value
Model	26	21271.6	818.14	403.51	0.000
Linear	6	14985.1	2497.51	1231.79	0.000
A	2	67.5	33.76	16.65	0.000
B	2	6151.0	3075.50	1516.85	0.000
C	2	8766.6	4383.29	2161.87	0.000
2^{nd} -Order Interactions	12	5892.4	491.03	242.18	0.000
A*B	4	234.8	58.70	28.95	0.000
A*C	4	252.5	63.12	31.13	0.000
B*C	4	5405.1	1351.28	666.46	0.000
3^{rd} -Order Interactions	8	394.1	49.26	24.30	0.000
A*B*C	8	394.1	49.26	24.30	0.000
Error	81	164.2	2.03		
Total	107	21435.8			

Table 8. Model Summary for Cr (III) on the Biosorption Capacity

S	R-sq	R-sq(adj)	R-sq(pred)
1.42392	99.23%	98.99%	98.64%

Table 9. ANOVA Table for Biosorption Capacity of the Pb (II)

Source	DF	Adj SS	Adj MS	F-value	P-value
Model	26	28198.3	1084.55	2657.06	0.000
Linear	6	22168.2	3694.70	9051.71	0.000
A	2	214.6	107.28	262.83	0.000
B	2	12617.7	6308.85	15456.16	0.000
C	2	9335.9	4667.96	11436.13	0.000
2^{nd} -Order Interactions	12	5714.6	476.22	1166.69	0.000
A*B	4	221.2	55.31	135.50	0.000
A*C	4	133.1	33.28	81.52	0.000
B*C	4	5360.3	1340.07	3283.06	0.000
3^{rd} -Order Interactions	8	315.5	39.44	96.62	0.000
A*B*C	8	315.5	39.44	96.62	0.000
Error	81	33.1	0.41		
Total	107	28231.4			

Table 10. Model Summary for Pb (II) on the Biosorption Capacity

S	R-sq	R-sq(adj)	R-sq(pred)
0.638887	99.88%	99.85%	99.79%

In this section, the main effects plots in Figure 5 were obtained shows that A(temperature), B (biosorbent dosage) and C (pH) effect on biosorption capacity for Cr (III) and Pb (II). In Figure 5(a), B and C have most significant effect on biosorption capacity, followed by A. This figure also shows that, B (biosorbent dosage) negatively impacting on biosorption capacity, while C (pH) have positive effect.

Similarly, In Figure 5(b), it was deduced that all the main factors A, B and C effective on biosorption capacity for Pb (II). Moreover, B (biosorbent dosage) and C (pH) greatest influence on biosorption capacity on the other hand A (Temperature) more less effect than these factors. Additionally, the results in Figure 9. shows both B (biosorbent dosage) and C (pH) have greatest effect on biosorption capacity for Pb (II) and the other hand A (temperature) have weakest effect on response variable. Also, this figure shows that in general, B (biosorbent dosage) has negatively effect on biosorption capacity and on the contrary C (pH) has positive effect.

After analyzing the main effects, the interaction plots for Pb (II) on biosorption capacity were obtained in Figure 6. These figures show that the significant interactions between temperature and biosorbent dosage, temperature and pH and also between biosorbent dosage and pH. In Figure 6(a), it is seen obviously that coded and quadratic combinations of A*B, A*C, and B*C are significant on biosorption capacity for Cr (III) as lines are non-parallel. Similarly, in Figure 6(b), it was concluded that all the interactions (A*B, A*C and B*C) are significant on biosorption capacity for Pb (II).

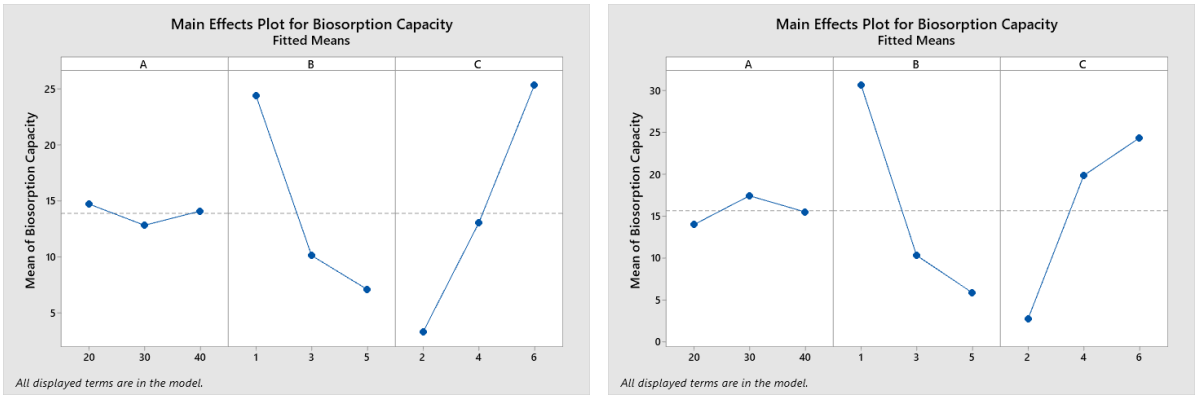

(**a**) (**b**)

Figure 5. (a): Main effects Plot for Cr (III) on the biosorption capacity. (b): Main Effects Plot for Pb (II) on the biosorption capacity.

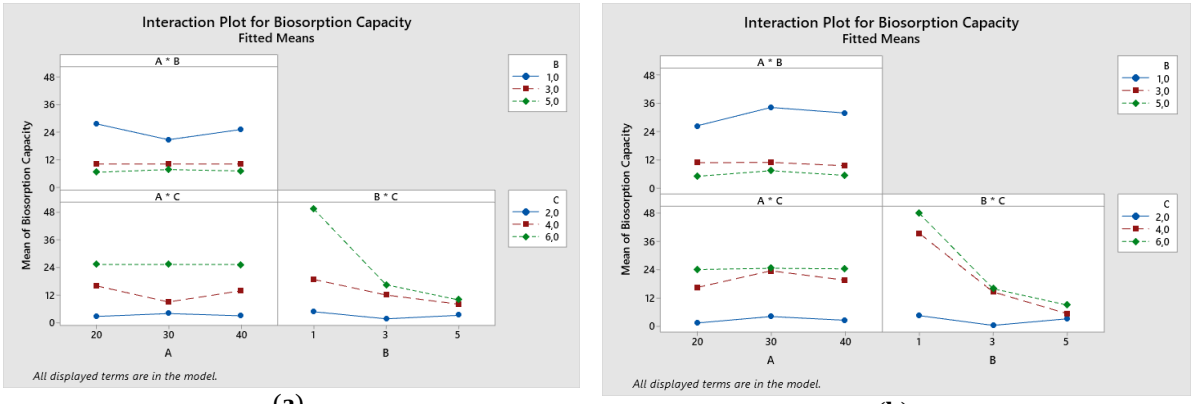

(**a**) (**b**)

Figure 6. (a): Interaction Plot for Cr (III) on the biosorption capacity. (b): Interaction Plot for Pb (II) on the biosorption capacity.

According to all the results were obtained, it was concluded that, all the factors considered are important on the Cr (III) and Pb (II) on biosorption capacity from wastewater. Similarly, each main factors and their second and third order interactions should be included in the regression model for optimization. In the next step, the results of the regression and optimization model will be examined with three factors and their interactions for biosorption capacity for Cr (III) and Pb (II).

The optimization analysis was implemented to determine convenient levels of all factors in ANOVA model and to obtain a regression equation for the removal efficiency. The regression equations were obtained in order to maximize Cr (III) (Eq. 4) and Pb (II) (Eq. 5) for removal efficiency response are given in below [12]. Besides, the optimization plots for Cr (III) and Pb (II) on removal efficiency are shown in Figure 7 and Figure 8.

$$y_{Biosorption\ Capacity\ for\ Cr} = 13.896 - 0.21A + 6.779B - 11.44C - 0.223AB - 0.24AC - 8.618BC - 0.256ABC \quad (4)$$

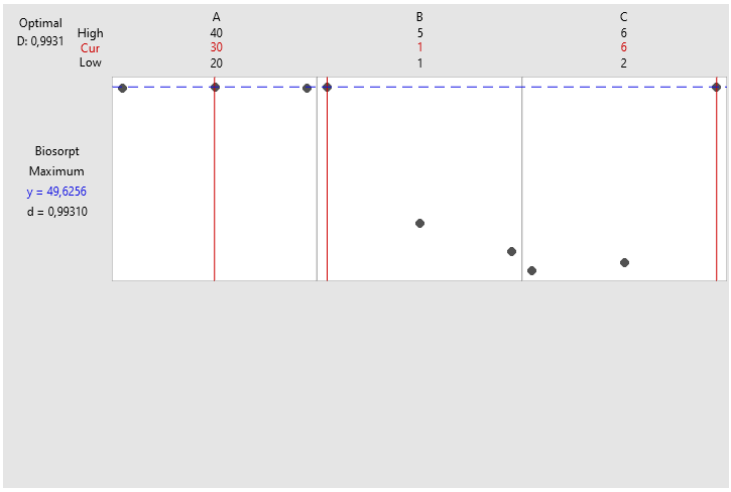

Figure 7. Optimization Plot for Cr (III) on the Biosorption Capacity.

According to Figure 7, for the optimization of the for Cr (III) on biosorption capacity as a response variable, value of the objective function was calculated as 0.99310. This value (0.99310) also means that determined values belonging to all the factors provide best conditions for biosorption capacity from wastewater. In case of A (temperature) 30 °C (medium level), B (biosorbent dosage) 1 g/L (low level) and C (pH) 6 pH (high level), the maximum value of biosorption capacity could reach 49.6256%.

$$y_{Biosorption\ Capacity\ for\ Pb} = 15.6611 + 0.1329A + 9.7593B - 8.6863C - 0.387AB + 0.151AC - 5.541BC - 0.73ABC \quad (5)$$

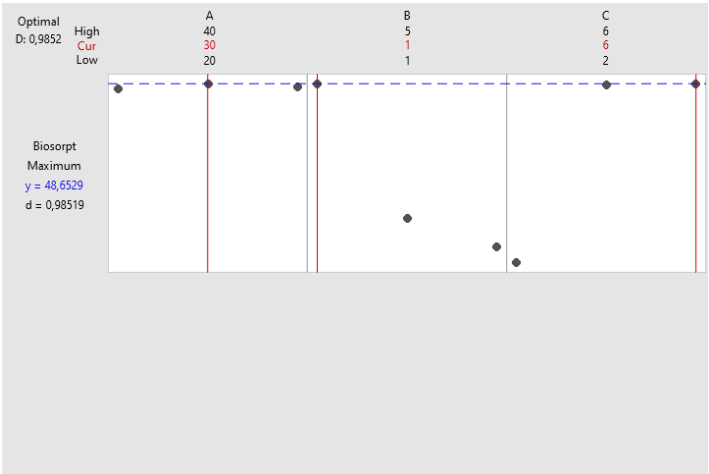

Figure 8. Optimization plot for Pb (III) on the biosorption capacity.

The optimization results of Figure 8 show that, for the optimization of the for Pb (II) on biosorption capacity as a response variable, value of the objective function was calculated as 0.98519. This value means that determined values belonging to all the factors provide best conditions for removal efficiency from wastewater. In case of A (temperature) 30 °C (medium level), B (biosorbent dosage) 1 g/L (low level) and C (pH) 6 pH (high level), the maximum value of biosorption capacity could reach 48.6529%.

4. CONCLUSION

In this study, 3^3 Factorial Experiment Design was applied to investigate the effect of each factor and their interactions) on Cr (III) and Pb (II) on removal efficiency and biosorption capacity. For this purpose, experimental data sets were obtained and the conditions under which the biosorption of Cr (III) and Pb (II) from wastewater yielded the best results were obtained by applying ANOVA and optimization analysis. For this purpose, by conducting ANOVA via Response Surface Methodology and by applying optimization analysis, more detailed results were obtained regarding the conditions under which biosorption of Cr (III) and Pb (II) from wastewater yielded the best results.

The ANOVA results show that temperature (°C), biosorbent dosage (g/L) and pH, and three levels belonging to these three main factors have significance effect for Cr (III) and Pb (II) on removal efficiency and biosorption capacity from wastewater. In addition to this, it was concluded that the most effective factors for the Cr (III) on removal efficiency as a response variable were the biosorbent dosage and pH, while the most influential factors for Pb (II) were temperature and pH. Similarly, while the most effective factors for the biosorption capacity response variable on Cr (III) was biosorbent dosage and pH, the same factors were also effective for the Pb (II). The main effects and their interactions in the ANOVA model also explain the removal efficiency and biosorption capacity response variables with quite high Adj. R-squared values. Moreover, based on interaction plots, all the second and third order interactions have significant effect for Cr (III) and Pb (II) on removal efficiency and biosorption capacity.

Optimization results were obtained depending on ANOVA results, on the other hand, show that all the factors' levels were obtained maximize the removal efficiency and biosorption capacity from wastewater in general. The optimum factors levels are temperature of 20 °C, biosorbent dosage of 1 g/L and pH of 6 for Cr (III) on removal efficiency. However, these levels are temperature of 30 °C, biosorbent dosage of 1 mg/L and pH of 6 for Pb (II) on removal efficiency. On the other hand, the optimum factor levels for Cr (III) on biosorption capacity was detected to be temperature of 30 °C, biosorbent dosage of 1 g/L and pH of 6. Also, in case of temperature of 30 °C, biosorbent dosage of 1 g/L and pH of 6, for the Pb (II) on biosorption capacity reach gave the highest value.

Consequently, in case the factor levels were considered (chosen) as indicated, optimum conditions were provided for both response variables in efficiency of metal removal from wastewater. With this study, it has been demonstrated that Factorial Experimental Design are quite applicable in the field of chemical experiments, and it is predicted that all these experiences make an example for other researchers.

CONFLICT OF INTEREST

The authors stated that there are no conflicts of interest regarding the publication of this article.

REFERENCES

[1] Elgarahy AM, Elwakeel, KZ, Mohammad SH, Elshoubaky GA. A critical review of biosorption of dyes, heavy metals and metalloids from wastewater as an efficient and green process. Cleaner Eng Technol 2021; 4: 100209.

[2] Beni AA, Esmaeili A. Biosorption, an efficient method for removing heavy metals from industrial effluents. A reviev. Environ Technol Innov 2020; 17: 100503.

[3] Priyadarshanee M, Das S. Biosorption and removal of toxic heavy metals by metal tolerating bacteria for bioremediation of metal contamination: A comprehensive review. J Environ Chem Eng 2021; 9: 10486.

[4] Esmaelli A, Darvish M. Evaluation of the marine alga *Sargassum glaucescens* for the adsorption of Zn (II) from aqueous solutions. Water Qual Res J 2014; 49: 339–345.

[5] Mondal NK, Samanta A, Dutta S, Chattoraj S. Optimization of Cr (VI) biosorption onto Aspergillus niger using 3-level box-behnken design: Equilibrium, kinetic, thermodynamic and regeneration studies. J Genet Eng Biotechnol 2017; 15: 151-160.

[6] Li D, Xu X, Yu H, Han X. Characterization of Pb2+ biosorption by psychrotrophic strain *Pseudomonas* sp. I3 isolated from permafrost soil of Mohe wetland in Northeast China. J Environ Manage 2017: 196, 8-15.

[7] Malkoc S, Yazici B, Gürsel C, Dikmen, S. Optimization of the removal of chromium and lead by *penicillium chrysogenum* using 2k factorial experiments. Environ Qual Manage 2022; 1-14.

[8] Majasan JO, Cho JIS, Maier M, Shearing PR, Brett DJL. Optimization of mass transport parameters in a polymer electrolyte membrane electrolyser using factorial design-of-experiment. Front Energy Res 2021; 9.

[9] Raj JVA, Kumar RP, Vijayakumar B, Gnansounou, E, Bharathiraja B. Modelling and process optimization for biodiesel production from *Nannochloropsis salina* using artificial neural network. Bioresour Technol 2021; 329: 124872.

[10] Rashad S, EL-Chaghaby G, Lima EC, Simoes Dos Reis G. Optimizing the ultrasonic-assisted extraction of antioxidants from *ulva lactuca* algal biomass using factorial design. Biomass Conv Bioref 22 April 2021.

[11] Jiju A. Design of Experiments for Engineers and Scientists: Second Edition. In Design of Experiments for Engineers and Scientists. 2014; 2nd ed. Amsterdam, Holland: Elsevier.

[12] Malkoc S, Anagun AS, Deniz N. A novel sustainable biosorbent (*ulocladium consortiale*) proposal with central composite design to reduce water pollution. Iran j. Sci Technol Trans Sci 2021; 45:1131-1141.

[13] Atalan A, Şahin H. Design of Experiments Optimization Application in Physics: A Case Study of the Damped Driven Pendulum Experiment. Sigma J Eng & Nat Sci 2021; 39(3): 322-330.

APPENDIX

Table 11. 3^3 Factorial Design Matrix for The Removal Efficiency of The Cr (III).

Experiments	Temperature (°C)	Biosorbent dosage (g/L)	pH	Response Values			
				1. Repetition	2. Repetition	3. Repetition	4. Repetition
1	20	1	2	11.555	9.890	9.822	99.363
2	20	1	4	56.118	56.945	57.782	9.935
3	20	1	6	99.897	99.902	99.868	56.206
4	20	3	2	11.821	11.063	11.001	99.880
5	20	3	4	71.404	70.581	71.851	11.846
6	20	3	6	99.645	99.832	99.570	73.935
7	20	5	2	13.694	14.644	13.146	99.872
8	20	5	4	82.897	82.221	83.377	14.244
9	20	5	6	99.758	99.545	99.485	82.306
10	30	1	2	10.356	10.696	10.551	99.603
11	30	1	4	14.111	14.152	14.545	10.294
12	30	1	6	99.929	99.601	99.926	14.676
13	30	3	2	11.307	10.322	10.588	99.924
14	30	3	4	69.584	76.437	69.584	10.717
15	30	3	6	99.871	99.203	99.045	76.437
16	30	5	2	53.610	51.805	52.373	98.738
17	30	5	4	80.756	80.154	79.893	51.604
18	30	5	6	99.747	100.236	98.819	79.959
19	40	1	2	7.085	6.955	9.583	99.497
20	40	1	4	45.149	48.834	26.627	11.123
21	40	1	6	99.852	99.803	99.983	52.421
22	40	3	2	10.745	10.021	9.554	99.898
23	40	3	4	76.228	71.023	75.180	10.463
24	40	3	6	99.719	99.329	99.848	71.473
25	40	5	2	8.473	11.978	11.059	99.805
26	40	5	4	83.351	80.758	80.410	12.783
27	40	5	6	99.747	99.647	9.822	79.697

Table 12. 3^3 Factorial Design Matrix for The Removal Efficiency of The Pb (II).

Experiments	Temperature (°C)	Biosorbent dosage (g/L)	pH	Response Values			
				1. Repetition	2. Repetition	3. Repetition	4. Repetition
1	20	1	2	2.000	1.980	2.900	4.200
2	20	1	4	63.540	62.620	56.920	61.040
3	20	1	6	95.964	96.044	96.148	96.280
4	20	3	2	2.000	1.980	2.900	4.200
5	20	3	4	93.710	93.454	92.400	93.396
6	20	3	6	97.548	97.094	97.616	97.792
7	20	5	2	29.840	23.640	20.660	29.640
8	20	5	4	34.900	37.420	37.420	39.780
9	20	5	6	88.972	83.746	84.902	85.190
10	30	1	2	9.800	11.260	12.100	9.360
11	30	1	4	97.360	97.322	97.382	97.586
12	30	1	6	98.349	98.987	97.684	97.314
13	30	3	2	2.000	1.980	2.900	4.200
14	30	3	4	97.636	97.638	97.896	97.528
15	30	3	6	97.042	96.214	95.814	95.722
16	30	5	2	70.500	67.152	71.860	66.020
17	30	5	4	59.900	60.580	53.800	66.240
18	30	5	6	95.930	90.588	90.744	90.634
19	40	1	2	11.920	17.600	15.400	12.840
20	40	1	4	80.160	76.260	83.566	83.958
21	40	1	6	97.460	94.250	99.158	95.628
22	40	3	2	2.000	1.980	2.900	4.200
23	40	3	4	75.230	73.240	71.120	71.120
24	40	3	6	93.270	95.094	95.652	94.334
25	40	5	2	2.000	1.980	2.900	4.200
26	40	5	4	77.720	61.680	60.160	59.560
27	40	5	6	91.742	90.958	96.284	98.064

Table 13. 3^3 Factorial Design Matrix for The Biosorption Capacity of The Cr (III).

Experiments	Temperature (°C)	Biosorbent dosage (g/L)	pH	Response Values			
				1. Repetition	2. Repetition	3. Repetition	4. Repetition
1	20	1	2	5.709	4.877	4.882	4.958
2	20	1	4	27.671	28.246	28.548	27.770
3	20	1	6	49.552	49.555	49.245	49.642
4	20	3	2	1.961	1.839	1.833	1.968
5	20	3	4	11.901	11.756	11.919	12.314
6	20	3	6	16.552	16.561	16.507	16.590
7	20	5	2	1.368	1.459	1.310	1.420
8	20	5	4	8.276	8.209	8.318	8.214
9	20	5	6	9.960	9.931	9.941	9.952
10	30	1	2	5.106	5.274	5.254	5.137
11	30	1	4	6.972	7.006	7.258	7.251
12	30	1	6	49.964	49.503	49.371	49.664
13	30	3	2	1.882	1.713	1.7576	1.781
14	30	3	4	11.574	12.680	11.551	12.706
15	30	3	6	16.623	16.512	16.464	16.608
16	30	5	2	5.357	5.170	5.235	5.152
17	30	5	4	8.056	7.996	7.970	7.977
18	30	5	6	9.959	9.964	9.854	9.923
19	40	1	2	3.521	3.464	4.735	5.528
20	40	1	4	22.440	24.271	13.208	26.002
21	40	1	6	49.530	49.310	49.497	49.357
22	40	3	2	1.790	1.665	1.447	1.734
23	40	3	4	12.679	11.813	12.480	11.865
24	40	3	6	16.587	16.522	16.564	16.546
25	40	5	2	0.847	1.196	1.105	9.984
26	40	5	4	8.325	8.060	8.022	7.944
27	40	5	6	9.929	9.965	9.928	9.946

Table 14. 3^3 Factorial Design Matrix for The Biosorption Capacity of The Pb (II).

Experiments	Temperature (°C)	Biosorbent dosage (g/L)	pH	Response Values			
				1. Repetition	2. Repetition	3. Repetition	4. Repetition
1	20	1	2	0.996	0.980	1.433	2.079
2	20	1	4	31.33	31.000	28.067	30.278
3	20	1	6	47.134	47.359	47.317	47,948
4	20	3	2	0333	0.329	0.481	0.698
5	20	3	4	15.546	15.514	15.349	15.504
6	20	3	6	16.236	16.129	16.226	16.255
7	20	5	2	2.979	2.360	2.062	2.958
8	20	5	4	3.479	3.904	3.738	3.972
9	20	5	6	8.869	8.368	8.463	8.509
10	30	1	2	4.851	5.585	6.002	4.634
11	30	1	4	48.583	48.179	48.401	48.406
12	30	1	6	48.979	48.810	48.263	48.560
13	30	3	2	0.332	0.329	0.481	0.700
14	30	3	4	16.186	16.208	16.294	16.211
15	30	3	6	16.163	15.961	15.948	15.911
16	30	5	2	7.039	6.696	7.169	6.591
17	30	5	4	5.973	6.041	5.378	6.608
18	30	5	6	9.582	9.041	9.056	9.045
19	40	1	2	5.901	8.765	7.639	6.344
20	40	1	4	39.527	37.903	41.125	41.979
21	40	1	6	48.152	46.751	49.381	47.624
22	40	3	2	0.332	0.330	0.483	0.700
23	40	3	4	12.488	12.205	12.166	11.798
24	40	3	6	15.473	15.838	15.889	15.639
25	40	5	2	0.200	0.197	0.290	0.419
26	40	5	4	7.744	6.158	5.997	5.954
27	40	5	6	9.145	9.085	9.613	9.783